Fluid Mechanics and Aerodynamics

Todd H. Rider thor@riderinstitute.org 13 November 2019

Any suggestions for improvements would be greatly appreciated.

On aircraft:

"There is as much pressure exerted by a substance against the air as by the air against the substance.

"Observe how the beating of its wings against the air suffices to bear up the weight of the eagle in the highly rarefied air which borders on the fiery element! Observe also how the air moving over the sea, beaten back by the bellying sails, causes the heavily laden ship to glide onwards!

"So that by adducing and expounding the reasons of these things you may be able to realize that man when he has great wings attached to him, by exerting his strength against the resistance of the air and conquering it, is enabled to subdue it and to raise himself upon it."

On parachutes:

"If a man have a tent made of linen of which the apertures have all been stopped up, and it be twelve braccia across and twelve in depth, he will be able to throw himself down from any great height without sustaining any injury."

On helicopters:

"I find that if this instrument made with a screw be well made–that is to say, made of linen of which the pores are stopped up with starch–and be turned swiftly, the said screw will make its spiral in the air and it will rise high."

Advice for test pilots:

"This machine should be tried over a lake, and you should carry a long wineskin as a girdle so that in case you fall you will not be drowned."

–Leonardo da Vinci, *The Notebooks* (ca. 1500)

Overview

Fluid mechanics and aerodynamics concerns the motion of liquids and gases or their interactions with objects such as pipes or aircraft. One fundamental factor affecting how to model the behavior of a fluid is whether the fluid is compressible, or in other words whether its density changes significantly when its pressure its increased. Another fundamental factor is viscosity, or whether the particles of the fluid seem to stick to each other and pull on each other. Therefore, it is most convenient to divide models of fluid behavior into four categories: (1) incompressible, inviscid fluids, (2) incompressible viscous fluids, (3) compressible inviscid fluids, and (4) compressible viscous fluids. Important applications of fluid mechanics include the design of ships and submarines, as well as helicopters, airplanes, parachutes, and spacecraft reentering the atmosphere. Other applications include fluids in pipes and lubricants in machinery, pressure and circulation in the ocean and atmosphere, and sound waves and shock waves.

Contents

1 Incompressible, Inviscid Fluid Mechanics

The simplest fluid mechanics cases to analyze are those in which both (1) the fluid is **incompressible** or has a constant density (or equivalently, in which any velocities are much less than the speed of sound in the fluid) and (2) the fluid is **inviscid** (it does not have any **viscosity**, or "stickiness") [1-15]. This section will introduce three important laws for any fluid (conservation of mass, conservation of momentum, and conservation of energy), then show that for incompressible inviscid fluids, the laws can be simplified to the Bernoulli equation and the equations for potential flow. This section will then apply these principles to several practical situations, including buoyancy, aerodynamic drag, aerodynamic lift, and helicopters.

1.1 Conservation of Mass (Continuity Equation)

The first important law for fluid mechanics is the conservation of mass, often called the **continuity equation**. Mass can move around or build up but cannot be created or destroyed (barring relativistic conversions between mass and energy). Specifically, a fluid has a mass density ρ and moves at a velocity $\mathbf{v}$, both of which are functions of position $\mathbf{x}$ and time t–the density and velocity may be different at different places or times. The integral form of the continuity equation is

$$\overbrace{\frac{\partial}{\partial t}\int_V \rho\, dV}^{\substack{\text{Change in mass}\\ \text{within control}\\ \text{volume } V}} + \overbrace{\oint_S \rho \mathbf{v}\cdot\mathbf{dS}}^{\substack{\text{Mass outflow across}\\ \text{surface } S \text{ enclosing}\\ \text{the control volume}}} = \overbrace{0}^{\text{Conserved}} \qquad \textbf{Continuity equation (integral form)} \tag{1}$$

Thus if there is a net (positive) outward flow of mass across the surface S enclosing a control volume, the remaining mass within that volume must be decreasing (negative $\partial/\partial t$). Note that the mass outflow is a product of mass density, velocity, and area dS–increasing any of these factors increases the mass outflow rate proportionately.

As discussed in *Applied Mathematics* 5.4, common physics equations such as the continuity equation can also be written in terms of differentials (gradients) instead of integrals. For a general vector variable $\mathbf{A}$, the two forms may be interconverted using

$$\oint_S \mathbf{A}\cdot\mathbf{dS} = \int_V (\nabla\cdot\mathbf{A})\, dV \qquad \textbf{Divergence theorem} \tag{2}$$

relating integrals over a volume V and the surface S enclosing that volume. By applying Eq. (2) to Eq. (1), the continuity equation may be written in its differential form:

$$\overbrace{\frac{\partial\rho}{\partial t}}^{\substack{\text{Change in mass}}} + \overbrace{\nabla\cdot(\rho\mathbf{v})}^{\substack{\text{Mass outflow}}} = \overbrace{0}^{\text{Conserved}} \qquad \textbf{Continuity equation (differential form)} \tag{3}$$

The meaning remains the same–if there is a net outward flow of mass from a point, the mass density at that point must be decreasing. Regardless of whether the integral or differential form is used, the continuity equation is usually used to show that the functions $\rho(\mathbf{x},t)$ and $\mathbf{v}(\mathbf{x},t)$ are interrelated. Specific solutions of the continuity equation depend on the particular situation being considered.

For incompressible fluids ($\nabla\rho = 0$ and $\partial\rho/\partial t = 0$), Eqs. (1) and (3) are greatly simplified:

$$\oint_S \mathbf{v}\cdot\mathbf{dS} = 0 \qquad \text{or} \qquad \nabla\cdot\mathbf{v} = 0 \qquad \textbf{Continuity equation (incompressible fluid)} \tag{4}$$

1.2 Conservation of Momentum (Euler or Navier-Stokes Equation)

Newton's second law for conservation of momentum is $d\mathbf{p}/dt = m(d\mathbf{v}/dt) = \Sigma_i \mathbf{F}_i$, in which $\mathbf{p}$ is momentum (not to be confused with pressure p), m is mass, and $\Sigma_i \mathbf{F}_i$ is the sum of the forces applied to the mass. In other words, momentum is constant or conserved unless external forces are applied. For a fluid, this law for conservation of momentum may be written per volume as

$$\overbrace{\rho\left(\frac{\partial}{\partial t} + \mathbf{v}\cdot\nabla\right)\mathbf{v}}^{\text{Mass} \times \text{acceleration}} = \overbrace{\rho\mathbf{g}}^{\substack{\text{Gravitational}\\ \text{force}}} - \overbrace{\nabla p}^{\substack{\text{Pressure}\\ \text{force}}} + \overbrace{\mathbf{F}_{\text{viscous}}}^{\substack{\text{Viscous}\\ \text{forces}}} \qquad \textbf{Momentum equation (differential form)} \tag{5}$$

The term $(\partial/\partial t + \mathbf{v}\cdot\nabla) \equiv d/dt$ is called the **convective derivative**. The $\partial/\partial t$ is actual variation with time, and the $\mathbf{v}\cdot\nabla$ accounts for apparent time variation of a quantity due to moving along a spatial gradient ∇ of the quantity at velocity $\mathbf{v}$. The integral form of the momentum equation is:

$$\overbrace{\frac{\partial}{\partial t}\int_V \rho\mathbf{v}\,dV + \oint_S \mathbf{v}(\rho\mathbf{v}\cdot\mathbf{dS})}^{\text{Mass} \times \text{acceleration}} = \overbrace{\int_V \rho\mathbf{g}\,dV}^{\substack{\text{Gravitational}\\ \text{force}}} - \overbrace{\oint_S p\,\mathbf{dS}}^{\substack{\text{Pressure}\\ \text{force}}} + \overbrace{\int_V \mathbf{F}_{\text{viscous}}\,dV}^{\substack{\text{Viscous}\\ \text{forces}}} \qquad \textbf{Momentum equation (integral form)} \tag{6}$$

The momentum conservation equation, Eq. (5), is sometimes called the Euler equation, especially when the viscous force term is neglected, and sometimes called the Navier-Stokes equation, especially when the viscous force term is included and defined more specifically (see Section 2.1).

1.3 Conservation of Energy

On a per mass basis, the total energy e of a fluid is just the sum of the internal (thermal) energy u, the kinetic energy $v^2/2$, and the gravitational potential energy gH, where H is height:

$$e = u + \frac{v^2}{2} + gH \tag{7}$$

By analogy with the equations for mass and momentum, conservation of energy may be written as:

$$\overbrace{\frac{\partial}{\partial t}\int_V \rho\left(u + \frac{v^2}{2} + gH\right)\,dV}^{\substack{\text{Change in energy within}\\ \text{control volume } V}} + \overbrace{\oint_S \rho\left(u + \frac{v^2}{2} + gH\right)\mathbf{v}\cdot\mathbf{dS}}^{\substack{\text{Energy outflow across surface}\\ S \text{ enclosing the control volume}}} \qquad \textbf{Energy equation (integral form)}$$

$$= \underbrace{\int_V \dot{q}_{\text{input}}\,dV}_{\substack{\text{Input heat}\\ \text{energy}}} + \underbrace{\int_V \dot{w}_{\text{input}}\,dV}_{\substack{\text{Input work}\\ \text{energy}}} - \underbrace{\oint_S p\mathbf{v}\cdot\mathbf{dS}}_{\substack{\text{Output work energy}\\ \text{by expanding pressure}}} + \underbrace{\int_V \phi_{\text{viscous}}\,dV}_{\substack{\text{Input energy from}\\ \text{friction with surroundings}}} \tag{8}$$

$$\overbrace{\frac{\partial}{\partial t}\left[\rho\left(u + \frac{v^2}{2} + gH\right)\right]}^{\text{Change in energy}} + \overbrace{\nabla\cdot\left[\rho\left(u + \frac{v^2}{2} + gH\right)\mathbf{v}\right]}^{\text{Energy outflow}} \qquad \textbf{Energy equation (differential form)}$$

$$= \underbrace{\dot{q}_{\text{input}}}_{\substack{\text{Input heat}\\ \text{energy}}} + \underbrace{\dot{w}_{\text{input}}}_{\substack{\text{Input work}\\ \text{energy}}} - \underbrace{\nabla\cdot(p\mathbf{v})}_{\substack{\text{Output work energy}\\ \text{by expanding pressure}}} + \underbrace{\phi_{\text{viscous}}}_{\substack{\text{Input energy from}\\ \text{friction with surroundings}}} \tag{9}$$

Section 2 will discuss viscous friction and Section 3.1 will discuss the heat and work energy terms.

1.4 Bernoulli Equation

Another favorite equation of fluid mechanicists is the **Bernoulli equation**:

$$\overbrace{\frac{1}{2}\rho v^2}^{\substack{\text{Kinetic energy}\\ \text{per volume}}} + \overbrace{\rho g H}^{\substack{\text{Gravitational}\\ \text{potential energy}\\ \text{per volume}}} + \overbrace{p}^{\substack{\text{Pressure}\\ \text{potential energy}\\ \text{per volume}}} = \overbrace{\text{constant (along a streamline)}}^{\substack{\text{Total energy}\\ \text{per volume}}} \tag{10}$$

in which H is the relative height of the fluid at a given point and a streamline is ones of the paths followed by particles in a fluid. Different streamlines may follow different paths (for example higher or lower), but as long as fluid particles keep following the same particular streamline, their energy on the right side of Eq. (10) is constant.

The Bernoulli equation is not a new and independent equation, but simply restates some of the principles of the equations for conservation of energy and momentum. There are at least three different ways to arrive at the Bernoulli equation:

1. It is simply a statement of the conservation of energy, expressing the total energy as the sum of different kinds of energy. If fluid following a streamline loses one type of energy (e.g., gravitational potential energy), it must gain more of another type (e.g., kinetic energy) to keep its total energy constant.
2. The Bernoulli equation may be derived from the more general Eq. (9) for energy conservation by neglecting time variation ($\partial/\partial t = 0$), thermal energy ($u = 0$), and input energies ($\dot{q}_{\text{input}} = \dot{w}_{\text{input}} = \phi_{\text{viscous}} = 0$), and integrating what is left to remove the $\nabla \cdot \mathbf{v}$.
3. The Bernoulli equation may be derived by simplifying and integrating Eq. (5) for momentum conservation (taking a sum of forces per volume and integrating them over distance yields a sum of energies per volume), as will be shown in Section 1.5.

Based on those connections to the more general equations for energy and momentum conservation, note that the Bernoulli equation does not account for and hence is invalid in the presence of:

- Time variation (the flow must be steady and constant).
- Compressibility (the fluid must be incompressible).
- Viscosity (the fluid must be inviscid) and friction between a fluid and its surroundings caused by that viscosity. A simple way to account for viscosity is to specify that frictional losses (say after passing through a certain length of pipe) reduce the total energy density (or from the Bernoulli equation, equivalently the pressure or corresponding gravitational height or **head**) by a certain amount. Frictional losses will actually be calculated in Section 2.2.
- Flow along different streamlines (different streamlines may have different, unrelated total energy constants).
- Pumps, propellers, turbines, or anything else that adds or removes work energy from the flow (thus altering the total energy constant partway along that streamline). The Bernoulli equation can be adapted to include these effects if one specifies how much extra energy density or equivalent pressure or gravitational height/head is added to the fluid flow passing through a pump, propeller, or turbine. An example will be given in Section 1.9 for fluid flow through a helicopter rotor.
- Heat transfer to or from the fluid.

Provided that one remembers those legal disclaimers, provisos, and caveats, the Bernoulli equation is handy for solving a number of fluid mechanics problems, such as those shown in Fig. 1:

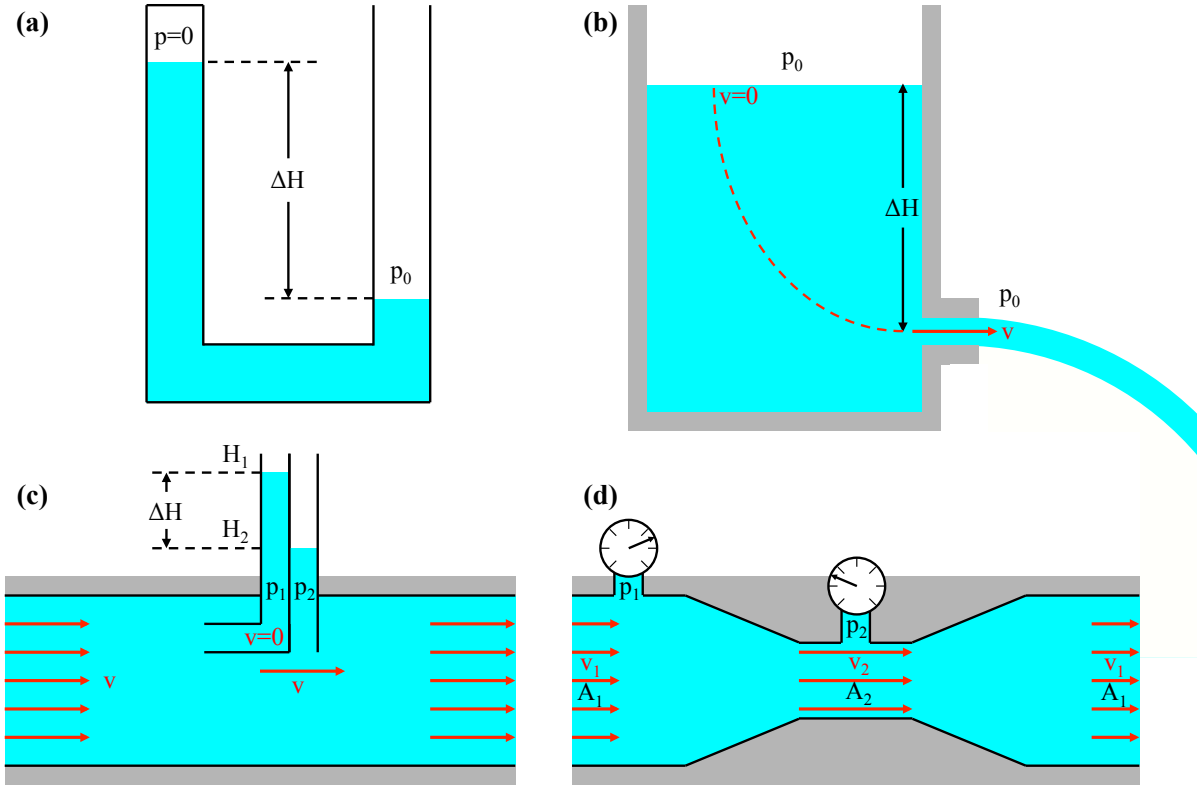

Fig. 1. Examples of applications of the Bernoulli equation. **(a)** Barometer. **(b)** Flow from a spout in a barrel. **(c)** Pitot tube. **(d)** Venturi meter.

(a) Pressure with depth

Neglecting any pressure at the top of a motionless fluid of depth H (in meters), Eq. (10) gives the pressure at the bottom of the fluid as:

$$p = \rho g H \approx \begin{cases} 9800\,H \text{ Pa} \approx 0.0967\,H \text{ Atm} & \text{for fresh water} \\ 10060\,H \text{ Pa} \approx 0.0993\,H \text{ Atm} & \text{for salt water} \\ 132,000\,H \text{ Pa} \approx 1.31\,H \text{ Atm} & \text{for mercury} \end{cases} \tag{11}$$

using the earth's surface gravitational acceleration $g \approx 9.807$ m/sec^2, average densities of 1000 kg/m^3 for fresh water, 1027 kg/m^3 for salt water in the ocean, and 13,500 kg/m^3 for mercury, and the earth's sea-level atmospheric pressure $p_0 = 1.013 \times 10^5$ Pa.

For example, Eq. (11) shows that at the deepest part (10,900 m) of the ocean, the Challenger Deep, the pressure is approximately 1080 times the pressure of the atmosphere.

Equation (11) also shows that in a **barometer** [Fig. 1(a)], sea-level atmospheric pressure p_0 is sufficient to support a $\Delta H = 760$ mm column of mercury if there is a vacuum ($p = 0$) above the mercury. (Actually the mercury vapor pressure above the liquid mercury is not zero, but is far smaller than atmospheric pressure and thus can be neglected.) A barometer, which compares atmospheric and vacuum pressures, is just one example of the more general class of **manometers**, configurations that use the relative heights of liquids in tubes to compare two pressures.

(b) Flow from a spout in a barrel

Consider a streamline that connects water at the top of a barrel to water flowing from a spout near the bottom of the barrel [Fig. 1(b)]. At both ends of the streamline, the water is exposed to atmospheric pressure p_0 and thus must have the same pressure, which may be neglected. At the top, the water is essentially motionless ($v = 0$) but has a gravitational potential energy density $\rho g \Delta H$ relative to the level of the spout. At the spout, the flow has zero gravitational potential energy but a kinetic energy density of $\rho v^2/2$. Equating the energy densities, the flow velocity is:

$$v \;=\; \sqrt{2\,g\,\Delta H} \tag{12}$$

Note that Eq. (12) is simply the usual velocity of a mass that has fallen from a height ΔH. The same principle applies to flow velocities from faucets on different floors of a building when the water is gravity-fed from a water tower at a certain height or pumped up to a certain pressure.

Assuming that the barrel drains slowly enough that Eq. (12) applies at all times, one can calculate the time Δt required to completely drain the barrel. If the surface of the water has cross-sectional area $A_{\rm barrel}$ and falls at a rate $d(\Delta H)/dt$ and the spout has area $A_{\rm spout}$ and flow velocity v from Eq. (12) , the continuity Eq. (1) requires that $\rho A_{\rm barrel} d(\Delta H)/dt = \rho A_{\rm spout} v$, or

$$\frac{d(\Delta H)}{dt} \;=\; \frac{A_{\rm spout}}{A_{\rm barrel}}\,v \;=\; \frac{A_{\rm spout}}{A_{\rm barrel}}\,\sqrt{2\,g\,\Delta H} \tag{13}$$

Separating the variables $d(\Delta H)$ and dt in Eq. (13) and integrating, the time to drain the barrel is

$$\Delta t \;=\; \frac{A_{\rm barrel}}{A_{\rm spout}}\,\sqrt{\frac{2\,\Delta H}{g}} \tag{14}$$

(c) Pitot tube

If a fluid is flowing steadily ($\partial/\partial t = 0$) at velocity v and two tubes (collectively called a **Pitot tube**) are inserted into the flow [Fig. 1(c)], one of which collects fluid and brings it to a stop and the other of which does not impede the fluid's velocity, the fluid velocity may be determined by using sensors to measure the pressure difference $\Delta p = p_1 - p_2$ between the two tubes, or alternatively the difference in fluid height $\Delta H = H_1 - H_2$ in a manometer configuration [Fig. 1(c)]. The difference in fluid kinetic energy density $\rho v^2/2$ is converted into a difference in pressure potential energy density Δp or a difference in gravitational potential energy density $\rho g \Delta H$, so the velocity is

$$v \;=\; \sqrt{\frac{2\,\Delta p}{\rho}} \;=\; \sqrt{2\,g\,\Delta H} \tag{15}$$

(d) Venturi meter

If fluid is flowing steadily ($\partial/\partial t = 0$) at velocity v_1 through a pipe of cross-sectional area A_1 and is forced to pass through a region of smaller area A_2 [Fig. 1(d)], the flow will accelerate to a higher velocity v_2 by the continuity Eq. (1), $\rho v_1 A_1 = \rho v_2 A_2$. One can determine the unconstricted flow velocity and mass flow rate using such a **Venturi meter** by measuring the fluid pressures p_1 before and p_2 at the constriction and using the Bernoulli Eq. (10), $\rho v_1^2/2 + p_1 = \rho v_2^2/2 + p_2$. Combining the continuity and Bernoulli equations, the unconstricted velocity v_1 and mass flow rate $\dot{m}$ are:

$$v_1 \;=\; \sqrt{\frac{2(p_1 - p_2)}{\rho(A_1^2/A_2^2 - 1)}} \tag{16}$$

$$\dot{m} \;=\; \rho v_1 A_1 \;=\; A_1\sqrt{\frac{2\rho(p_1 - p_2)}{(A_1^2/A_2^2 - 1)}} \tag{17}$$

1.5 Potential Flow

Potential flow is a mathematical method of defining the local velocity components of a fluid as derivatives of a higher function, which can make it easier to solve certain fluid mechanics problems. Using $(\mathbf{v}\cdot\nabla)\mathbf{v} = \nabla(v^2/2) - \mathbf{v}\times(\nabla\times\mathbf{v})$, Eq. (5) for conservation of momentum becomes

$$\rho\frac{\partial\mathbf{v}}{\partial t} \;+\; \rho\nabla\left(\frac{v^2}{2}\right) \;-\; \rho\mathbf{v}\times(\nabla\times\mathbf{v}) \;=\; \rho\mathbf{g} \;-\; \nabla p \;+\; \mathbf{F}_{\text{viscous}} \tag{18}$$

The third term in Eq. (18) involves the **vorticity**, which is twice the local angular fluid velocity:

$$\omega \;=\; \nabla\times\mathbf{v} \qquad\qquad \textbf{Vorticity} \tag{19}$$

If fluid flow is incompressible (ρ = constant), inviscid ($\mathbf{F}_{\text{viscous}} = 0$), steady-state ($\partial/\partial t = 0$), and **irrotational** ($\omega = \nabla\times\mathbf{v} = 0$), Eq. (18) can be integrated along a streamline to obtain the Bernoulli Eq. (10), and the fluid velocity components can be expressed as derivatives of a higher function. One suitable higher function is the velocity potential ϕ, defined such that fluid always flows from regions of lower potential to regions of higher potential. Except for the fluid mechanics convention of omitting a minus sign, that is similar to charged particles moving from regions of higher to lower electric potential energy, or particles diffusing from regions of higher to lower concentrations. An alternative higher function is the stream function ψ, defined to be constant along streamlines of fluid motion. Fluid always moves directly along lines of constant ψ and directly across lines of constant ϕ, so lines of constant ϕ and ψ are always perpendicular to each other. For two-dimensional flows (constant in the third dimension) the velocity components may be found from the velocity potential or stream function in either rectangular or polar coordinates:

$$v_x \;=\; \frac{\partial\phi}{\partial x} \;=\; \frac{\partial\psi}{\partial y} \quad\text{and}\quad v_y \;=\; \frac{\partial\phi}{\partial y} \;=\; -\frac{\partial\psi}{\partial x}\,, \quad\text{or} \tag{20}$$

$$v_r \;=\; \frac{\partial\phi}{\partial r} \;=\; \frac{1}{r}\,\frac{\partial\psi}{\partial\theta} \quad\text{and}\quad v_\theta \;=\; \frac{1}{r}\,\frac{\partial\phi}{\partial\theta} \;=\; -\frac{\partial\psi}{\partial r} \tag{21}$$

Using Eq. (20), lines of constant velocity potential ϕ obey:

$$\begin{aligned} 0 \;&=\; d\phi \;=\; \frac{\partial\phi}{\partial x}\,dx \;+\; \frac{\partial\phi}{\partial y}\,dy \;=\; v_x\,dx \;+\; v_y\,dy \\ \Longrightarrow\quad \left(\frac{dy}{dx}\right)_{\phi=\text{constant}} \;&=\; -\,\frac{v_x}{v_y} \end{aligned} \tag{22}$$

Likewise, using Eq. (20), lines of constant stream function ψ obey:

$$\begin{aligned} 0 \;&=\; d\psi \;=\; \frac{\partial\psi}{\partial x}\,dx \;+\; \frac{\partial\psi}{\partial y}\,dy \;=\; -v_y\,dx \;+\; v_x\,dy \\ \Longrightarrow\quad \left(\frac{dy}{dx}\right)_{\psi=\text{constant}} \;&=\; \frac{v_y}{v_x} \;=\; -\,\frac{1}{(dy/dx)_{\phi=\text{constant}}} \end{aligned} \tag{23}$$

As expected from the definitions of the velocity potential and stream function, Eq. (23) shows that lines of constant ψ are indeed perpendicular to lines of constant ϕ.

Applying the incompressible continuity Eq. (4) to $\mathbf{v} = \nabla\phi$ shows that the velocity potential satisfies Laplace's equation. Similarly, applying the condition for irrotationality to the stream function shows that the stream function also satisfies Laplace's equation:

$$\nabla\cdot\mathbf{v} \;=\; \nabla\cdot(\nabla\phi) \;=\; 0 \qquad\Longrightarrow\qquad \nabla^2\phi \;=\; 0 \tag{24}$$

$$\nabla\times\mathbf{v} \;=\; -\hat{\mathbf{z}}\nabla^2\psi \;=\; 0 \qquad\Longrightarrow\qquad \nabla^2\psi \;=\; 0 \tag{25}$$

Laplace's equation arises in many different fields and has well-known solutions, as discussed in *Applied Mathematics* 5.7. Some common situations and solutions for potential flow are:

(a) Uniform flow at velocity v_∞ in the x direction [as shown in Fig. 2(a)], which has the following velocity potential, stream function, and velocity components:

$$\phi = v_\infty x = v_\infty r\cos\theta \qquad \text{or} \qquad \psi = v_\infty y = v_\infty r\sin\theta \tag{26}$$

$$v_x = v_\infty \qquad \text{and} \qquad v_y = 0 \tag{27}$$

$$v_r = v_\infty\cos\theta \qquad \text{and} \qquad v_\theta = -v_\infty\sin\theta \tag{28}$$

(b) Line source at $x = y = 0$, of infinite extent in the z direction [Fig. 2(b)], producing Λ volume per z length per second of fluid (or a line sink consuming fluid if Λ is negative):

$$\phi = \frac{\Lambda}{2\pi}\ln r \qquad \text{or} \qquad \psi = \frac{\Lambda}{2\pi}\theta \tag{29}$$

$$v_x = \frac{\Lambda}{2\pi}\frac{x}{x^2+y^2} \qquad \text{and} \qquad v_y = \frac{\Lambda}{2\pi}\frac{y}{x^2+y^2} \tag{30}$$

$$v_r = \frac{\Lambda}{2\pi r} \qquad \text{and} \qquad v_\theta = 0 \tag{31}$$

(c) Line vortex centered at $x = y = 0$, as shown in Fig. 2(c). A vortex is like a source with ϕ and ψ switched, since the velocity is purely radial for a source and purely angular for a vortex.

$$\phi = \frac{\Gamma}{2\pi}\theta \qquad \text{or} \qquad \psi = \frac{\Gamma}{2\pi}\ln r \tag{32}$$

$$v_x = -\frac{\Gamma}{2\pi}\frac{y}{x^2+y^2} \qquad \text{and} \qquad v_y = \frac{\Gamma}{2\pi}\frac{x}{x^2+y^2} \tag{33}$$

$$v_r = 0 \qquad \text{and} \qquad v_\theta = -\frac{\Gamma}{2\pi r} \tag{34}$$

(d) Line doublet or combined source and sink centered at $x = y = 0$, as illustrated in Fig. 2(d). Note that the doublet is similar to an electric dipole from *Electromagnetism and Acoustics* ?.?.

$$\phi = \frac{\kappa}{2\pi}\frac{\cos\theta}{r} \qquad \text{or} \qquad \psi = -\frac{\kappa}{2\pi}\frac{\sin\theta}{r} \tag{35}$$

$$v_x = -\frac{\kappa}{2\pi}\frac{x^2-y^2}{(x^2+y^2)^2} \qquad \text{and} \qquad v_y = -\frac{\kappa}{2\pi}\frac{2xy}{(x^2+y^2)^2} \tag{36}$$

$$v_r = -\frac{\kappa}{2\pi}\frac{\cos\theta}{r^2} \qquad \text{and} \qquad v_\theta = -\frac{\kappa}{2\pi}\frac{\sin\theta}{r^2} \tag{37}$$

(e) Flow around a rotating cylinder [Fig. 2(e)] may be regarded as the sum of simpler uniform, doublet, and vortex flows. This is one example of how more complex flow patterns can be constructed from simpler flow solutions. Flow around a rotating cylinder is also related to the much more common case of flow around aircraft wings, as will be discussed in Section 1.8.

$$\phi = (v_\infty r\cos\theta)\left(1+\frac{R^2}{r^2}\right)+\frac{\Gamma}{2\pi}\theta \qquad \text{or} \qquad \psi = (v_\infty r\sin\theta)\left(1-\frac{R^2}{r^2}\right)+\frac{\Gamma}{2\pi}\ln\left(\frac{r}{R}\right) \tag{38}$$

$$v_r = (v_\infty\cos\theta)\left(1-\frac{R^2}{r^2}\right) \qquad \text{and} \qquad v_\theta = -(v_\infty\sin\theta)\left(1+\frac{R^2}{r^2}\right)-\frac{\Gamma}{2\pi r} \tag{39}$$

ϕ can be extended to a third dimension ($v_z = \partial\phi/\partial z$) but only holds for irrotational flows. ψ exists even for rotational flows but cannot be extended to a third dimension, although one can apply it to any two dimensions in any coordinate system (rectangular, cylindrical, or spherical). The flow rate per unit depth between two streamlines is the difference of their stream functions, $q = \psi_2 - \psi_1$. [1]

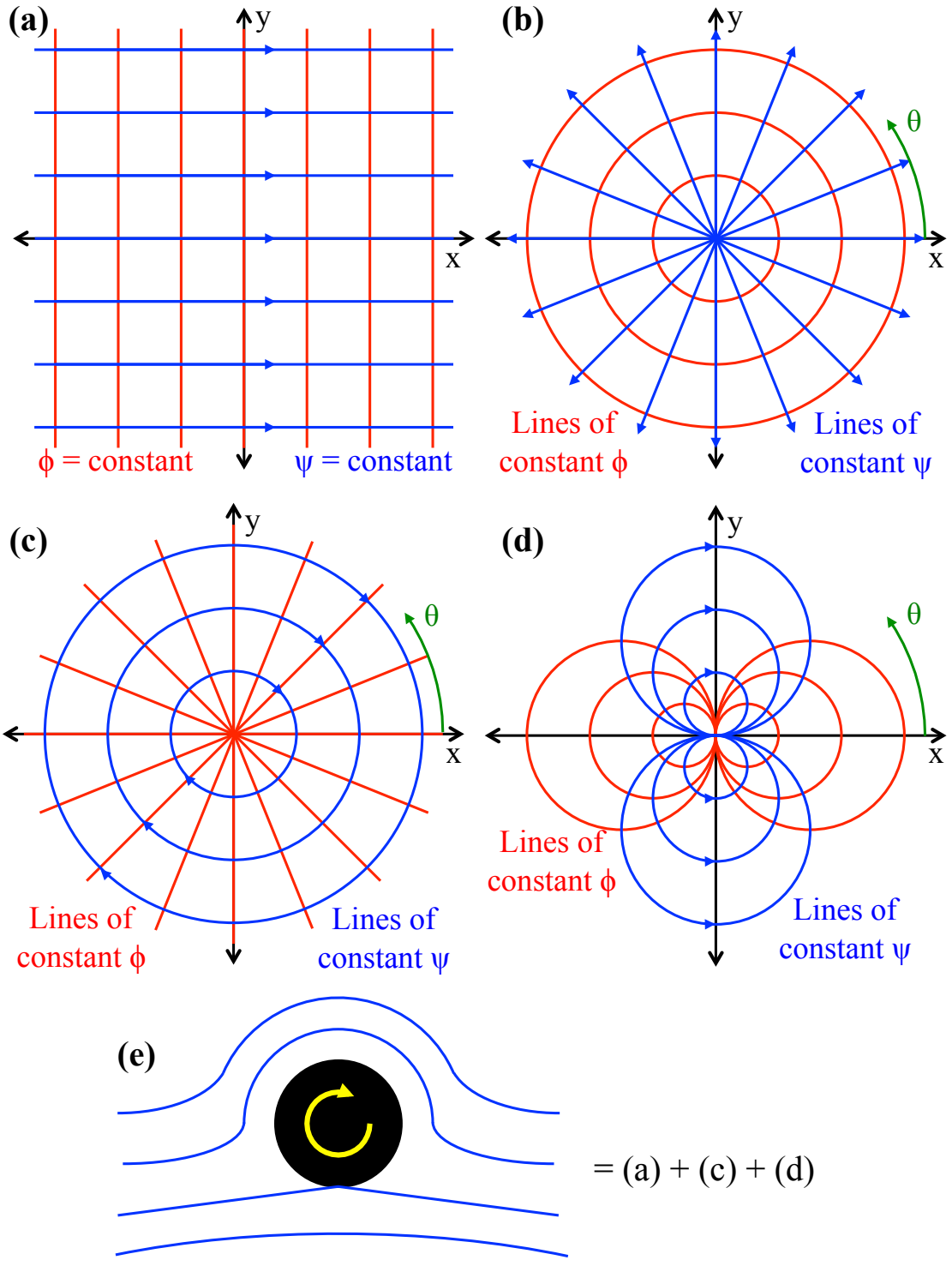

Figure 2. Some simple two-dimensional potential flows. Fluid flows from regions of lower potential ϕ to regions of higher potential, moving along streamlines with constant values of the stream function ψ. **(a)** Uniform flow. **(b)** Line source. (A line sink is identical but with inward flow.) **(c)** Vortex flow. **(d)** Doublet (or combined source and sink) flow. **(e)** Flow around a rotating cylinder may be regarded as the superposition of uniform, vortex, and doublet flows.

1.6 Buoyancy

If an object is immersed in a fluid and there is a downward gravitational force, the fluid will exert an upward **buoyant force** on the object, as illustrated in Fig. 3. Buoyancy is basically the densest material, fluid, or object wanting to be as low in the gravitational field as possible, and therefore trying to hold up everything less dense above itself.

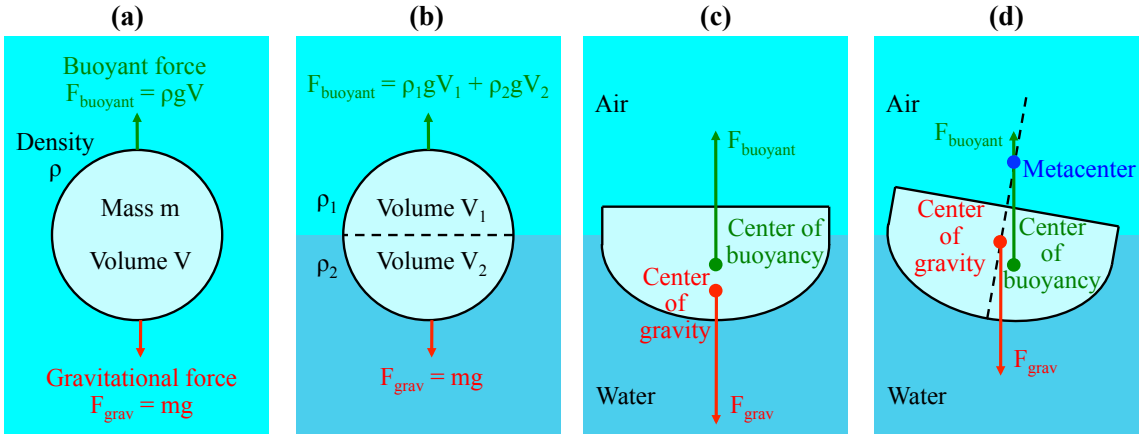

Figure 3. Buoyancy. **(a)** Upward buoyant force and downward gravitational force acting on an object of mass m and volume V immersed in a fluid of density ρ. **(b)** Forces acting on an object floating at the interface between two fluids with densities ρ_1 and ρ_2. **(c)** An object immersed in one fluid or floating at the interface between two fluids is stable (will not tip over) if its center of buoyancy is above its center of gravity. **(d)** An object floating at the interface between two fluids can also be stable if its center of buoyancy is below its center of gravity but the center of buoyancy shifts to the lower side to counteract any tipping motion.

If the other terms in Eq. (5) are neglected, integrating the remaining $\nabla p = \rho g$ over an object of volume V fully immersed in a fluid of density ρ gives the upward buoyant force on the object:

$$F_{\text{buoyant}} \;=\; \rho g V \qquad \textbf{Buoyant force for object in one fluid} \tag{40}$$

Archimedes' principle summarizes Eq. (40) by stating that the buoyant force is equal to the weight of the fluid displaced by the object.

If the object has total mass m, it will also experience a downward gravitational force $F_{\text{grav}} = mg$ [Fig. 3(a)]. Writing the object's average density as $\rho_{\text{object}} = m/V$, the net force on the object is:

$$F_{\text{net}} \;=\; F_{\text{buoyant}} - F_{\text{grav}} \;=\; \left(\rho - \frac{m}{V}\right) gV \;=\; (\rho - \rho_{\text{object}})\, gV \tag{41}$$

In water ($\rho \approx 1000$ kg/m^3), gas bubbles or air-filled floats have negligible density, so from Eq. (41) they experience a large net upward force of $F_{\text{net}} \approx 9800$ N per m^3 of gas volume.

From the ideal gas law (to be reviewed in Section 3.1), two gases at the same temperature and pressure have densities proportional to their molecular weights. Therefore, in air ($\rho \approx 1.225$ kg/m^3 and average molecular weight $M.W._{\text{air}} \approx 29$), a balloon of gas with molecular weight $M.W._{\text{gas}}$ experiences a net upward force (neglecting the mass of the balloon itself or of any cargo):

$$F_{\text{net}} \;\approx\; 12.0\left(1 - \frac{M.W._{\text{gas}}}{M.W._{\text{air}}}\right) \frac{\text{N}}{\text{m}^3} \;\approx\; 12.0\left(1 - \frac{M.W._{\text{gas}}}{29}\right) \frac{\text{N}}{\text{m}^3} \tag{42}$$

Equation (42) shows that hydrogen (H_2, $M.W._{\text{gas}} \approx 2$) balloons experience a net upward force $F_{\text{net}} \approx 11.2$ N per m^3 of gas volume, and helium (He, $M.W._{\text{gas}} \approx 4$) balloons experience a net upward force $F_{\text{net}} \approx 10.4$ N per m^3 of gas volume.

Also from the ideal gas law, two gases of the same molecular weight and pressure have densities inversely proportional to their temperatures above absolute zero. Therefore, the net upward force on a hot-air balloon surrounded by colder atmospheric air (again neglecting the mass of the balloon itself or of any cargo) is:

$$F_{\text{net}} \approx 12.0 \left(1 - \frac{T_{\text{atmosphere}}}{T_{\text{hot air}}}\right) \frac{\text{N}}{\text{m}^3} \tag{43}$$

For atmospheric air at the freezing temperature ($T_{\text{atmosphere}} = 273^o$K) and hot air at the boiling temperature of water ($T_{\text{hot air}} = 373^o$K), Eq. (43) shows that a hot air balloon experiences a net upward force $F_{\text{net}} \approx 3.2$ N per m^3 of hot air volume.

Buoyancy also applies to fluids themselves. If two fluids do not readily mix and have different densities, buoyancy makes the less dense fluid float on top of the denser fluid, just as oil floats on water, water floats on corn syrup, or the atmosphere floats on the ocean.

If an object is floating at the interface between two fluids with densities ρ_1 and ρ_2, displacing a volume V_1 from the first fluid and volume V_2 from the second fluid [Fig. 3(b)], the upward buoyant force exerted on the object by the fluids is:

$$F_{\text{buoyant}} = \rho_1 g V_1 + \rho_2 g V_2 \qquad \textbf{Buoyant force for object in two fluids} \tag{44}$$

If an object is floating at the interface between two fluids and one fluid is much less dense than the other (e.g., air is $> 800\times$ less dense than water), the buoyancy contribution from the less dense fluid may be neglected in Eq. (44). Although the steel of a ship's hull would readily sink, it encloses air-filled spaces that displace water volume, and so the average density of the ship is less than water. Submarines vary the amount of water or air in their ballast tanks to adjust their buoyancy.

Just as gravitational and inertial forces may be regarded as acting at the center of mass or center of gravity of an object (*Classical Mechanics* ?.?), the buoyant force may be regarded as acting at an object's center of buoyancy, which is the point that would have been the center of gravity of all the fluid that the object displaced.

As shown in Fig. 3(c), an object that is completely immersed in one fluid, or an object that is floating at the interface between two fluids, is stable (will not tip over) if its center of buoyancy is above its center of gravity. That way the buoyant force tries to pull the upper part of the object upward and the gravitational force tries to pull the lower part of the object downward, so the object does not want to flip over.

As illustrated in Fig. 3(d), an object floating at the interface between two fluids can also be stable if its center of buoyancy is below its center of gravity but the center of buoyancy shifts to the lower side to counteract any tipping motion. (If the center of buoyancy shifts toward the higher side, the object just keeps tipping until you get a bath.) A more complicated way to state this principle is that the **metacenter**, the point where the vertical buoyancy force and the centerline of the tilting object intersect, must be above the center of gravity for the object to be stable, as shown in Fig. 3(d). If the object is unstable and its center of buoyancy shifts toward the higher side, the metacenter where the vertical line of buoyant force and the tipping centerline of the object intersect will be below the object's center of gravity. This method of achieving stability does not apply to an object that is completely immersed in a single fluid, since the center of buoyancy would not shift its relative location within the tipping object.

1.7 Aerodynamic Drag

If an object moves with velocity v through a fluid, or equivalently if a fluid moves with velocity v past a stationary object (Fig. 4), the fluid creates a **drag force** as it collides with the object.

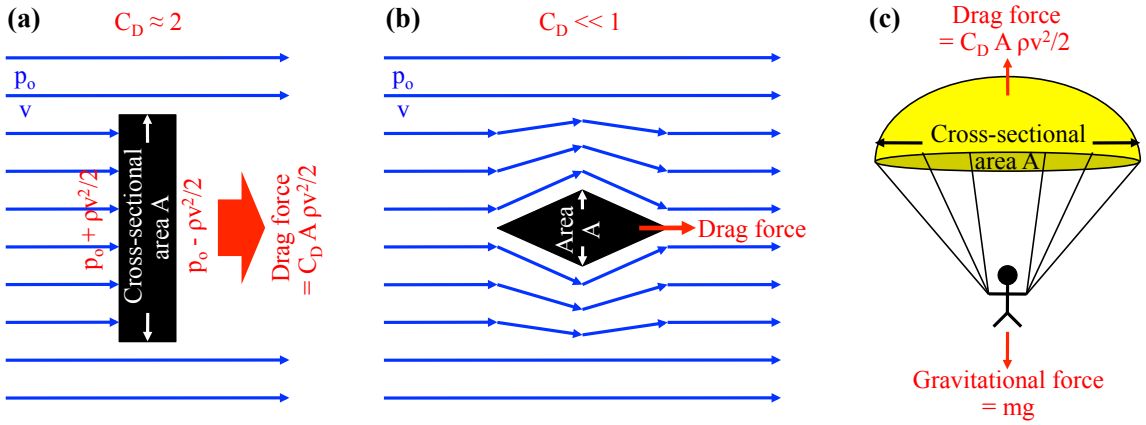

Figure 4. Aerodynamic drag. **(a)** An object that is broad and flat in front and in back collides with the flow to create a large overpressure in front and a large underpressure in back, and thus has a drag coefficient approaching 2. **(b)** An object that is very streamlined in front and in back deflects but does not greatly slow the flow, so its drag coefficient is relatively small. **(c)** The upward drag force on a parachute helps to counteract the downward gravitational force.

For simplicity, consider a very broad object that is flat on front and on back [Fig. 4(a)]. If the fluid's ambient pressure is p_o and its kinetic energy per volume is $\rho v^2/2$, the collision with the flat front of the object stops the fluid and converts all of its kinetic energy into extra pressure energy, creating a pressure of $p_o + \rho v^2/2$ on the front surface. Likewise there is a corresponding pressure of $p_o - \rho v^2/2$ on the flat rear surface of the object (the object pulls a partial vacuum in its wake), since the fluid has trouble filling in behind the object. The difference between the front overpressure and the rear underpressure on the object produces a net rearward drag force D:

$$D = \frac{1}{2} C_D A \rho v^2 \tag{45}$$

in which A is the cross-sectional area of the object as seen by the oncoming flow. If the object is very broad, the overpressure across the front and the underpressure across the rear are uniform, and fluid diversion around the object's edges is minimal, the **drag coefficient** C_D will approach its maximum possible value of 2. In contrast, an object that is very streamlined in front and back deflects but does not greatly slow the fluid flow [Fig. 4(b)], so there is little difference between the front overpressure and the rear underpressure, and the object's drag coefficient will be $C_D \ll 1$.

The drag force in Eq. (45) varies like v^2, so it rapidly increases as the velocity increases. Minimizing the cross-sectional area of an object helps minimize its drag. The drag coefficient C_D depends on the object's shape and its angle of attack (tilt to one side relative to the oncoming flow). In addition to pressure as considered here, drag can be created by friction of the fluid sticking to the sides of the object (as will be seen in Section 2.4) and by shock waves if the object is moving faster than the speed of sound (Sections 3.8-3.10); these added effects can make C_D vary with the velocity.

In the absence of forces other than gravity, a falling object will keep accelerating until it hits the ground. However, if the upward drag force D from Eq. (45) is large enough to balance the downward gravitational force mg on an object of mass m under gravitational acceleration g, the object will stop accelerating once its downward speed reaches the **terminal velocity** v_{terminal}:

$$v_{\text{terminal}} = \sqrt{\frac{2mg}{C_D A \rho}} \tag{46}$$

Equivalently, an object must have a cross-sectional area A to reach a given terminal velocity:

$$A = \frac{2mg}{C_D \rho v_{\text{terminal}}^2} \tag{47}$$

Using Eq. (47) for a skydiver [Fig. 4(c)] with a total mass of 100 kg including the parachute, gravitational acceleration $g \approx 9.807$ m/sec^2 near the surface of the earth, drag coefficient $C_D \approx 1$ for a parachute that efficiently creates an overpressure beneath it but negligible underpressure above it (the air fills in smoothly over the canopy), atmospheric pressure $\rho \approx 1.2$ kg/m^3 near the earth's surface, and maximum acceptable terminal velocity of $v_{\text{terminal}} \approx 6$ m/sec (equivalent to an unhindered fall from approximately 2 meters), the parachute must have a deployed cross-sectional area $A \approx 45$ m^2, or a deployed diameter of approximately 7.6 m if it is round.

1.8 Aerodynamic Lift

Aircraft wings are used to generate an upward aerodynamic **lift force** perpendicular to the direction of travel (or direction of incoming flow, if the aircraft is regarded as motionless in moving air) in order to overcome the downward gravitational force and keep the aircraft aloft. As will be described, lift on an aircraft wing can be produced by two independent mechanisms: (1) If the leading edge of the wing is tilted upward, incoming flow will be diverted downward, producing an equal and opposite upward lift force on the wing. (2) If the upper surface of the wing has more curvature than its lower surface, flow will move faster above the wing and hence have lower pressure than flow below the wing, producing a net upward lift force.

An airfoil is a cross-section through an aircraft wing along the direction of incoming flow, as shown in Fig. 5(a). As illustrated in Fig. 5(b), the chord line of length c is a straight line from the leading edge to the trailing edge of an airfoil, and the mean camber line is the halfway point between the upper and lower surfaces of the airfoil. Airfoils or wing shapes are usually designed to be thicker and more rounded on top and thinner and flatter on bottom, so the mean camber line deviates upward from the chord line by an amount called the camber h. The maximum thickness t of the airfoil is usually much less than the chord length c, $t/c \ll 1$; therefore airfoils can typically be treated as fairly thin. Aircraft usually have flaps on the trailing edge of the wing. By aligning the flaps with the rest of the wing or angling them lower or higher, one can adjust the effective camber of the wing and hence its lift and drag properties.

If a surface is inclined at angle of attack α relative to the incoming flow, the higher pressure $p_o + \rho v^2/2$ on the leading surface and lower pressure $p_o - \rho v^2/2$ on the trailing surface produce a net pressure $\Delta p = \rho v^2$ normal to the surface. From the red triangle in Fig. 5(c), a factor of $\sin\alpha$ times this pressure contributes to the drag in the direction of the flow, while a factor of $\cos\alpha$ times this pressure produces lift perpendicular to the flow. Thus the pressure drag and lift forces are

$$L = A_{\text{effective}} \cos\alpha \, \rho v^2 \tag{48}$$

$$D_{\text{pressure}} = A_{\text{effective}} \sin\alpha \, \rho v^2 \tag{49}$$

in which $A_{\text{effective}}$ is the effective cross-sectional area of the surface seen by the oncoming flow.

If the actual area of one side of the surface is A, the area intercepted by the flow is $A \sin\alpha$. However, flow within a region of comparable area ($\sim A \sin\alpha$) above the surface is distorted by the presence of the surface, and likewise flow within a region of comparable area below the surface is also affected. Thus the effective cross-sectional area including both the surface and the regions above and below it is $A_{\text{effective}} \sim 3A \sin\alpha$. Substituting this into Eqs. (48) and (49), the lift and pressure drag are:

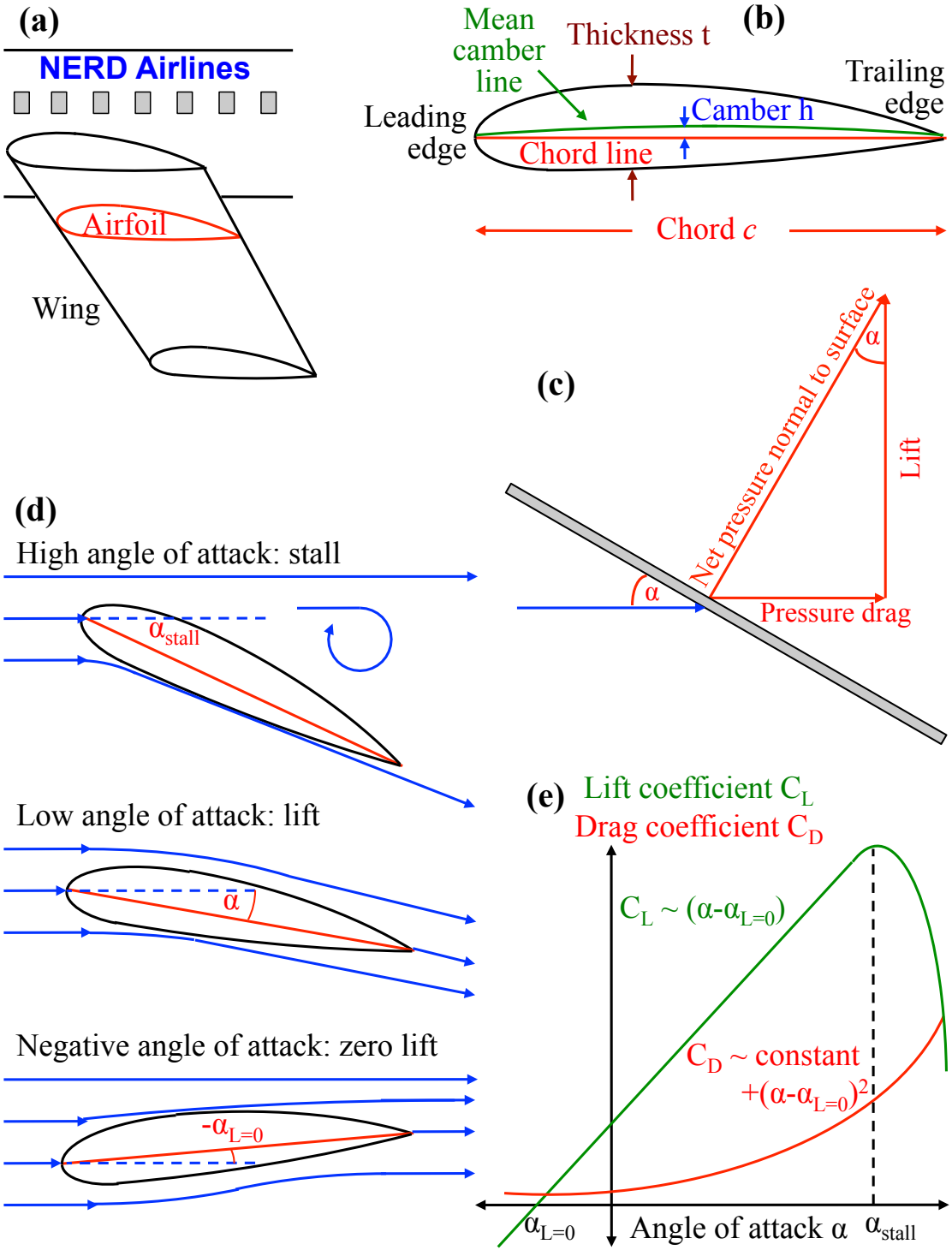

Figure 5. Aerodynamic lift. **(a)** An airfoil is a cross-section through an aircraft wing along the direction of incoming flow. **(b)** Airfoils are usually cambered, with asymmetric upper and lower surfaces. **(c)** For an angle of attack α between a surface and incoming flow, the force normal to the surface may be separated into drag and lift components. **(d)-(e)** A cambered airfoil produces zero lift at a negative angle of attack $\alpha_{L=0}$, linearly increasing lift for increasing angles of attack, and decreasing lift (stalling) above α_{stall}. Its drag is much smaller but increases parabolically.

$$L \approx 3 \sin\alpha \cos\alpha \, A \rho v^2 \approx 3\alpha \, A\rho v^2 \qquad \text{for small } \alpha \tag{50}$$

$$D_{\text{pressure}} \approx 3 \sin^2\alpha \; A \; \rho v^2 \approx 3\alpha^2 A\rho v^2 \qquad \text{for small } \alpha \tag{51}$$

By analogy with Eq. (45), but using A to denote wing surface area and not area perpendicular to the flow, the lift force can be written as:

$$L = \frac{1}{2} C_L \, A \, \rho \, v^2 \tag{52}$$

From Eqs. (50) and (52), the coefficient of lift is $C_L \approx 6\alpha$. Much scarier and more accurate calculations [1, 9] show that

$$C_L \approx 2\pi\alpha \tag{53}$$

Thus our seat-of-the-pants estimate was actually quite good. Even the 2π value will vary a bit depending on the exact airfoil thickness and shape, as found from wind tunnel measurements.

While a flat plate or other symmetrical (equally thick and equally shaped on top and bottom) airfoil generates no lift when $\alpha = 0$ in accordance with Eq. (53), an asymmetric or cambered airfoil does generate lift even at zero angle of attack. If the upper surface of the airfoil is thicker and more curved than the lower surface, as shown in Fig. 5(b), flow above the airfoil will be "squished" to pass through a smaller cross-sectional area than flow below it. Since the density cannot increase for incompressible flow, conservation of mass flow means that air passing above the airfoil must have a higher velocity than air passing below it. By the Bernoulli equation, the pressure exerted on the upper surface by the faster air will be less than the pressure exerted on the lower surface by the slower air, creating a net upward lift force, even when the airfoil is at zero angle of attack. The airfoil must actually be tilted down to a small negative angle of attack before the lift becomes zero, as shown at the bottom of Fig. 5(d). If h is the maximum camber of the airfoil, the zero-lift angle is $\alpha_{L=0} \sim -2h/c \sim -2^o$ to -3^o for most cambered airfoils [1], and the lift coefficient becomes

$$C_L \approx 2\pi(\alpha - \alpha_{L=0}) \tag{54}$$

From Eq. (54), the lift increases linearly with the angle of attack [Fig. 5(e)]. However, for angles of attack $\alpha > \alpha_{\text{stall}}$, the flow separates from the upper rear of the airfoil [Fig. 5(d) top], greatly decreasing the lift. This condition of **stalling** occurs at $\alpha_{\text{stall}} \sim 10 - 15^o$ for typical airfoils. In addition to generating more lift than a flat plate, the shape of asymmetric airfoils reduces flow separation from the upper surface, thereby both increasing α_{stall} and reducing the pressure drag.

Making these same modifications $3 \to \pi$ and $\alpha \to \alpha - \alpha_{L=0}$ to Eq. (51), the pressure drag coefficient per wing surface area A is

$$C_{D\,\text{pressure}} \approx 2\pi(\alpha - \alpha_{L=0})^2 \approx \frac{C_L^2}{2\pi} \tag{55}$$

The total drag is the sum of pressure drag, which we have just calculated, and viscous drag of the flow "sticking" to the surface and producing friction, as will be covered in Section 2.4. For now it suffices to say that this viscous drag component is typically much smaller than the pressure drag component or the lift, and that it is approximately independent of the angle of attack α, provided that $\alpha < \alpha_{\text{stall}}$ so the flow does not separate from the airfoil. Thus the total drag is parabolic with respect to $\alpha - \alpha_{L=0}$ as shown in Fig. 5(e):

$$D \approx D_{\text{viscous}} + D_{\text{pressure}} \approx D_{\text{viscous}} + \pi(\alpha - \alpha_{L=0})^2 A\rho v^2 \tag{56}$$

If the viscous drag component is neglected, the lift-to-drag ratio from the triangle in Fig. 5(c) is

$$\frac{L}{D} \;=\; \cot\alpha \;\approx\; \frac{1}{\alpha} \tag{57}$$

More detailed calculations [1, 9] show that for any thin airfoil, the center of pressure is located along the chord a distance of $c/4$ behind the leading edge. Thus for purposes of balancing the aircraft, the lift force supporting the wing and aircraft may be assumed to be centered at that location.

By focusing on plane flow around an airfoil thus far, we have essentially assumed that the wings are infinitely long. Real aircraft wings will have a finite aspect ratio:

$$(A.R.) \;=\; \frac{(\text{wingspan } b)^2}{\text{wing area } A} \;=\; \frac{\text{wingspan } b}{\text{average chord } c_{\text{average}}} \tag{58}$$

By convention, the aspect ratio generally assumes that the aircraft body between the two wings is negligibly small or merely serves as part of the wings. Since the wingspan b includes both wings, the aspect ratio is 2 for square wings, larger for longer wings, and infinite for infinitely long wings.

For infinitely long wings, incoming flow can only travel around the leading edge of the wing to pass below or above the wing, producing high pressure below and low pressure above the wing. However, for finite wings, some of the flow can "leak" around the wingtips to escape from the high pressure region to the low pressure region [Fig. 6(a)], thereby reducing the net pressure difference and the effective lift of the wing. The flow around the wingtips also creates vortices that trail after the aircraft and can create turbulence for other aircraft that follow too closely. For an aspect ratio of 2, the wings are square, with wingtips as long as the leading edges. Thus as much of the flow can leak around the wingtips as passes around the leading edge, cutting the effective lift in half. For lower aspect ratios, the lift reduction will be even more severe, and for an infinite aspect ratio, there is no lift reduction. To account for this effect, the coefficient of lift from Eq. (54) is modified:

$$C_L \;\approx\; \frac{2\pi}{1 + 2/(A.R.)}\,(\alpha - \alpha_{L=0}) \tag{59}$$

By analogy with Eq. (55) for infinite wings, detailed calculations [1, 9] show that the pressure drag coefficient for finite wings is:

$$C_{D\,\text{pressure}} \;\approx\; \frac{C_L^2}{\pi\;(A.R.)} \tag{60}$$

On some aircraft, the wingtips bend upward to form fins or winglets to minimize these end effects.

More detailed calculations of lift [1, 9] use two mathematical techniques that will only be mentioned here. As illustrated in Fig. 6(b), flow around an airfoil may be viewed as a superposition of uniform flow at velocity v_∞ and pure **circulation** Γ, resulting in net flow with a higher velocity above and lower velocity below the airfoil. In a sense, then, the lift is due solely to the circulation:

$$\frac{L}{b} \;=\; \rho v_\infty \Gamma \qquad \textbf{Kutta-Joukowsky theorem} \tag{61}$$

$$\Gamma \;=\; \oint_C \mathbf{v}\cdot d\mathbf{l} \qquad \textbf{Circulation} \tag{62}$$

where L/b is the lift per unit wingspan, and Γ is evaluated along any closed contour C around the airfoil by integrating the local fluid velocity component that is parallel to the contour. An important criterion in determining Γ is the **Kutta condition** that the flows rejoining from above and below the airfoil must have the same velocities at the trailing edge of the airfoil.

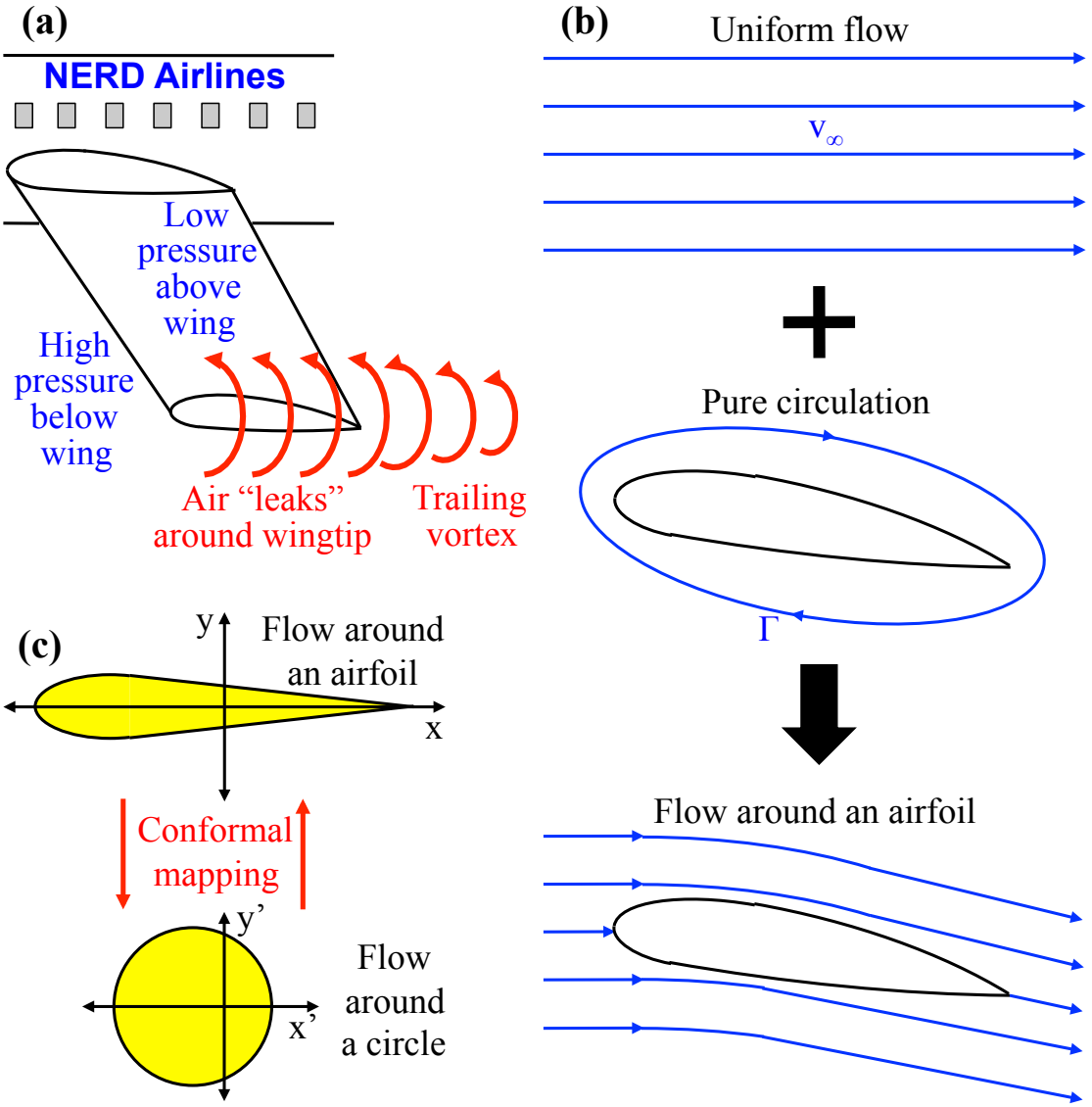

Figure 6. More detailed analysis of aerodynamic lift. **(a)** For a wing of finite length, flow can leak around the wingtip from the high-pressure region below the wing to the low-pressure region above the wing, reducing the lift of the wing and creating a vortex that trails behind the wing. **(b)** Flow around an airfoil may be regarded as the sum of uniform flow and pure circulation. Lift is due entirely to the circulation. **(c)** Conformal mapping uses mathematical coordinate transformations to relate flow around a complex airfoil shape to much more easily analyzed flow around a circle.

The second technique, **conformal mapping**, is a method of using mathematical transformations to redefine the real coordinates x and y in terms of highly distorted coordinates x' and y', as explained in *Applied Mathematics* 5.7 and illustrated in Fig. 6(c). This can allow the flow around a complex airfoil shape to be found from the flow around a much simpler shape, such as the rotating cylinder from Fig. 2(e). Using conformal mapping to calculate the circulation can be particularly powerful, provided one is willing to slog through several pages of contour integrals to get an answer.

The same principles that have been developed for aircraft wings can be applied to sails on boats. A sail is just a vertical airfoil that creates drag parallel to the wind direction and lift perpendicular to the wind direction, and that can be controlled by adjusting its shape and angle of attack.

1.9 Helicopters

Helicopters must be treated differently than other aircraft [15]. In particular, a helicopter's main rotor may be regarded as a rotating wing that is always moving forward and thus can generate lift even if the helicopter itself is motionless. As will be shown, this confers on helicopters both their advantages, such as their ability to hover or even fly backwards, and their disadvantages, such as their high fuel consumption and limited speed relative to fixed-wing aircraft.

Figure 7 shows the airflow through a helicopter rotor. For simplicity, the effects of individual blades can be ignored; generally the actual blades occupy $\sim 1/10$ of the rotor area A. Air far above the rotor is at the ambient atmospheric pressure p_0 and has downward velocity v_0, which is zero when the helicopter is hovering (not ascending or descending). All of the velocities involved are generally slow enough compared to the speed of sound that the air density ρ can be treated as a constant. The airflow speeds up by an amount v_i by the time it is sucked into the rotor; since ρ is constant, by conservation of mass the cross-sectional area of the airflow must therefore contract as it approaches the rotor (Fig. 7). Air passes through plane 1 just above and plane 2 just below the rotor. The cross-sectional area for each plane is $A_1 \approx A_2 \approx A$, so by conservation of mass the downward air velocities above and below the rotor are the same, $v_1 \approx v_2 \approx v_i + v_0$.

The rotor imparts an extra pressure $\Delta p = p_2 - p_1$ to the air passing through it. As the air pressure drops back to the ambient pressure p_0 at plane 3, the energy of that extra pressure is converted to a net increase v_w in airflow velocity, so $v_3 = v_w + v_0$. Specifically, the Bernoulli Eq. (10) gives:

$$p_2 - p_1 \;=\; \frac{1}{2}\rho(v_w + v_0)^2 - \frac{1}{2}\rho v_0^2 \;=\; \frac{1}{2}\rho v_w(v_w + 2v_0) \tag{63}$$

The helicopter's thrust T can be calculated from the rotor's area and pressure difference:

$$T \;=\; (p_2 - p_1)A \;=\; \frac{1}{2}\rho v_w(v_w + 2v_0)A \tag{64}$$

Alternatively, one can write the thrust in terms of the momentum change for the air that has passed through the rotor, using the mass flow rate $\dot{m} = \rho A(v_i + v_0)$ through the rotor:

$$T \;=\; \dot{m}(v_3 - v_0) \;=\; \dot{m}v_w \;=\; \rho A(v_i + v_0)v_w \tag{65}$$

By equating expressions (64) and (65) for the thrust, one finds

$$v_w \;=\; 2v_i \tag{66}$$

From Eq. (66) and mass conservation, the wake at plane 3 thus contracts to

$$A_3 \;=\; \frac{v_i + v_0}{2v_i + v_0}\,A \;=\; \frac{1}{2}\,A \;\text{ if }\; v_0 = 0 \tag{67}$$

The airflow velocity induced by the rotor is proportional to the velocity of the rotor tip, $v_i = v_{\text{tip}}\lambda_h$, where the constant of proportionality λ_h is called the induced inflow ratio. As the speed of sound $v_s \approx 1200$ km/hr (at sea level) is approached, very large amounts of power are required to overcome compressibility effects (Section 3.8). Therefore, it is preferable to limit the tip speed to $v_{\text{tip}} \sim v_s/2 \approx 600$ km/hr to minimize such effects.

Inserting Eq. (66) into Eq. (65) shows that the thrust is proportional to v_i^2 (or v_{tip}^2) if $v_0 = 0$:

$$T \;=\; 2\dot{m}v_i \;=\; 2\rho A v_i(v_i + v_0) \tag{68}$$

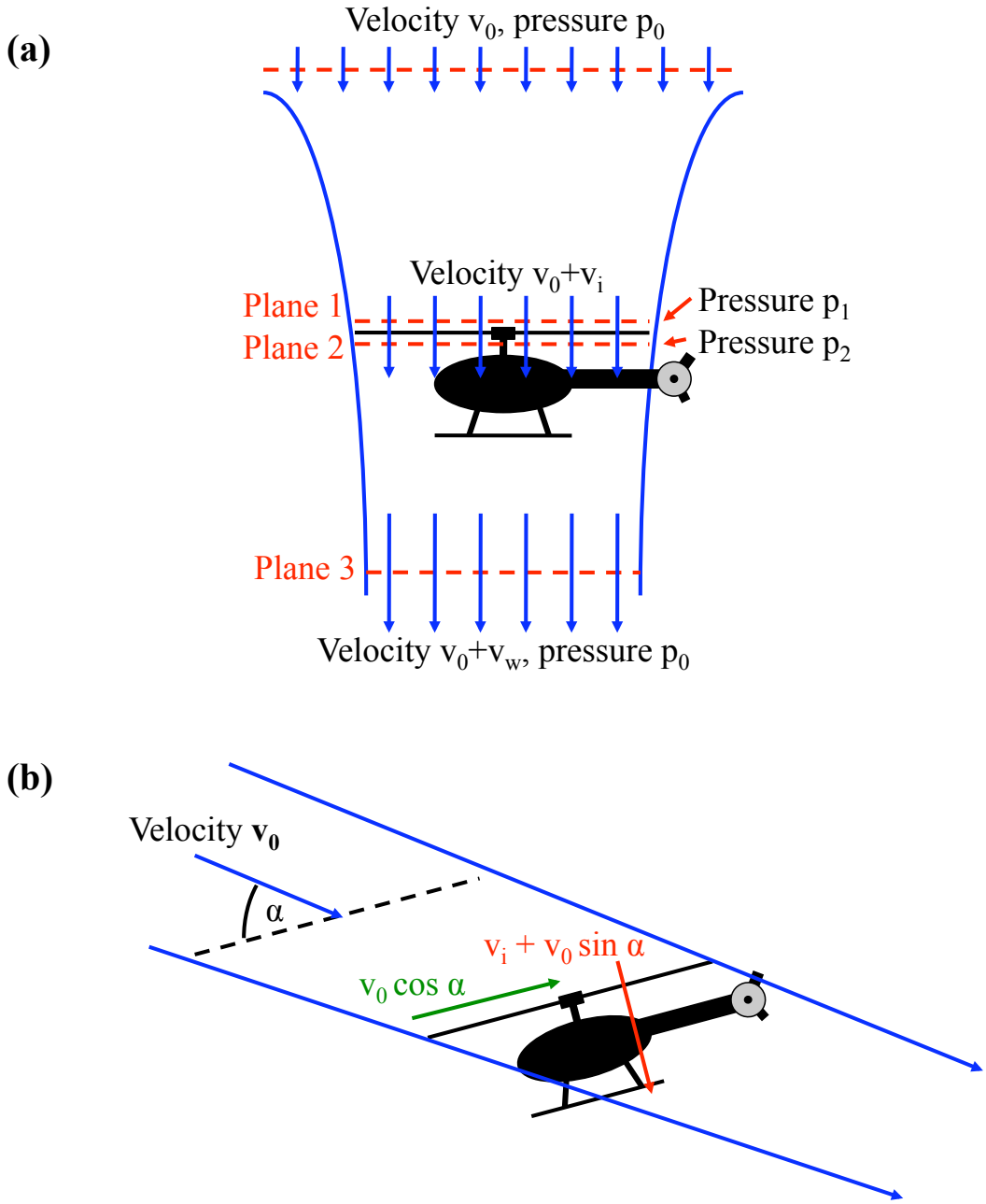

Figure 7. Airflow through a helicopter rotor. **(a)** Helicopter in vertical flight. **(b)** Helicopter in forward flight.

Likewise, the required power varies with the cube of the velocity, $P \propto v_i^3 \propto v_{\text{tip}}^3$, if $v_0 = 0$:

$$P \;=\; T(v_i + v_0) \;=\; 2\rho A v_i (v_i + v_0)^2 \tag{69}$$

The required power per given thrust is:

$$\frac{P}{T} \;=\; v_i + v_0 \;=\; \sqrt{\frac{T}{2\rho A}} \;\text{ if }\; v_0 = 0 \tag{70}$$

The thrust per rotor area or pressure difference $T/A = \Delta p$ is called the **disk loading**. Equation (70) shows that a lower disk loading (hence a larger rotor and lower v_1 and $v_{\rm tip}$) is more power efficient. A typical helicopter with thrust ~ 30 kN (to support a mass of 3000 kg) and rotor radius $R \sim 5$ m has $T/A = T/(\pi R^2) \sim 400$ Pa; disk loadings are generally $\sim 250 - 500$ Pa. Using Eq. (70) with a sea-level atmospheric density $\rho \approx 1.225$ kg/m^3, the power per thrust is thus $P/T \sim 10 - 15$ W/N. The actual power required by a helicopter is $\sim 20\%$ higher than this estimate due to nonuniform inflow, tip losses (vortex trails at the rotor tips), wake swirl, less than ideal wake contraction, the finite number of blades in the rotor, and power required by the tail rotor.

Equation (69) gives the power output required for a helicopter to climb vertically at velocity v_0 or hover at $v_0 = 0$. Unfortunately, it is difficult to apply this sort of analysis to vertical descents, since air might be passing either downward or upward through the rotor, depending on the descent speed. A special case that can be easily analyzed is a **windmill brake descent**, in which the downward motion of the helicopter through the air contributes to rotation of the rotor, which in turn slows the descent. In this case, the helicopter receives from the air a power *input* given by Eq. (69), where v_i is still downward and positive but v_0 is now negative because it is upward.

To move forward or in another horizontal direction, a helicopter tilts slightly toward the chosen direction, so that the rotor thrust has components causing both vertical lift and horizontal propulsion. Airflow to and from the rotor is then altered as in Fig. 7. The velocity $\mathbf{v_0}$ of air far upstream from the rotor is now inclined at an angle of attack α relative to the rotor. Air entering the rotor still gains an additional velocity $\mathbf{v_i}$ perpendicular to the rotor. Thus air at the rotor has a velocity component $v_0 \cos\alpha$ parallel to the rotor and $v_i + v_0 \sin\alpha$ perpendicular to it, or a net velocity V:

$$V \;=\; \sqrt{(v_0\cos\alpha)^2 + (v_0\sin\alpha + v_i)^2} \;=\; \sqrt{v_0^2 + 2v_0 v_i \sin\alpha + v_i^2} \tag{71}$$

Using $T = 2\dot{m}v_i$ from Eq. (68) with $\dot{m} = \rho A V$, the required thrust is

$$T \;=\; 2\dot{m}v_i \;=\; 2\rho A v_i V \tag{72}$$

The power is the thrust times the air velocity component $v_i + v_0 \sin\alpha$ that is parallel to it:

$$P \;=\; T(v_i + v_0\sin\alpha) \;=\; 2\rho A v_i V (v_i + v_0 \sin\alpha) \tag{73}$$

Two effects limit helicopters to a maximum forward speed $\sim v_s/4 \sim 300$ km/hour: (1) That speed plus the blade rotation make the advancing blade's tip velocity $\sim \frac{3}{4}v_s$, requiring large amounts of power to overcome compressibility effects. (2) Air rushing by at that speed is essentially motionless relative to the reverse velocity $v_{\rm tip}/2 \approx v_s/4$ at the mid-point of the retreating blade; thus most of the retreating blade cannot contribute much to the lift, making the helicopter vibrate and/or stall.

Of course, a helicopter must have some method of counteracting the rotor torque so that the helicopter body won't spin wildly in the opposite direction from the rotor's rotation. Generally a tail fin and tail rotor aimed to the side serve this purpose, though some larger helicopters avoid the problem by having two counter-rotating rotors on top.

The **autogiro**, a 1920s predecessor of true helicopters, is also worthy of mention. This was an airplane with unpowered, free-spinning rotor on top that was tilted slightly toward the rear of the craft. As the autogyro flew forward with its primary aircraft engine, the airflow spun the rotor, creating extra lift. This effect made the autogiro virtually stall proof at low forward speeds, although it could not hover completely motionless like a true helicopter with a powered rotor.

2 Incompressible, Viscous Fluid Mechanics

We will now consider cases in which the fluid is still incompressible but in which viscosity plays a major role. This section will begin by considering the relevant fundamental equations, then apply those to various specific situations including Poiseuille pressure- or gravity-driven flow through a conduit, Couette or lubricating flow between two surfaces that are moving with respect to each other, and flow over a flat plate.

2.1 Basic Equations

For an incompressible viscous fluid, one may still use the continuity equation (4), since viscosity plays no role in mass conservation.

For a viscous fluid, the term $\mathbf{F}_{\text{viscous}}$ in the momentum conservation equation (5) is important and must be defined in more detail. Whereas inviscid fluids have negligible stickiness, allowing fluid to slide frictionlessly past a wall or permitting different parts of a fluid to slide freely past each other, viscous fluids have a tendency to stick to themselves and to their surroundings. This stickiness creates a friction force that partially resists differences in velocity between a fluid and a wall, or between different parts of the fluid. As shown in Fig. 8(a), if there is a velocity gradient dv/dx, adjacent fluid elements that are moving at different velocities will try to stick to each other and hence exert viscous shear forces $\tau = \mu\, dv/dx$ on each other, with the shear forces trying to slow down the faster fluid elements and speed up the slower elements. The shear stress has units of force per area, and the constant of proportionality is the viscosity μ with units of Pa·sec. Generalizing to three dimensions, τ becomes a vector and d/dx becomes a gradient ∇:

$$\tau \;=\; \mu\nabla\mathbf{v} \tag{74}$$

The viscosity term $\mathbf{F}_{\text{viscous}}$ in Eq. (5) is the net viscous force per volume on an infinitesimal cube of fluid. If the same shear force τ is exerted in one direction on one side of a fluid element and in the other direction on the other side, those shear forces will essentially cancel each other out. A net force on the fluid element results when there is a gradient $d\tau/dx = \mu\, d^2v/dx^2$ in the shear force, making the shear force in one direction on one side of the element greater than the shear force in the other direction on the other side [Fig. 8(b)]. Taking the spatial derivative also converts the force per area τ into a force per volume $\mathbf{F}_{\text{viscous}}$. Thus the viscosity term involves the second derivative of the local fluid velocity:

$$\mathbf{F}_{\text{viscous}} \;=\; \mu\nabla^2\mathbf{v} \tag{75}$$

The viscosity μ varies with pressure and temperature, but for simplicity one can usually ignore such variations within the fluid, except for some special cases that will be covered in Section 4. In a few weird (**non-Newtonian**) fluids, viscosity can even vary with velocity–fluids such as quicksand or cornstarch in water resist fast motions more than they resist slow motions. If the viscosity μ or density ρ are indeed variable, the viscous force term is considerably more complicated than Eq. (75). More generally, there may be different shear forces acting in different directions on different sides of a fluid element, with the shear becoming a 3x3 matrix or tensor τ_{ij} having nine different components from τ_{xx} through τ_{zz} [Fig. 8(c)]:

$$\tau_{ij} \;=\; \begin{pmatrix} \tau_{xx} & \tau_{xy} & \tau_{xz} \\ \tau_{yx} & \tau_{yy} & \tau_{yz} \\ \tau_{zx} & \tau_{zy} & \tau_{zz} \end{pmatrix} \tag{76}$$

We won't worry about any of that here, but see [2] if you are glutton for punishment.

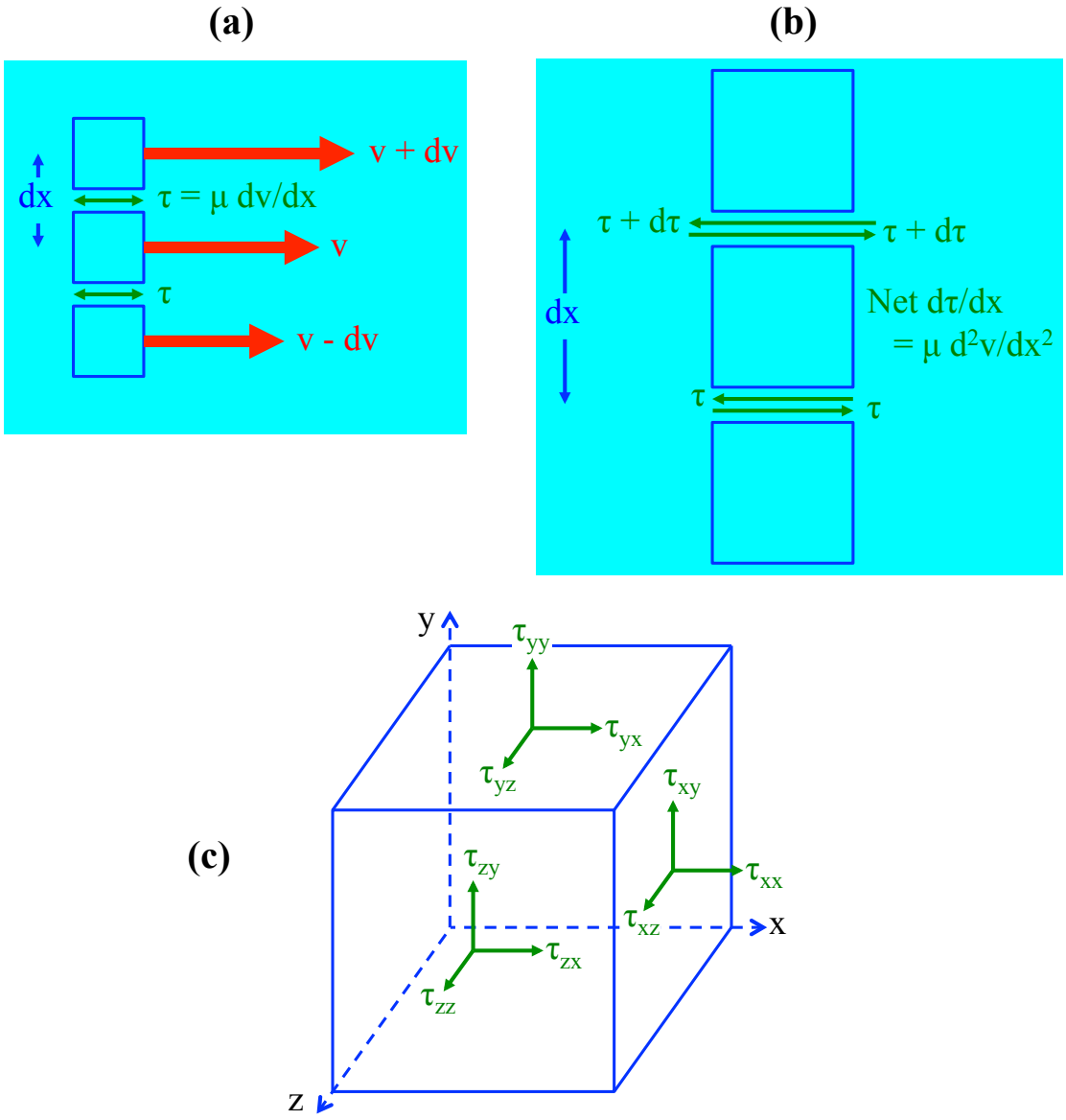

Figure 8. Viscous shear forces on an infinitesimal element within a fluid. **(a)** If there is a velocity gradient dv/dx, adjacent fluid elements that are moving at different velocities will try to stick to each other and hence exert viscous shear forces $\tau = \mu\, dv/dx$ on each other, with the shear forces trying to slow down the faster fluid elements and speed up the slower elements. **(b)** If the same shear force τ is exerted in one direction on one side of a fluid element and in the other direction on the other side, those shear forces will essentially cancel each other out. A net force on the fluid element results when there is a gradient $d\tau/dx = \mu\, d^2v/dx^2$ in the shear force, making the shear force in one direction on one side of the element greater than the shear force in the other direction on the other side. **(c)** More generally, there may be different shear forces acting in different directions on different sides of a fluid element, with the shear becoming a 3x3 matrix or tensor having nine different components from τ_{xx} through τ_{zz}.

Inserting Eq. (75) into Eq. (5), the Navier-Stokes momentum equation for constant ρ and μ is:

$$\rho\left(\frac{\partial}{\partial t}+\mathbf{v}\cdot\nabla\right)\mathbf{v} \;=\; \rho\mathbf{g} \;-\; \nabla p \;+\; \mu\nabla^2\mathbf{v} \qquad \textbf{Navier-Stokes equation} \tag{77}$$

Sometimes all terms in Eq. (77) are divided by ρ, and the kinematic viscosity is defined as

$$\nu \;=\; \frac{\mu}{\rho} \tag{78}$$

Some representative viscosities are given in Table 1.

Fluid	ρ **(kg/m^3)**	μ **(Pa·sec)**	ν **(m^2/sec)**
Air	1.20	1.82×10^{-5}	1.51×10^{-5}
Water	998	1.00×10^{-3}	1.00×10^{-6}
Ethanol	789	1.20×10^{-3}	1.50×10^{-6}
Mercury	13,500	1.56×10^{-3}	1.18×10^{-7}
SAE 10 motor oil	857	0.065	7.58×10^{-5}
SAE 40 motor oil	872	0.319	3.66×10^{-4}
Glycerine	1260	1.49	1.18×10^{-3}

Table 1. Density ρ, viscosity μ, and kinematic viscosity ν of common fluids at 20^{o}C and standard atmospheric pressure. The exact values differ slightly in different references.

As a boundary condition to solve the Navier-Stokes Eq. (77), it is generally assumed that fluid in contact with a solid surface is moving at the same velocity as the solid surface at that boundary. This is often called the **non-slip boundary condition**.

The Navier-Stokes equation is sufficiently complex that it can only be solved exactly for a small number of simple cases, many of which will be considered in Sections 2.2 and 2.3. In other cases, the Navier-Stokes equation can be simplified by estimates to arrive at approximate solutions, as will be shown in Section 2.4. In practice, the Navier-Stokes equation is often solved by numerical or computer methods for a wide variety of cases.

The inertial forces allowing a fluid to flow freely are on the order of the momentum density $\rho\sim v_\infty\rho$, in which v_∞ is the fluid velocity far from any obstacles. These freely flowing inertial forces are opposed by viscous drag forces, which from Eq. (74) vary like $\sim\mu/L$, in which L is a characteristic length over which change occurs in the fluid system. The ratio of these two types of forces is called the **Reynolds number** and indicates which effects predominate:

$$\mathrm{Re}_L \;=\; \frac{\text{Inertial forces}}{\text{Viscous forces}} \;=\; \frac{v_\infty\rho L}{\mu} \;=\; \frac{v_\infty L}{\nu} \tag{79}$$

If velocity gradients are small or zero, fluid flow is inviscid and well-behaved like the cases considered in Section 1. If velocity gradients are large and the Reynolds number is less than some transitional value $(\mathrm{Re}_L)_{\text{transition}}$, the flow is viscous but **laminar**, or smooth and orderly. If velocity gradients are large and the Reynolds number is greater than $(\mathrm{Re}_L)_{\text{transition}}$, the flow is viscous and **turbulent**, or randomly fluctuating and chaotic. The transitional Reynolds number $(\mathrm{Re}_L)_{\text{transition}}$ separating laminar and turbulent flow depends on the geometry through which the fluid is flowing. For example, $(\mathrm{Re}_L)_{\text{transition}}$ is ~ 3000 for flow through a circular pipe of diameter L and $\sim 300,000$ for flow over a flat plate of length L.

When scale aircraft or car models are tested in a wind tunnel, or when scale ship models are tested in a water channel, one must adjust the fluid's velocity, density, viscosity, etc. for the smaller scale so that the Reynolds number (and any other relevant dimensionless parameters) and hence the type of flow will correctly model the full-scale situation.

2.2 Poiseuille Flow

Poiseuille flow is viscous flow through a conduit, driven by a pressure gradient and/or gravitational force along the conduit. It is especially relevant to viscous flow through pipes, ducts, and channels. The major cases we will consider are (a) plane Poiseuille flow between flat plates, (b) plane Poiseuille flow above one flat plate, (c) Poiseuille flow through a circular pipe, and (d) Poiseuille flow through conduits of other shapes.

(a) Plane Poiseuille flow between flat plates

For steady-state, laminar, plane Poiseuille flow between two infinite parallel plates separated by a gap of height H in the y direction, where the lower plate is at $y = -H/2$ and the upper plate is at $y = H/2$ as shown in Fig. 9(a), the Navier-Stokes Equation (77) reduces to:

$$-\frac{1}{\mu}\left(\left|\frac{dp}{dx}\right| + \rho g \sin\theta\right) = \frac{d^2 v_x}{dy^2} \tag{80}$$

in which the flow is driven by a negative pressure gradient dp/dx along the length of the channel and/or gravitational force if the channel slopes downhill at an angle θ relative to horizontal.

Matching the boundary conditions $v_x = 0$ at $y = -H/2$ and $y = H/2$ (the non-slip boundary condition, such that the fluid immediately adjacent to the motionless plates is itself motionless), the solution of Eq. (80) is:

$$v_x = \frac{1}{2\mu}\left(\left|\frac{dp}{dx}\right| + \rho g \sin\theta\right)\left[\left(\frac{H}{2}\right)^2 - y^2\right] \tag{81}$$

The shear stress at any point in the flow is

$$\tau = \mu \frac{dv_x}{dy} = -\left(\left|\frac{dp}{dx}\right| + \rho g \sin\theta\right) y \tag{82}$$

Using Eq. (82), the shear stress on the lower and upper plates is

$$\tau(y = \pm H/2) = \mp\left(\left|\frac{dp}{dx}\right| + \rho g \sin\theta\right)\frac{H}{2} \tag{83}$$

For a channel of width Δz into the page in Fig. 6(a), the total flow rate Q (in kg/second) between the plates is

$$Q = \rho\,\Delta z \int_{-H/2}^{H/2} v_x dy = \rho\,\Delta z\,\frac{H^3}{12\mu}\left(\left|\frac{dp}{dx}\right| + \rho g \sin\theta\right) \tag{84}$$

Using Eqs. (81) and (84), the maximum and average flow velocities are

$$(v_x)_{\max} = v_x(y = 0) = \frac{H^2}{8\mu}\left(\left|\frac{dp}{dx}\right| + \rho g \sin\theta\right) \tag{85}$$

$$(v_x)_{\text{avg}} = \frac{Q}{\rho\, H\, \Delta z} = \frac{2}{3}(v_x)_{\max} \tag{86}$$

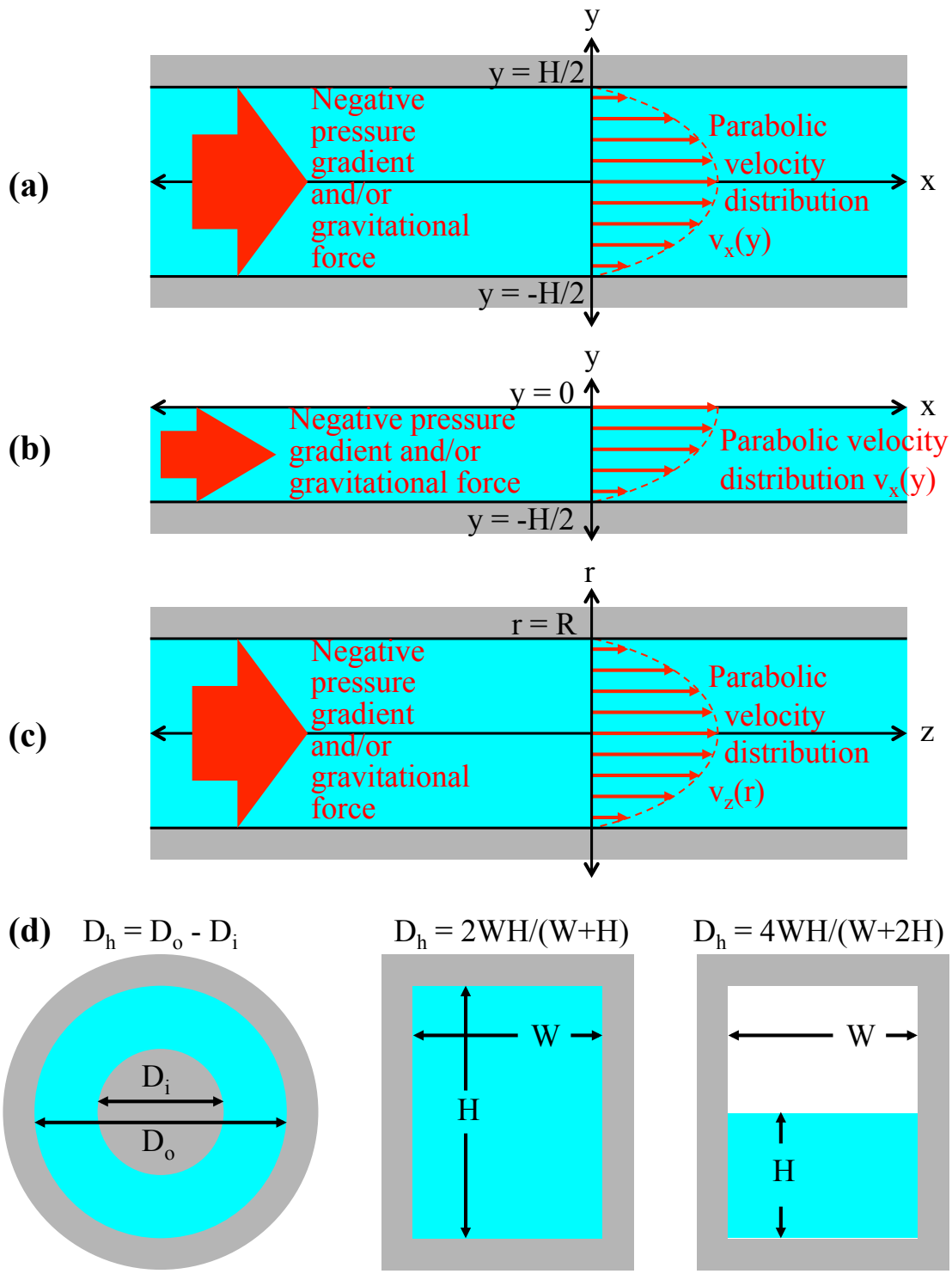

Figure 9. Poiseuille flow (a) between flat plates [parabolic velocity distribution as shown for laminar flow], (b) above one flat plate [laminar], (c) through a circular pipe [laminar], and (d) through conduits of other shapes shown in cross-section with their effective hydraulic diameters D_h.

(b) Plane Poiseuille flow above one flat plate

For steady-state plane Poiseuille flow above one infinite flat plate in the y direction, where the plate is at $y = -H/2$ and the upper surface of the liquid is at $y = 0$ as shown in Fig. 9(b), the solution of Eq. (81) is still valid, but now it only extends from $y = -H/2$ to $y = 0$ instead of $y = H/2$. Note that the flow velocity is maximum at the upper surface, where there is no adjacent solid wall to provide friction. The total flow volume is half the value of Q from Eq. (84):

$$Q \;=\; \frac{\rho\,\Delta z}{3\mu}\,\left(\frac{H}{2}\right)^3\left(\left|\frac{dp}{dx}\right| \;+\; \rho g\sin\theta\right) \tag{87}$$

Sometimes this case appears in the form of viscous flow down a vertical wall, or $|dp/dx| = 0$ and $\sin\theta = 1$ in Eq. (87).

(c) Poiseuille flow through a circular pipe

For steady-state, laminar, plane Poiseuille flow in the z direction through an infinitely long circular pipe of radius R as shown in Fig. 9(c), the Navier-Stokes Equation (77) reduces to:

$$-\,\frac{1}{\mu}\left(\left|\frac{dp}{dx}\right| \;+\; \rho g\sin\theta\right) \;=\; \frac{1}{r}\,\frac{d}{dr}\left(r\,\frac{dv_z}{dr}\right) \tag{88}$$

Matching the non-slip boundary condition $v_z = 0$ at $r = R$, the solution of Eq. (88) is:

$$v_z \;=\; \frac{1}{4\mu}\left(\left|\frac{dp}{dx}\right| \;+\; \rho g\sin\theta\right)(R^2 \;-\; r^2) \tag{89}$$

The shear stress at any point in the flow is

$$\tau \;=\; \mu\,\frac{dv_z}{dr} \;=\; -\frac{1}{2}\left(\left|\frac{dp}{dx}\right| \;+\; \rho g\sin\theta\right) r \tag{90}$$

The shear stress at the pipe wall is

$$\tau(r = R) \;=\; -\frac{1}{2}\left(\left|\frac{dp}{dx}\right| \;+\; \rho g\sin\theta\right) R \tag{91}$$

The total flow rate through the circular pipe is

$$Q \;=\; \rho\int_0^R v_z\,2\pi r\,dr \;=\; \frac{\pi\rho R^4}{8\mu}\left(\left|\frac{dp}{dx}\right| \;+\; \rho g\sin\theta\right) \tag{92}$$

Using Eqs. (89) and (92), the maximum and average flow velocities are

$$v_{\max} \;=\; v_z(r = 0) \;=\; \frac{R^2}{4\mu}\left(\left|\frac{dp}{dx}\right| \;+\; \rho g\sin\theta\right) \tag{93}$$

$$v_{\text{avg}} \;=\; \frac{Q}{\pi\rho R^2} \;=\; \frac{R^2}{8\mu}\left(\left|\frac{dp}{dx}\right| \;+\; \rho g\sin\theta\right) \;=\; \frac{1}{2}(v_z)_{\max} \tag{94}$$

Note that the physical situation and results of Eqs. (89)-(94) for Poiseuille flow through a circular pipe are very similar to the physical situation and results of Eqs. (81)-(86) for Poiseuille flow between flat plates, apart from fairly minor differences in the numerical factors.

Using $R = D/2$ and $|dp/dx| = \Delta p/L$, and ignoring downhill flow for the moment ($\theta = 0$), Eq. (94) may be rewritten in terms of the fluid pressure drop Δp caused by viscous drag on the walls after flowing through a pipe of length L:

$$v_{\text{avg}} \;=\; \frac{D^2}{32\mu}\,\frac{\Delta p}{L} \tag{95}$$

Turning Eq. (95) around, the pressure drop is called the Hagen-Poiseuille law:

$$\Delta p \;=\; \frac{32\,\mu\,v_{\text{avg}}\,L}{D^2} \;=\; \frac{64}{\text{Re}_D}\,\frac{L}{D}\,\frac{\rho\,v_{\text{avg}}^2}{2} \tag{96}$$

where the Reynolds number for this case is defined as $\text{Re}_D \equiv \rho v_{\text{avg}} D/\mu$. It is customary to express viscous pressure or energy losses in terms of the Darcy friction factor f. From Eq. (96), the friction factor for laminar flow through a circular pipe is:

$$f \;\equiv\; \frac{\Delta p}{\rho v_{\text{avg}}^2/2}\,\frac{D}{L} \;=\; \frac{64}{\text{Re}_D} \tag{97}$$

Written in terms of the Darcy friction factor in order to generalize the results to flows other than just laminar flow in a circular pipe, the head loss, energy loss, and pressure loss after fluid has passed through a length L of pipe are:

$$\Delta h \;=\; \frac{f\,L\,v_{\text{avg}}^2}{2\,D\,g} \tag{98}$$

$$\Delta E \;=\; g\,\Delta h \;=\; \frac{f\,L\,v_{\text{avg}}^2}{2\,D} \tag{99}$$

$$\Delta p \;=\; \rho\,g\,\Delta h \;=\; \frac{f\,L\,\rho\,v_{\text{avg}}^2}{2\,D} \tag{100}$$

(Just to create confusion, sometimes folks use the Fanning friction factor, which is defined to be one quarter of the Darcy friction factor, $f_{\text{Fanning}} = f_{\text{Darcy}}/4$.)

For pipes in series, the head, energy, or pressure losses from each section of pipe are additive, just as voltage losses across individual electrical components are additive when the components are in series. For pipes in parallel, the head (or energy or pressure) loss between the junction where the pipes separate from each other and the junction where the pipes rejoin must be the same for each parallel branch of pipe, just as the voltage losses across parallel electrical circuits must be the same. The same rules apply if pumps are included, except each pump adds head (or energy or pressure, just as a battery adds voltage in a circuit), whereas each frictional loss subtracts head.

All of the preceding laminar results are valid for sufficiently low flow velocities and low Reynolds numbers, $\text{Re}_D = \rho v_{\text{avg}} D/\mu < 2000$. The transition from laminar to turbulent flow in a pipe generally occurs for Reynolds numbers between roughly 2000 and 4000. Higher-velocity flows with Reynolds numbers $\text{Re}_D > 4000$ are typically fully turbulent except for a very thin still-laminar region near the wall. Although turbulent flow is fluctuating and difficult to calculate, experimental measurements indicate that the time-averaged velocity profile varies approximately as:

$$v_z \;\approx\; (v_z)_{\text{max}} \left(1 - \frac{r}{R}\right)^{1/7} \tag{101}$$

Note that the turbulent velocity profile $v/v_{\text{max}} \approx (1 - r/R)^{1/7}$ is much "flatter" and has much less variation across the pipe than the laminar parabolic velocity profile $v/v_{\text{max}} \approx 1 - (r/R)^2$ from Eq. (89), since turbulent fluctuations tend to mix and homogenize the flow (at least in the time-averaged sense) everywhere except in a thin laminar region near the wall. By integrating the turbulent velocity profile in Eq. (101) across the pipe, the average velocity of the flow is:

$$(v_z)_{\text{avg}} \;\approx\; \frac{49}{60}\,(v_z)_{\text{max}} \;\approx\; 0.817\,(v_z)_{\text{max}} \tag{102}$$

From experimental measurements, an empirical relationship for the Darcy friction factor f for turbulent flow in a pipe is the Colebrook equation:

$$\frac{1}{\sqrt{f}} \approx -2.0 \log_{10}\left(\frac{\epsilon/D}{3.7} + \frac{2.51}{\mathrm{Re}_D\sqrt{f}}\right) \tag{103}$$

in which ϵ is the height of bumps inside the pipe. ϵ is typically negligible for glass and plastic tubing, $\sim 10^{-6} - 10^{-4}$ m for metal pipe (with smooth copper pipe at the low end and rough cast iron pipe at the high end of that range), and $\sim 10^{-3}$ m for concrete.

Equation (103) is an implicit equation for f, but the dependence on f in the right-hand side of the equation is relatively weak, so one can quickly arrive at an approximate solution by using an initial estimate of f in the right-hand side to obtain a better estimate on the left-hand side, then iterating a couple of times to refine the estimate. For a wide range of roughness values ϵ and Reynolds numbers Re_D, the friction factor f generally varies between approximately 0.005 and 0.1; thus $f \sim 0.03$ is a good first guess for the right-hand side.

Note that for very smooth pipes, the term $(\epsilon/D)/3.7$ in Eq. (103) vanishes and f is completely determined by the Reynolds number, so f varies with the flow velocity. In contrast, for very rough pipes, the term $2.51/(\mathrm{Re}_D\sqrt{f})$ in Eq. (103) is negligible and f is completely determined by the roughness, remaining constant regardless of the flow velocity.

(d) Poiseuille flow through conduits of other shapes

There are exact solutions for Poiseuille flow through conduits of many other shapes [2]. However, as a simple approximation, one may define an effective hydraulic diameter D_h for a conduit of arbitrary cross-sectional shape, then use Eqs. (89)-(94) for Poiseuille flow through a "circular" conduit of radius D_h. The results should be approximately correct to within a factor of 2 or so in most cases. The hydraulic diameter of a conduit with a certain cross-sectional area and wetted perimeter (perimeter of the fluid in contact with conduit walls) is

$$D_h \equiv \frac{4 \times \text{area}}{\text{wetted perimeter}} \tag{104}$$

Sometimes fluid mechanicists use the effective hydraulic radius R_h instead, and just to be confusing, they usually definite it to be 1/4 (not 1/2) of the hydraulic diameter:

$$R_h \equiv \frac{\text{area}}{\text{wetted perimeter}} = \frac{D_h}{4} \tag{105}$$

For a given cross-sectional area of flow, frictional losses at the wall will be minimized if the wetted perimeter of the wall is minimized, which means if the conduit is circular and either full or half-full.

For infinite flat plates of width $W \to \infty$ separated by distance H as in Fig. 9(a), the hydraulic diameter is $D_h = 4(HW)/(2W+2H) = 4(HW)/(2W) = 2H$, or the hydraulic radius is $R_h = H/2$. Note that in calculating the wetted perimeter in the denominator, the finite height H is negligible compared to the infinite width W.

For flow of depth $H/2$ above one infinite flat plate of width $W \to \infty$ as in Fig. 9(b), the hydraulic diameter is $D_h = 4(HW/2)/(W+H) = 4(HW/2)/(W) = 2H$, or the hydraulic radius is $R_h = H/2$. Note that for calculating the wetted perimeter in the denominator, the upper liquid surface of width W is not bounded by a wall and hence does not count.

For a circular pipe of diameter D as in Fig. 9(c), the hydraulic diameter is $D_h = 4(\pi D^2/4)/(\pi D) = D$, or comfortingly enough the actual diameter. Sadly, though, the hydraulic radius is only half the actual radius, $R_h = D/4$.

For flow between two concentric cylinders of diameters D_o and D_i as in the left side of Fig. 9(d), the hydraulic diameter is $D_h = 4(\pi D_o^2/4 - \pi D_i^2/4)/(\pi D_o + \pi D_i) = D_o - D_i$. The hydraulic radius is $R_h = (D_o - D_i)/4$.

For flow that fully fills a rectangular conduit of width W and height H as in the center of Fig. 9(d), the hydraulic diameter is $D_h = 4(WH)/(2W + 2H) = 2WH(W + H)$, and the hydraulic radius is $R_h = WH(W + H)/2$.

For flow of depth H that partially fills a rectangular conduit of width W as in the right side of Fig. 9(d), the hydraulic diameter is $D_h = 4(WH)/(W + 2H)$, and the hydraulic radius is $R_h = (WH)/(W + 2H)$. Note that for calculating the wetted perimeter in the denominator, the upper liquid surface of width W is not bounded by a wall and hence does not count.

A common situation of interest is **uniform flow** (flow with constant cross section) slightly downhill in an **open channel**, such as a river, canal, or partially full sewer pipe. This situation may be simplified by treating the flow as purely one-dimensional with an average and constant velocity v_{avg}. For constant velocity, the downhill slope of the channel is simply the head height loss per length along the channel:

$$S_o = \frac{\Delta h}{L} \tag{106}$$

Using Eq. (106) and the hydraulic radius $R_h = D/4$, Eq. (98) may be rewritten as the **Chezy formula** for uniform flow in an open channel:

$$v_{\text{avg}} = \sqrt{\frac{8gR_hS_o}{f}} = C\, R_{h,\,\text{meters}}^{1/2}\, S_o^{1/2} \;\; \frac{\text{m}}{\text{sec}} \tag{107}$$

in which the Chezy coefficient is defined as

$$C \equiv \sqrt{\frac{8g}{f}} \tag{108}$$

Since flow in channels will generally be turbulent, the Darcy friction factor f may be found from Eq. (103) with $R_h = D/4$, and then used in Eq. (108) to find the Chezy coefficient.

A simpler and therefore more commonly used empirical correlation for the Chezy coefficient was developed by Manning:

$$C = \frac{1}{n}\, R_{h,\,\text{meters}}^{1/6} \tag{109}$$

The **Manning roughness parameter** n varies from 0.01 for perfectly smooth (e.g., glass or brass) channels to 0.02 for smooth excavated earth channels to 0.03 for clean, straight natural channels to 0.04 for sluggish, deep pools.

Combining Eqs. (107) and (109), the complete **Chezy-Manning formula** for uniform flow in an open channel is:

$$v_{\text{avg}} = \frac{1}{n}\, R_{h,\,\text{meters}}^{2/3}\, S_o^{1/2} \;\; \frac{\text{m}}{\text{sec}} \tag{110}$$

If the cross-sectional area of the flow is A, the total mass flow per second will simply be

$$Q = \rho\, A\, v_{\text{avg}} \tag{111}$$

in which v_{avg} may be found from either Eq. (107) or Eq. (110).

For examples of non-uniform open channel flows and how they can be estimated, see [1, 3].

2.3 Couette Flow

Couette flow is viscous flow between two surfaces, driven by movement of one surface relative to the other. It is especially relevant to cases in which a lubricant reduces the friction between two moving surfaces. The most common geometries are (a) plane Couette flow between flat plates, (b) axial Couette flow between concentric cylinders, and (c) angular Couette flow between concentric cylinders. Since these cases usually involve viscous lubricants, the flows are generally laminar, and we will not consider the corresponding turbulent solutions.

(a) Plane Couette flow between fixed and moving flat plates

For steady-state plane Couette flow between two infinite parallel plates separated by a gap of height H in the y direction, where the lower plate at $y = -H/2$ is motionless and the upper plate at $y = H/2$ is moving at velocity v_{upper} in the x direction as shown in Fig. 10(a), the Navier-Stokes Equation (77) reduces to:

$$0 \;=\; \frac{d^2 v_x}{dy^2} \tag{112}$$

Matching the non-slip boundary conditions $v_x = 0$ at $y = -H/2$ and $v_x = v_{\text{upper}}$ at $y = H/2$, the solution of Eq. (112) is:

$$v_x \;=\; v_{\text{upper}} \left(\frac{y}{H} + \frac{1}{2} \right) \tag{113}$$

The shear stress is uniform throughout the flow:

$$\tau \;=\; \mu \, \frac{dv_x}{dy} \;=\; \frac{\mu \, v_{\text{upper}}}{H} \tag{114}$$

Since the flow velocity increases linearly with height and has an average of $v_{\text{avg}} = v_{\text{upper}}/2$, the total flow rate for a channel of width Δz into the page in Fig. 7(a) is simply

$$Q \;=\; \rho \, \frac{v_{\text{upper}}}{2} \, H \, \Delta z \tag{115}$$

More complicated flow problems can sometimes be solved by superposition of simpler solutions. For example, if flow between two infinite parallel plates is due to one of the plates moving as in the Couette case and also a pressure gradient or gravitational force as in the Poiseuille case, the solution may be expressed as the superposition of the appropriate Couette and Poiseuille solutions, with constants matched to the appropriate boundary conditions.

(b) Axial Couette flow between axially moving concentric cylinders

For steady-state axial Couette flow between two infinitely long concentric cylinders, where the inner cylinder of radius r_i is motionless and the outer cylinder of radius r_o is moving at velocity v_o in the axial z direction as shown in Fig. 10(b), the Navier-Stokes momentum equation (77) is simply:

$$0 \;=\; \frac{1}{r} \, \frac{d}{dr} \left(r \, \frac{dv_z}{dr} \right) \tag{116}$$

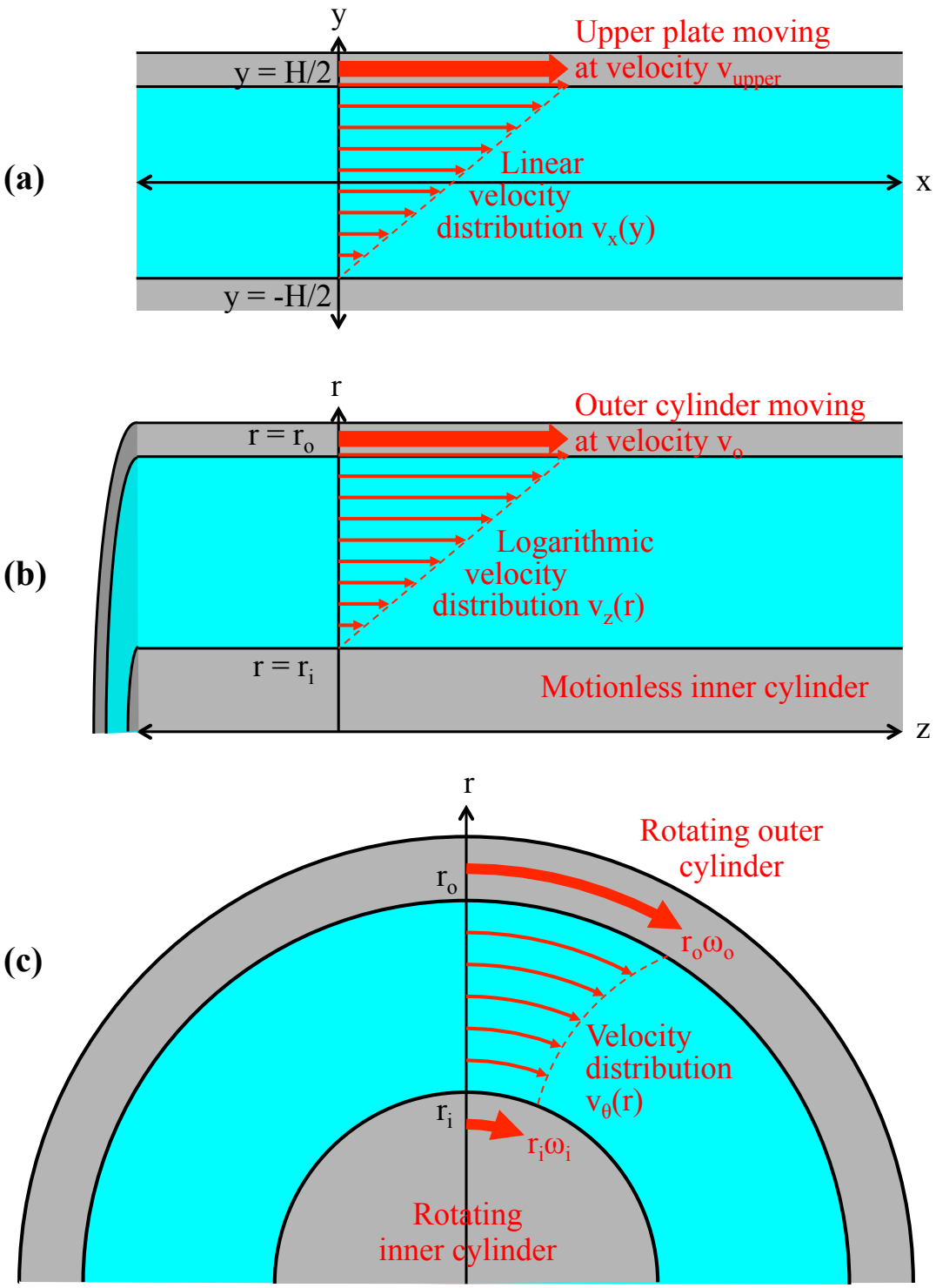

Figure 10. Couette flow between (a) a fixed lower and moving upper flat plate, (b) a fixed inner and axially moving outer concentric cylinder, and (c) inner and outer concentric cylinders in relative angular motion.

For the boundary conditions $v_z = 0$ at $r = r_i$ and $v_z = v_o$ at $r = r_o$, the solution of Eq. (116) is:

$$v_z \;=\; v_o \,\frac{\ln(r/r_i)}{\ln(r_o/r_i)} \tag{117}$$

The shear stress at any point in the flow is

$$\tau \;=\; \mu\,\frac{dv_z}{dr} \;=\; \frac{\mu\, v_o}{r\ln(r_o/r_i)} \tag{118}$$

The total axial flow rate between the concentric cylinders is

$$Q \;=\; \rho\int_{r_i}^{r_o} v_z\, 2\pi r\, dr \;=\; \pi\rho v_o r_o^2 \;-\; \frac{\pi\rho v_o(r_o^2 - r_i^2)}{2\ln(r_o/r_i)} \tag{119}$$

In the limit of infinitely large cylinders separated by a finite gap, $r_i \to \infty$ and $r_o = r_i + H$, axial Couette flow reduces to the previous case of Couette flow between infinite flat plates.

(c) Angular Couette flow between rotating concentric cylinders

For steady-state angular Couette flow between two infinitely long concentric cylinders, where the inner cylinder of radius r_i is rotating at an angular rate ω_i and the outer cylinder of radius r_o is rotating at an angular rate ω_o as shown in Fig. 10(c), the Navier-Stokes Equation (77) reduces to:

$$0 \;=\; \frac{d^2 v_\theta}{dr^2} \;+\; \frac{d}{dr}\left(\frac{v_\theta}{r}\right) \tag{120}$$

The solution of Eq. (120) for boundary conditions $v_\theta = r_i\omega_i$ at $r = r_i$ and $v_\theta = r_o\omega_o$ at $r = r_o$ is:

$$v_\theta \;=\; \left[\frac{\omega_o r_o^2 - \omega_i r_i^2}{r_o^2 - r_i^2}\right] r \;+\; \left[\frac{(\omega_i - \omega_o) r_i^2 r_o^2}{r_o^2 - r_i^2}\right]\frac{1}{r} \tag{121}$$

The shear stress at any point in the flow is

$$\tau \;=\; \mu\,\frac{dv_\theta}{dr} \;=\; \mu\left[\frac{\omega_o r_o^2 - \omega_i r_i^2}{r_o^2 - r_i^2}\right] \;-\; \mu\left[\frac{(\omega_i - \omega_o) r_i^2 r_o^2}{r_o^2 - r_i^2}\right]\frac{1}{r^2} \tag{122}$$

The total angular flow rate between the concentric cylinders of length Δz is

$$Q \;=\; \rho\,\Delta z\int_{r_i}^{r_o} v_\theta\, dr \;=\; \rho\,\Delta z\left\{\left[\frac{\omega_o r_o^2 - \omega_i r_i^2}{r_o^2 - r_i^2}\right]\frac{r_o^2 - r_i^2}{2} \;+\; \left[\frac{(\omega_i - \omega_o) r_i^2 r_o^2}{r_o^2 - r_i^2}\right]\ln\left(\frac{r_o}{r_i}\right)\right\} \tag{123}$$

In the limit of infinitely large cylinders separated by a finite gap, $r_i \to \infty$ and $r_o = r_i + H$, angular Couette flow reduces to the first case of Couette flow between infinite flat plates.

2.4 Boundary Layers

Viscous flow that encounters a surface will form a boundary layer as it moves past that surface. Fluid within the boundary layer will cling to the surface and move more slowly than the surrounding fluid outside the boundary layer. Specifically, the fluid velocity at the surface will be zero relative to the surface, and the fluid velocity will steadily increase further out in the boundary layer until it matches the surrounding flow velocity at the edge of the boundary layer. The most commonly considered cases are (a) a laminar boundary layer on a flat plate, (b) a turbulent boundary layer on a flat plate, and (c) boundary layer effects for Poiseuille flow entering a channel or pipe.

(a) Laminar boundary layer on a flat plate

For steady-state ($\partial/\partial t = 0$) flow in the absence of significant gravitational and pressure forces, the Navier-Stokes momentum equation (77) simplifies to:

$$\rho(\mathbf{v}\cdot\nabla)\mathbf{v} \;=\; \mu\nabla^2\mathbf{v} \tag{124}$$

As shown in Fig. 11(a), fluid flowing in the x direction past a flat plate will form a boundary layer of thickness $\delta(x)$ in the y direction, where $\delta(x)$ will vary along the length of the plate. If the velocity of the flow far from the plate is v_∞, the fluid velocity in the boundary layer must match the boundary conditions (a) $v_x = 0$ at $y = 0$ and (b) $v_x = v_\infty$ at $y = \delta(x)$. The shear will also be maximum at the plate and zero at the edge of the boundary layer [boundary condition (c), $dv_x/dy = 0$ at $y = \delta(x)$] where the flow returns to uniform. For simplicity, one can assume that the velocity will vary parabolically with y just as it did for Poiseuille flow above a flat plane [Section 2.2, case (b)]. The most general parabolic velocity profile would have the form $v_x \approx C_0 + C_1 y + C_2 y^2$. Matching the boundary conditions (a), (b), and (c) just listed determines the constants C_0, C_1, and C_2 and yields the velocity profile:

$$v_x \;\approx\; v_\infty\left\{2\frac{y}{\delta(x)} - \left[\frac{y}{\delta(x)}\right]^2\right\} \tag{125}$$

Using the approximate velocity profile of Eq. (125), the right-hand side of Eq. (124) is

$$\left|\mu\nabla^2 v\right| \;\approx\; \frac{2v_\infty}{\delta^2(x)} \tag{126}$$

Since the flow is predominantly in the x direction, the left-hand side of Eq. (124) will be primarily x components. Although the velocity within the boundary layer will vary with position, as a rough approximation one could assume an average velocity $\sim v_\infty/2$ intermediate between the zero surface and maximum v_∞ flow velocities. In fact, the aerodynamics of the boundary layer is dominated by interactions near the surface, where the flow is moving even more slowly than this, so using a representative boundary layer flow velocity $\sim v_\infty/4$ will yield an even better final result:

$$|\rho(\mathbf{v}\cdot\nabla)\mathbf{v}| \;\sim\; \rho v_x\frac{d}{dx}v_x \;\sim\; \rho\,\frac{v_\infty}{4}\,\frac{1}{x}\,\frac{v_\infty}{4} \tag{127}$$

Substituting Eq. (127) into the left side of Eq. (124) and Eq. (126) into the right side yields:

$$\rho\,\frac{v_\infty^2}{16x} \;\sim\; \mu\,\frac{2\,v_\infty}{\delta^2(x)}\;, \quad \text{or} \tag{128}$$

$$\delta(x) \;\sim\; \sqrt{\frac{32\mu x}{\rho v_\infty}} \;\approx\; 5.7\sqrt{\frac{\mu x}{\rho v_\infty}} \tag{129}$$

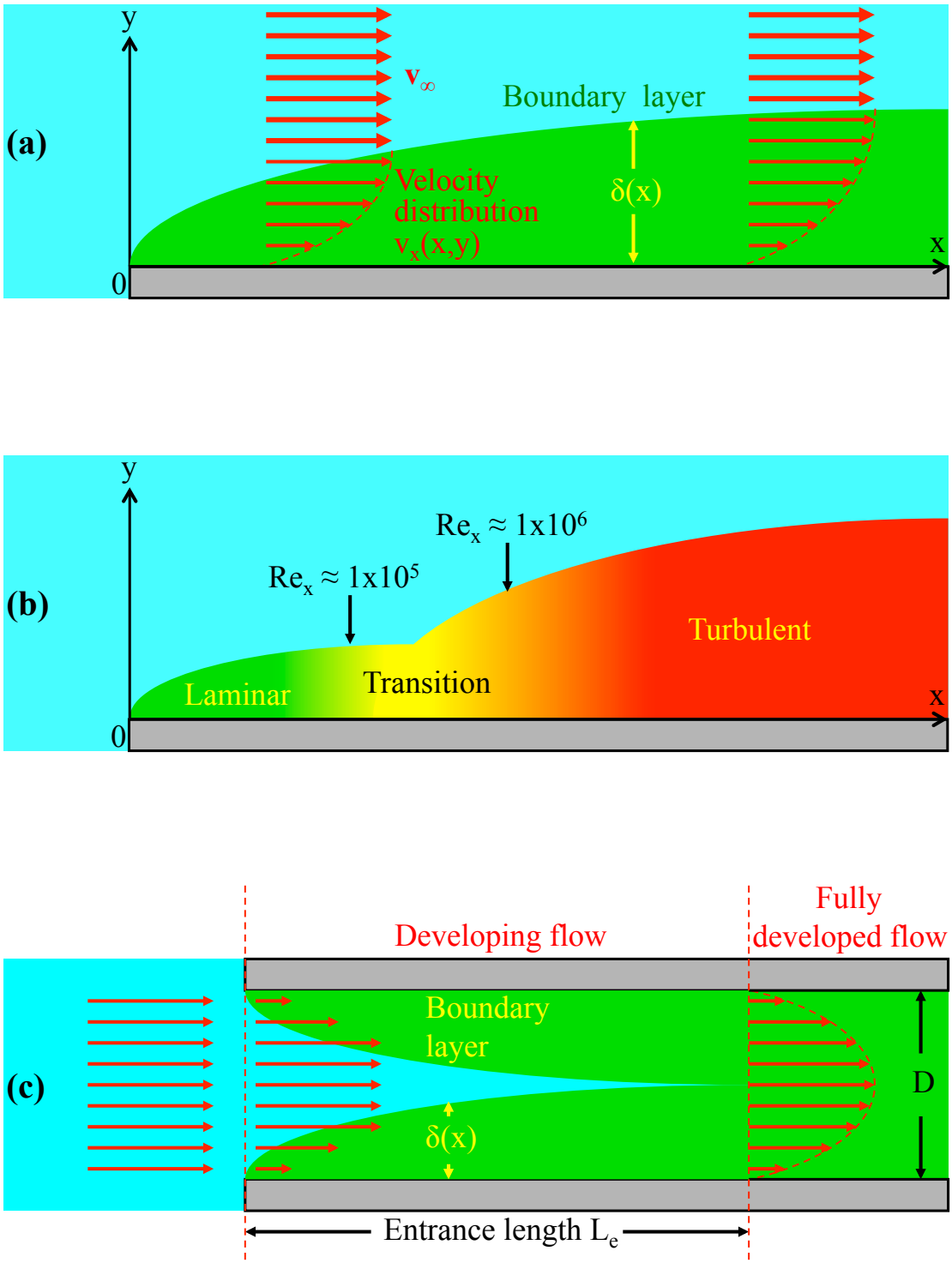

Figure 11. Boundary layers for (a) laminar flow past a flat plate, (b) turbulent flow past a flat plate, and (c) Poiseuille flow entering a pipe.

Much scarier and more accurate calculations yield basically the same answer for the boundary layer thickness as Eq. (129), only with a slightly different constant; this is called the **Blasius solution**:

$$\delta(x) \;\approx\; 5.0\sqrt{\frac{\mu x}{\rho v_\infty}} \;=\; 5.0\,\frac{x}{\mathrm{Re}_x^{1/2}} \tag{130}$$

Equation (130) is applicable as long as the flow remains laminar.

Using Eqs. (125) and (130), the shear stress at any point x along the surface of the plate is

$$\tau(x) \;=\; \mu\left[\frac{dv_x}{dy}\right]_{y=0} \;\approx\; 2\,\mu\,\frac{v_\infty}{\delta(x)} \;\approx\; \frac{2}{5}\,v_\infty\sqrt{\frac{\mu\rho v_\infty}{x}} \tag{131}$$

Integrating the shear force from Eq. (131) over the length L of the plate in the x direction, and assuming uniform flow across the plate width W in the y direction, one finds the drag force F_D exerted on one side of the plate (ignoring flow past the other side of the plate):

$$F_D \;=\; W\int_0^L dx\,\tau(x) \;\approx\; \frac{4}{5}\,W v_\infty\sqrt{\mu\rho v_\infty L} \tag{132}$$

Using Eq. (132), the drag coefficient due to viscous friction may be defined as:

$$C_f \;\equiv\; \frac{F_D}{(1/2)\rho v_\infty^2 W L} \;\approx\; \frac{8}{5}\sqrt{\frac{\mu}{\rho v_\infty L}} \;=\; \frac{1.6}{\sqrt{\mathrm{Re_L}}} \tag{133}$$

The velocity profile in Eq. (125) that led to Eq. (133) is only approximate, so this result is only approximate. More precise calculations yield a slightly lower numerical coefficient:

$$C_f \;\approx\; \frac{1.328}{\sqrt{\mathrm{Re_L}}} \tag{134}$$

(b) Turbulent boundary layer on a flat plate

In general, turbulent flow is very difficult to calculate, but experimental measurements indicate that the boundary layer thickness for turbulent flow over a flat plate [Fig. 11(b)] varies as [2]:

$$\delta(x) \;\approx\; 0.16\,\frac{x}{\mathrm{Re}_x^{1/7}} \tag{135}$$

Likewise, for turbulent flow, experimental measurements show that the frictional drag coefficient (or coefficient of friction) for viscous flow over one side of a flat plate is [2]:

$$C_f \;\approx\; 0.027\,\frac{1}{\mathrm{Re}_x^{1/7}} \tag{136}$$

(c) Entrance length for Poiseuille flow

As shown in Fig. 11(c), fluid flow entering a pipe or duct will form a boundary layer that grows from the walls until it meets in the center of the pipe after an entrance length L_e. While the boundary layer is growing, the velocity profile is said to be a **developing flow** with an inviscid core. Once the boundary layers meet in the center, the velocity profile becomes a fully developed viscous flow as analyzed in Section 2.2. Empirically, the entrance length for a circular pipe of diameter D is [2]:

$$L_e \;\approx\; \begin{cases} 0.06D(\mathrm{Re}_D + 10) & \text{for laminar flow } (\mathrm{Re}_D < 2000) \\ 4.4D\mathrm{Re}_D^{1/6} & \text{for turbulent flow } (\mathrm{Re}_D > 4000) \end{cases} \tag{137}$$

The turbulent entrance length is often considered to be $L_e \sim 25$ for the typical range $\mathrm{Re}_D \sim 10^4 - 10^5$.

3 Compressible, Inviscid Fluid Mechanics

For fluids in which compressibility cannot be neglected, the fluid density is no longer constant and must be considered a variable. This is especially true when objects travel at velocities approaching or exceeding the velocity of sound in the surrounding fluid, since the objects can significantly compress the fluid in the process. Thankfully, fluid viscosity may be safely neglected in a variety of circumstances, making the calculations more tractable than they would otherwise be. Compressible, inviscid fluid mechanics is relevant to many applications, including atmospheric pressure, sound waves, compressible flow through ducts, shock waves, explosions and implosions, subsonic flow around objects traveling slower than the speed of sound in the surrounding fluid, transonic flow around objects passing through the speed of sound, supersonic flow around objects exceeding the speed of sound, and hypersonic flow around objects greatly exceeding the speed of sound.

3.1 Basic Equations

If viscosity is ignored, one may still use Eqs. (3) for conservation of mass, (5) for conservation of momentum, and (9) for conservation of energy.

Several equations derived in *Statistical Physics* ?.? for ideal gases are also needed. When compressibility of the fluid must be taken into account, the fluid density $\rho(\mathbf{x},t)$ at a given position and time is no longer constant and may be found from the **ideal gas law**:

$$p(\mathbf{x},t) = \rho(\mathbf{x},t)\, R\, T(\mathbf{x},t) \qquad \textbf{Ideal gas law} \tag{138}$$

in which $p(\mathbf{x},t)$ is the fluid's pressure at that position and time, $T(\mathbf{x},t)$ is the fluid's absolute temperature (in ^{o}K) at that position and time, and R is the gas constant for that fluid. For a gas of molecules with molecular weight $M.W.$, the gas constant is

$$R \approx \frac{8314}{M.W.} \frac{\text{J}}{\text{kg }^o\text{K}} \tag{139}$$

Different fluids have different gas constants. Normal air is mostly diatomic nitrogen molecules (N_2) with a molecular weight of approximately $14 \times 2 = 28$. As listed in Table 2, air also contains some diatomic oxygen (O_2) and other molecules that increase the average molecular weight a bit to $M.W. \approx 28.97$, giving a gas constant of $R \approx 287$ J/(kg ^{o}K) for standard air.

The total volume V increases as the density ρ of the gas decreases: $V \propto 1/\rho$. The specific volume v (not to be confused with velocities also denoted by v), or volume per unit mass of the gas, is convenient when the other properties are also considered in terms of their amounts per unit mass. Density is mass per volume, so the volume per mass is simply the inverse of the density:

$$v = \frac{1}{\rho} \tag{140}$$

The energy per unit mass of a gas, or specific energy u, is proportional to the gas's temperature:

$$u(\mathbf{x},t) = c_v T(\mathbf{x},t) \tag{141}$$

in which the constant of proportionality c_v is the specific heat capacity at constant volume. For a gas composed of atoms or molecules with N degrees of freedom, the specific heat is

$$c_v = \frac{N}{2} R \tag{142}$$

In a monatomic gas such as helium, each atom has three degrees of freedom in which it can move [translation in the x, y, and z dimensions, as shown in Fig. 12(a)], so the specific heat is $c_v = (3/2)R$. Air is mainly composed of diatomic nitrogen and oxygen, as summarized in Table 2. Each diatomic molecule has five degrees of freedom [translation in the x, y, and z dimensions, plus rotation in two angular directions–spinning the molecule on its axis does not count, as shown in Fig. 12(b)], so the specific heat is $c_v = (5/2)R \approx 718$ J/(kg ^{o}K) for air.

Component	Chemical formula	By number of molecules	By mass
Nitrogen	N_2	78.1%	75.5%
Oxygen	O_2	20.9%	23.1%
Argon	Ar	0.9%	1.3%
Carbon dioxide	CO_2	$\sim 0.4\%$	$\sim 0.6\%$
Water vapor	H_2O	$\sim 0 - 4\%$	$\sim 0 - 3\%$
Other components		$< 1\%$	$< 1\%$

Table 2. Approximate composition of air. Due to rounding of the numbers and variations in the amount of water vapor, the numbers may not sum to 100%. The precise composition will vary depending on location, altitude, time of year, pollution, and other factors.

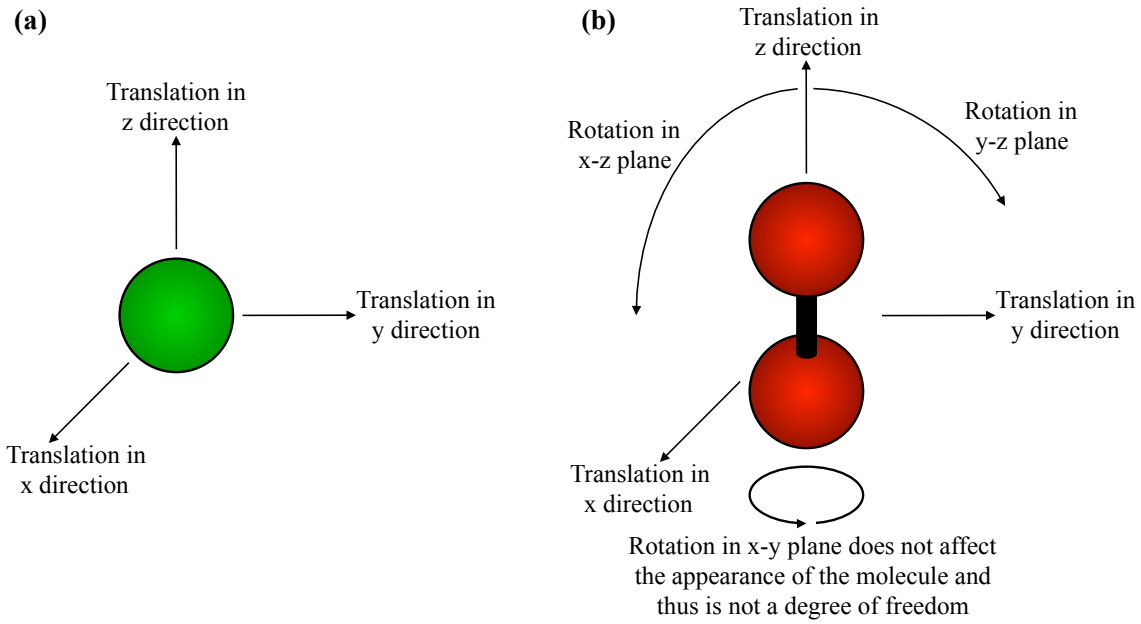

Figure 12. The number of degrees of freedom of particles in a gas determines the specific heat capacity values for that gas. (a) A monatomic gas has 3 degrees of freedom. **(b)** A diatomic gas molecule has 5 degrees of freedom.

From *Statistical Physics* ?.? or *Thermodynamics and Propulsion* ?.?, a fluid can gain internal energy du per unit mass by absorbing heat energy dq per unit mass. Since dq is heat energy, it is proportional to the temperature T, and since heat energy is the random, disorderly motion of molecules, dq is also proportional to the added entropy or disorder ds per unit mass: $dq = T\,ds$. Likewise, a fluid can lose internal energy if the fluid does work dw per mass on its surroundings by expanding by an amount dv while exerting a pressure p on its surroundings: $dw = -p\,dv$. The **First Law of Thermodynamics** is a form of the energy conservation equation that relates changes du to the internal energy of a fluid to the input heat energy dq imparted to the fluid and the output work energy dw done by the fluid on its surroundings:

$$dq = du - dw \tag{143}$$

$$T\,ds = du + p\,dv \tag{144}$$

If the volume of a fluid is held constant [$dv = 0$ in Eq. (144)], the input heat energy required to give the fluid a final internal energy u and temperature T (starting from zero) is $q = u = c_v T$ from Eq. (141). However, if the fluid is allowed to expand at constant pressure, the input heat energy must provide both the internal energy u and the work energy pv done by the fluid in expanding:

$$q \;=\; u \,+\, pv \;=\; u \,+\, \frac{p}{\rho} \tag{145}$$

In compressible fluid mechanics, fluids are generally allowed to expand freely, so the quantity $u+p/\rho$ in Eq. (145) is much more relevant than just the internal energy density u. This total of the internal thermal energy and the pressure work energy is called the **enthalpy**. The specific enthalpy h or enthalpy per unit mass of a fluid is proportional to its temperature:

$$h(\mathbf{x},t) \;=\; u(\mathbf{x},t) + \frac{p(\mathbf{x},t)}{\rho(\mathbf{x},t)} \;=\; c_v T(\mathbf{x},t) + RT(\mathbf{x},t) \tag{146}$$

$$\;=\; c_p T(\mathbf{x},t) \tag{147}$$

in which Eq. (146) used the ideal gas law from Eq. (138). In Eq. (147), the constant of proportionality c_p is the specific heat capacity at constant pressure, and it is simply:

$$c_p \;=\; c_v + R \tag{148}$$

Thus $c_p = (7/2)R \approx 1005$ J/(kg ^{o}K) for air.

The ratio of c_p and c_v is designated the **specific heat ratio** γ:

$$\gamma \;\equiv\; \frac{c_p}{c_v} \;=\; \frac{N+2}{N} \tag{149}$$

For a monatomic gas, there are $N = 3$ degrees of freedom, so $\gamma = 5/3 \approx 1.67$. For diatomic gases such as air, there are $N = 5$ degrees of freedom and $\gamma = 7/5 = 1.4$.

From Eqs. (148) and (149), one can express c_v and c_p in terms of γ:

$$\gamma \;=\; \frac{c_v + R}{c_v} \qquad \Longrightarrow \qquad c_v \;=\; \frac{1}{\gamma - 1} R \tag{150}$$

$$\gamma \;=\; \frac{c_p}{c_p - R} \qquad \Longrightarrow \qquad c_p \;=\; \frac{\gamma}{\gamma - 1} R \tag{151}$$

From Eq. (144), the incremental change in entropy ds in a gas is:

$$ds \;=\; \frac{du}{T} \,+\, \frac{p\,dv}{T}$$

$$\;=\; c_v \,\frac{dT}{T} \,+\, R\,\frac{dv}{v} \tag{152}$$

in which Eq. (152) used Eqs. (138) and (141).

Integrating Eq. (152), the change in entropy $s_2 - s_1$ when a gas moves from conditions with subscript 1 to conditions with subscript 2 is:

$$s_2 - s_1 \;=\; c_v \,\ln\!\left(\frac{T_2}{T_1}\right) \,+\, R\,\ln\!\left(\frac{v_2}{v_1}\right)$$

$$\;=\; c_v \,\ln\!\left(\frac{T_2}{T_1}\right) \,-\, R\,\ln\!\left(\frac{\rho_2}{\rho_1}\right) \tag{153}$$

Alternatively, Eq. (153) may be rewritten using $c_v = c_p - R$:

$$\begin{aligned} s_2 - s_1 &= c_p \ln\left(\frac{T_2}{T_1}\right) - R \ln\left(\frac{T_2}{T_1}\right) - R \ln\left(\frac{\rho_2}{\rho_1}\right) = c_p \ln\left(\frac{T_2}{T_1}\right) - R \ln\left(\frac{\rho_2 R T_2}{\rho_1 R T_1}\right) \\ &= c_p \ln\left(\frac{T_2}{T_1}\right) - R \ln\left(\frac{p_2}{p_1}\right) \end{aligned} \tag{154}$$

A very common condition is an adiabatic state, in which there is no heat added to or removed from a fluid–the fluid is not remotely heated by a laser, cooled by a refrigerator, heated by chemical or nuclear reactions inside or outside the fluid, etc. With no heat flow there is no entropy flow, so for an adiabatic fluid, the entropy change in Eqs. (153) and (154) is $s_2 - s_1 = 0$:

$$0 = c_v \ln\left(\frac{T_2}{T_1}\right) - R \ln\left(\frac{\rho_2}{\rho_1}\right) = c_p \ln\left(\frac{T_2}{T_1}\right) - R \ln\left(\frac{p_2}{p_1}\right) \tag{155}$$

Rearranging Eq. (155) yields several relations for adiabatic changes in a gas:

$$\frac{T_2}{T_1} = \left(\frac{\rho_2}{\rho_1}\right)^{R/c_v} = \left(\frac{\rho_2}{\rho_1}\right)^{\gamma-1} \tag{156}$$

$$\frac{T_2}{T_1} = \left(\frac{p_2}{p_1}\right)^{R/c_p} = \left(\frac{p_2}{p_1}\right)^{(\gamma-1)/\gamma} \tag{157}$$

$$\frac{p_2}{p_1} = \left(\frac{\rho_2}{\rho_1}\right)^{\gamma} \tag{158}$$

Equations (156) and (157) made use of Eqs. (150) and (151), and Eq. (158) was found by equating Eqs. (156) and (157) to eliminate the temperatures. Under such adiabatic conditions, the only temperature changes of the fluid are due to changes in its pressure and density, in accordance with the ideal gas law. Equation (158) may also be written as:

$$\frac{p}{\rho^\gamma} = \text{constant} \qquad \Longrightarrow \qquad dp = \gamma \frac{p}{\rho}\, d\rho \qquad \textbf{Adiabatic relation} \tag{159}$$

For an adiabatic fluid flow, the energy includes internal thermal energy ρu per volume, pressure energy p per volume, kinetic energy $\rho v^2/2$ per volume (v is velocity again from now on), and gravitational potential energy $\rho g H$ per volume (H is height) and is conserved:

$$\begin{aligned} \rho u + p + \frac{1}{2}\rho v^2 + \rho\, g\, H &= \text{total energy per volume} = \text{constant}, \quad \text{or} \\ u + \frac{p}{\rho} + \frac{1}{2} v^2 + g\, H &= \text{total energy per mass} = \text{constant}, \quad \text{or} \\ h + \frac{1}{2} v^2 + g\, H &= \text{total energy per mass} = \text{constant} \end{aligned} \tag{160}$$

Thus for a steady (not time-varying) adiabatic flow, the enthalpy, velocities, and heights at points 1 and 2 are related by

$$h_1 + \frac{v_1^2}{2} + g\, H_1 = h_2 + \frac{v_2^2}{2} + g\, H_2 \tag{161}$$

In other words, since there is no heat input in an adiabatic flow, the only energy sources available to change the enthalpy are the kinetic energy $v^2/2$ and the gravitational potential energy gH of the flow itself. Usually the gravitational term is negligible. If the flow slows down, the kinetic energy is converted to thermal energy and/or pressure energy contained within the enthalpy.

3.2 Atmospheric Pressure

A useful application of compressible fluid mechanics is to determine the variation of the earth's atmospheric pressure p and density ρ with height H above sea level. Neglecting all terms in Eq. (5) except $\nabla p = dp/dH$ and the gravitational term ρg, the pressure variation dp/dH is governed by the gravitational acceleration $g \approx 9.807$ m/sec^2 near the earth's surface and the local density of the atmosphere:

$$\frac{dp}{dH} \;=\; -\rho g \tag{162}$$

Using the ideal gas law from Eq. (138) for the atmosphere, with $R \approx 287$ J/(kg ^{o}K) for air, Eq. (162) becomes

$$\frac{dp}{dH} \;=\; -\frac{g}{RT}\,p \tag{163}$$

In the **isothermal atmosphere** approximation, T is a constant independent of the altitude. Integrating Eq. (163), one then finds that the atmospheric pressure and density decay exponentially with increasing altitude, starting from the sea level values $p_o \approx 1.013\times10^5$ Pa and $\rho_o \approx 1.225$ kg/m^3:

$$p \;=\; p_o\, e^{-H/H_o} \tag{164}$$

$$\rho \;=\; \rho_o\, e^{-H/H_o} \tag{165}$$

$$\text{where } H_o \;\equiv\; \frac{RT}{g} \;\approx\; 29.3\, T_{^o\mathrm{K}} \text{ m} \qquad \textbf{Atmospheric scale height} \tag{166}$$

For the temperature $T \approx 220$ ^{o}K typical of the upper atmosphere, the scale height is $H_o \approx 6.5$ km. Physically, higher air weighs on lower air, making it more dense, and all of that weighs even more on air below that, making the pressure and density vary exponentially in Eqs. (164) and (165).

Actually the atmospheric temperature does vary somewhat with altitude (Fig. 13), and the nonzero temperature gradient $dT/dH \equiv L$ is called the **lapse rate**. For a constant lapse rate, the temperature is

$$T \;=\; T_o \,+\, LH \tag{167}$$

Separating variables in Eq. (163) and integrating with the aid of Eq. (167) yields the pressure:

$$\int_{p_o}^{p} \frac{dp}{p} \;=\; -\frac{g}{R}\int_0^H \frac{dH}{T} \;=\; -\frac{g}{R}\int_0^H \frac{dH}{T_o + LH}$$

$$\Longrightarrow\quad p \;=\; p_o \left(\frac{T}{T_o}\right)^{-\frac{g}{LR}} \;=\; p_o \left(1 + \frac{LH}{T_o}\right)^{-\frac{g}{LR}} \tag{168}$$

The density may be obtained from Eq. (168) and the ideal gas law of Eq. (138):

$$\rho \;=\; \rho_o \,\frac{p}{p_o}\,\frac{T_o}{T} \;=\; \rho_o \left(1 + \frac{LH}{T_o}\right)^{-\frac{g}{LR}} \tag{169}$$

Yes Virginia, Eqs. (167)-(168) really do reduce to Eqs. (164)-(165) in the limit $L \to 0$.

By convention, the earth's atmosphere is usually divided into several layers. The **troposphere** is the lowest, extending from the ground up to $H \sim 10$ km. Because the ground is heated by the sun each day and then heats the troposphere via convection, the troposphere has a relatively large lapse rate, $L \approx -6.5$ ^{o}K/km on average, and can be described to a good approximation by Eqs.

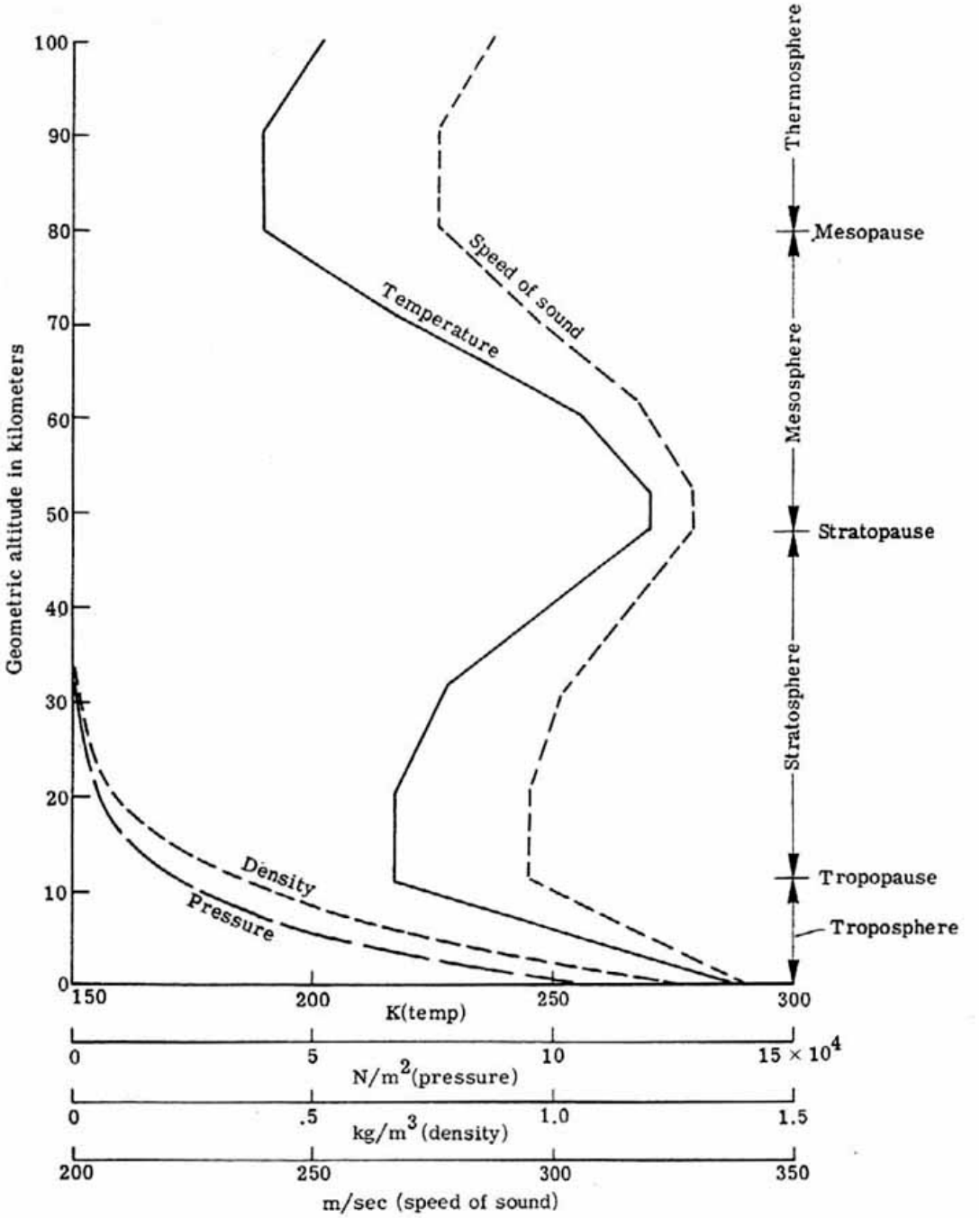

Figure 13. Pressure, density, temperature, speed of sound, and layers in the atmosphere. (1962 U.S. Standard Atmosphere graphed by NASA and in the public domain, from http://www.centennialofflight.gov/essay/Theories_of_Flight/atmosphere/TH1G1.htm.)

(167)-(169). The next layer, the **stratosphere**, extends from $\sim$ 10 km altitude up to $\sim$ 50 km. Temperatures vary fairly slowly with altitude in the stratosphere, so the exponential atmosphere approximation of Eqs. (164)-(165) is reasonable for high-altitude aircraft and spacecraft reentering the atmosphere. Higher layers of the atmosphere have very low densities, and their specific properties can vary significantly due to factors such as the charged particle flux arriving from space. These higher layers will not be discussed here. For more information on the atmosphere, see *Meteorology*.

3.3 Sound Waves and Acoustics

Waves may be either transverse (wiggling up and down or side to side relative to the direction the wave travels) or longitudinal (alternately stretched and compressed along the same axis the waves travel), as shown in Fig. 14. Compressible fluids can have sound waves, or longitudinal waves in which the particles of the fluid are alternately compressed and rarified. Generally fluids cannot wiggle themselves from side to side, so they cannot support transverse waves (except in cases in which there is some "connection" between the particles, as in highly viscous fluids, magnetofluids, electrically charged fluids or plasmas, or solid substances). **Acoustics** is the science of sound waves and will be briefly covered here. For more detailed coverage of the topic, see *Electromagnetism and Acoustics* ? or references [16]-[18].

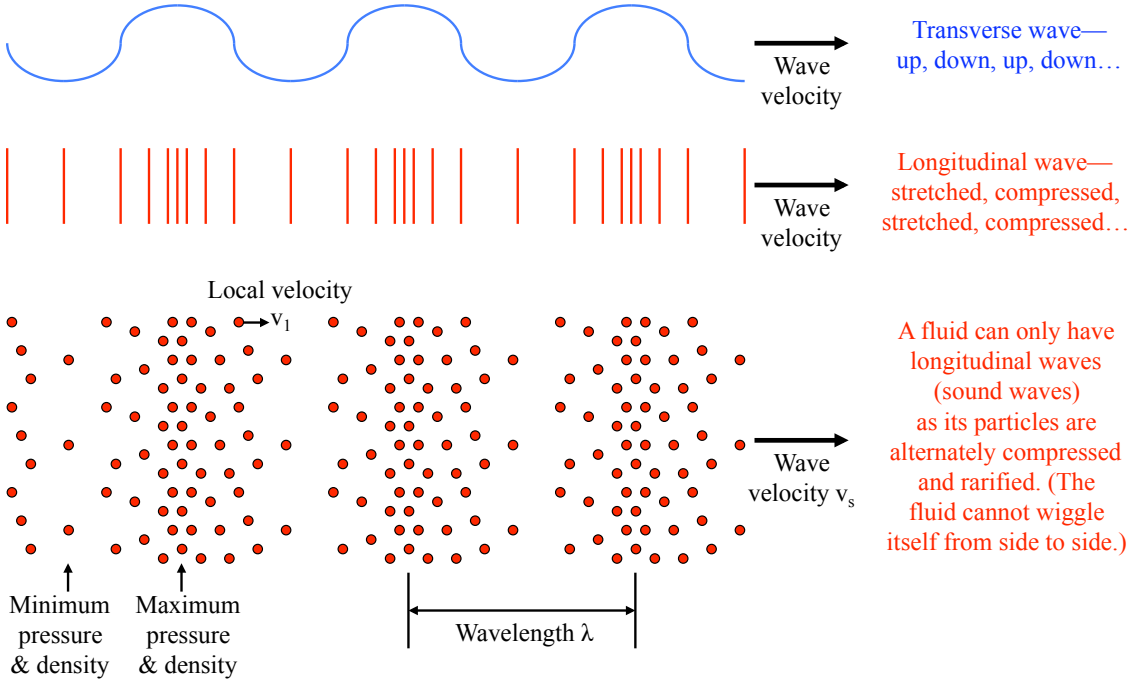

Figure 14. Waves may be transverse (wiggling up and down or side to side relative to the direction the wave travels) or longitudinal (being stretched and compressed in the direction the wave travels. Sound waves are longitudinal.

Fundamental Equations for Sound Waves

The full fluid equations describing sound waves are very complex and nonlinear, but may be greatly simplified and linearized assuming that the amplitudes and velocities of particle motion involved in the waves remain small. To linearize the equations, one can begin by assuming that the local pressure, density, and velocity in a fluid at a given position and time are the constant background values (denoted with a subscript 0) plus some small perturbation (denoted with a subscript 1):

$$p(\mathbf{x},t) = p_0 + p_1(\mathbf{x},t) \qquad p_1 \ll p_0 \tag{170}$$

$$\rho(\mathbf{x},t) = \rho_0 + \rho_1(\mathbf{x},t) \qquad \rho_1 \ll \rho_0 \tag{171}$$

$$\mathbf{v}(\mathbf{x},t) = 0 + \mathbf{v_1}(\mathbf{x},t) \qquad |\mathbf{v_1}| \ll v_s \tag{172}$$

Note that the uniform background fluid velocity is assumed to be zero, $\mathbf{v_0} = 0$, in Eq. (172). The back-and-forth velocity v_1 of particles in the fluid is assumed to be much less than the speed of sound waves v_s in the fluid, which we will derive very shortly.

Neglecting higher order terms containing two or more small perturbation factors, the linearized forms of Eqs. (3) for mass conservation, (5) for momentum conservation, and (159) for the adiabatic relation are:

$$\frac{\partial \rho_1}{\partial t} + \rho_0 \nabla \cdot \mathbf{v_1} \approx 0 \qquad \textbf{linearized continuity equation} \tag{173}$$

$$\frac{\partial \mathbf{v_1}}{\partial t} + \frac{\nabla p_1}{\rho_0} \approx 0 \qquad \textbf{linearized momentum equation} \tag{174}$$

$$p_1 \approx \gamma \frac{p_0}{\rho_0} \rho_1 \qquad \textbf{linearized adiabatic relation} \tag{175}$$

Taking the time derivative of Eq. (173) and the divergence of Eq. (174) [using $\nabla \cdot (\nabla p_1) = \nabla^2 p_1$], and combining the resulting equations with Eq. (175) leads to a wave equation:

$$\frac{\partial^2 p_1}{\partial t^2} = \gamma \frac{p_0}{\rho_0} \nabla^2 p_1 \tag{176}$$

$$= v_s^2 \nabla^2 p_1 \tag{177}$$

in which the speed of sound waves is:

$$v_s = \sqrt{\gamma \frac{p_0}{\rho_0}} = \sqrt{\gamma R T} \tag{178}$$

For air with $\gamma = 1.4$ and $R \approx 287$ J/(kg ^{o}K):

$$v_s \approx 331.3 \sqrt{1 + \frac{T_{\text{Celsius}}}{273}} \text{ m/sec} \tag{179}$$

At room temperature ($T \approx 25^o$C), the velocity of sound is

$$v_s \approx 346 \text{ m/sec} = 1246 \text{ km/hr} = 774 \text{ miles/hr} \tag{180}$$

The physical meaning of the wave equation in Eq. (177) is that energy can exist as kinetic energy (vibration back and forth of molecules in the fluid, introducing a $\partial/\partial t$ dependence) or potential energy (pressure of the fluid in compressed regions relative to that in neighboring rarified regions, introducing a ∇ dependence). Energy sloshes back and forth between the two different forms, creating a wave motion that propagates through the fluid away from its point of creation. This same physical insight shows that v_s in Eq. (177) is indeed the wave velocity, since it relates the number of wiggles per length on the right side of that equation to the number of wiggles per time on the left side.

Solutions of Eq. (177) are of the form

$$p_1 = \text{Re}\{P_1 \exp[\pm i(\mathbf{k} \cdot \mathbf{x} - \omega t)]\}$$

$$= \text{Re}\{P_1 [\cos(\mathbf{k} \cdot \mathbf{x} - \omega t) \pm i \sin(\mathbf{k} \cdot \mathbf{x} - \omega t)]\} \qquad \textbf{Wave solution} \tag{181}$$

in which $\mathbf{k}$ is the wavevector and ω is the angular frequency of the wave. Re in Eq. (181) means to take only the real part of this complex expression, to avoid ascribing imaginary values to physical quantities. Usually scientists are too lazy to explicitly write the Re. In practice the final solution usually boils down to a simple sine or cosine. If you stand in one spot, you can ignore spatial variations and just watch the amplitude of a wave oscillate back and forth with time.

Plugging the solution from Eq. (181) into Eq. (177) yields

$$v_s k \;=\; \omega\,, \qquad \text{or} \qquad f\lambda \;=\; v_s \qquad\qquad \textbf{Simple dispersion relation} \tag{182}$$

where $\lambda = 2\pi/k$ is the wavelength (in meters) and $f = \omega/2\pi$ is the frequency of the wave (in cycles per second or Hertz, Hz). For sound waves of reasonable amplitude in air, waves of all frequencies travel at the same velocity v_s. For very large amplitudes or in certain media, nonlinearities that we have ignored in our linearized derivation of sound waves become important, and different frequencies travel at different velocities, leading to dispersion or separation of waves of different frequencies that originate from the same source.

Using Eqs. (181) and (182), Eq. (174) gives the back-and-forth perturbation velocity v_1 in terms of the perturbation wave pressure p_1:

$$v_1 \;=\; \frac{p_1}{(\omega/k)\rho_0} \;=\; \frac{p_1}{v_s\rho_0} \tag{183}$$

The quantity $v_s\rho_0$ that appears in Eq. (183) and will recur again is called the **acoustic impedance**. It has units of kg/(m^2 sec) or Pa sec/m. For air at standard temperature and pressure, the acoustic impedance is

$$v_s\rho_0 \;\approx\; \left(346\,\frac{\text{m}}{\text{sec}}\right)\left(1.23\,\frac{\text{kg}}{\text{m}^3}\right) \;\approx\; 425\,\frac{\text{Pa sec}}{\text{m}} \tag{184}$$

The **displacement** or back-and-forth distance that particles within the wave travel is

$$\Delta x \;\approx\; \frac{v_1}{\omega} \;=\; \frac{p_1}{\omega v_s\rho_0} \tag{185}$$

Using Eq. (178), Eq. (175) gives the perturbation density ρ_1 in terms of the perturbation pressure p_1:

$$\rho_1 \;=\; \frac{p_1}{v_s^2} \tag{186}$$

Loudness

Since power is force times velocity, the intensity I or power per area of a sound wave is the wave's force per area (perturbation pressure p_1) times its perturbation velocity v_1:

$$I(t) \;=\; p_1 v_1 \;=\; \frac{p_1^2}{v_s\rho_0} \;=\; v_s\rho_0\, v_1^2 \tag{187}$$

The intensity fluctuates as waves pass. Averaging over the wave cycle, the average intensity is

$$\langle I\rangle \;=\; \frac{\langle p_1^2\rangle}{v_s\rho_0} \;=\; v_s\rho_0\left\langle v_1^2\right\rangle \tag{188}$$

Averaging over a sinusoidal wave such as Eq. (181) gives

$$\left\langle p_1^2\right\rangle \;=\; \frac{1}{2}P_1^2 \tag{189}$$

In other words, the root-mean-squared pressure is $1/\sqrt{2}$ of the peak wave pressure, $\langle p_1^2\rangle^{1/2} = P_1/\sqrt{2}$. Likewise, the root-mean-squared perturbation velocity is $1/\sqrt{2}$ of the peak perturbation velocity, $\langle v_1^2\rangle^{1/2} = V_1/\sqrt{2}$. By convention, usually the root-mean-squared values are cited for sound waves.

As an example, the approximate lower limit of human hearing is $\langle I \rangle \approx 10^{-12}$ W/m^2. From Eq. (188), this corresponds to a wave pressure of $\langle p_1^2 \rangle^{1/2} = \sqrt{v_s \rho_0 \langle I \rangle} \approx 2.0 \times 10^{-5}$ Pa. From Eq. (186), the corresponding perturbation density is $\langle \rho_1^2 \rangle^{1/2} = \langle p_1^2 \rangle^{1/2} / v_s^2 \approx 1.7 \times 10^{-10}$ kg/m^3. From Eq. (183), the corresponding perturbation velocity is $\langle v_1^2 \rangle^{1/2} = \langle p_1^2 \rangle^{1/2} / (v_s \rho_0) \approx 4.7 \times 10^{-8}$ m/sec. For a sound wave of frequency $f = 1$ kHz or $\omega = 2\pi f \approx 6280$ sec^{-1}, the distance traveled by particles in the wave is $\Delta x \approx v_1 / \omega \approx 7.5 \times 10^{-12}$ m, or less than the width of an atom ($\sim 10^{-10}$ m). Thus the conditions from Eqs. (170)-(172) that $p_1 \ll p_0$, $\rho_1 \ll \rho_0$, and $v_1 \ll v_s$ are easily fulfilled; the sound wave is an extremely small perturbation of the background fluid values.

To consider sound waves of other intensities, it is customary to use the sound pressure level (SPL) or loudness of a sound wave, which is defined as:

$$SPL \equiv 10 \log_{10} \left(\frac{\langle I \rangle}{10^{-12} \text{ W/m}^2} \right) \text{ dB} = 20 \log_{10} \left(\frac{\langle p_1^2 \rangle^{1/2}}{2 \times 10^{-5} \text{ Pa}} \right) \text{ dB} \tag{190}$$

in which the sound pressure level is given in units of decibels (dB). By convention, the lower limit of human hearing (10^{-12} W/m^2 of power or 2×10^{-5} Pa of pressure) is chosen as 0 dB. A sound that has 10 times more loudness or intensity (or $\sqrt{10} \approx 3.16$ times more pressure) than that would be 10 dB, a sound 100x louder would be 20 dB, a sound 1000x louder would be 30 dB, and so forth. Table 3 lists the loudness levels of a variety of sound sources. The human ear can perceive sound over a wide range and generally works in a logarithmic fashion, for example easily perceiving that one sound is 10x or 100x louder than another, but not readily detecting that one sound is 1.2x louder than another. Continuous exposure to sounds above ~ 85 dB can cause hearing loss in people. Sound becomes physically painful around 130 dB or so.

Note that for the loudest sounds listed in Table 3, the root-mean-squared perturbation pressure and density are significant fractions of the normal background atmospheric pressure $p_0 \approx 1.0 \times 10^5$ Pa and density $\rho_0 \approx 1.2$ kg/m^3, and the root-mean-squared perturbation velocity is a significant fraction of the speed of sound $v_s \approx 346$ m/sec. (Remember also that the peak values are $\sqrt{2}$ larger than the root-mean-squared values.) For waves that are even louder or stronger than these, Eqs. (170)-(172) underlying the derivation of sound waves break down, and the waves must be treated as shock waves as will be shown in Section 3.5, instead of simple sound waves. Note too that for the loudest sounds listed in Table 3, the displacement is measured in millimeters or centimeters; thus sufficiently loud sound waves or shock waves can produce such large vibrations that they can do physical damage even to structures that are much more resilient than the human ear.

Many sound sources can be approximated as point sources with sound waves propagating spherically outward in all directions from the origin. Since the wave intensity is the total power emitted divided by the expanding surface area $4\pi r^2$ as the wave travels a distance r from the origin, the intensity of a spherical sound wave is

$$\langle I \rangle = \frac{\text{Power}}{4\pi r^2} \tag{191}$$

Whereas the intensity drops as $1/r^2$, from Eqs. (191) and (188), the wave pressure drops as $1/r$:

$$\left\langle p_1^2 \right\rangle^{1/2} = \sqrt{\frac{v_s \rho_0 \text{ Power}}{4\pi}} \frac{1}{r} \tag{192}$$

Sound source (and distance)	**Loudness** SPL (dB)	**Intensity** $\langle I \rangle$ (W/m^2)	**Pressure** $\langle p_1^2 \rangle^{1/2}$ (Pa)	**Density** $\langle \rho_1^2 \rangle^{1/2}$ (kg/m^3)	**Velocity** $\langle v_1^2 \rangle^{1/2}$ (m/sec)	**Displacement** Δx (m) at 1 kHz
Mosquito (3 m)	0	10^{-12}	2.0×10^{-5}	1.7×10^{-10}	4.7×10^{-8}	7.5×10^{-12}
Breathing (3 m)	10	10^{-11}	6.3×10^{-5}	5.1×10^{-10}	1.5×10^{-7}	2.4×10^{-11}
Leaves rustling	20	10^{-10}	2.0×10^{-4}	1.7×10^{-9}	4.7×10^{-7}	7.5×10^{-11}
Empty auditorium	30	10^{-9}	6.3×10^{-4}	5.1×10^{-9}	1.5×10^{-6}	2.4×10^{-10}
Outside at night	40	10^{-8}	2.0×10^{-3}	1.7×10^{-8}	4.7×10^{-6}	7.5×10^{-10}
Quiet restaurant	50	10^{-7}	6.3×10^{-3}	5.1×10^{-8}	1.5×10^{-5}	2.4×10^{-9}
Normal conversation	60	10^{-6}	2.0×10^{-2}	1.7×10^{-7}	4.7×10^{-5}	7.5×10^{-9}
Automobile traffic	70	10^{-5}	6.3×10^{-2}	5.1×10^{-7}	1.5×10^{-4}	2.4×10^{-8}
Vacuum cleaner	80	10^{-4}	2.0×10^{-1}	1.7×10^{-6}	4.7×10^{-4}	7.5×10^{-8}
Noisy factory	90	10^{-3}	6.3×10^{-1}	5.1×10^{-6}	1.5×10^{-3}	2.4×10^{-7}
Power tools (1 m)	100	10^{-2}	2	1.7×10^{-5}	4.7×10^{-3}	7.5×10^{-7}
Motorcycle (5 m)	110	10^{-1}	6.3	5.1×10^{-5}	1.5×10^{-2}	2.4×10^{-6}
Rock concert	120	1	20	1.7×10^{-4}	4.7×10^{-2}	7.5×10^{-6}
Jackhammer (2 m)	130	10^{1}	63	5.1×10^{-4}	1.5×10^{-1}	2.4×10^{-5}
Jet engine (3 m)	140	10^{2}	2.0×10^{2}	1.7×10^{-3}	4.7×10^{-1}	7.5×10^{-5}
Handgun (1 m)	150	10^{3}	6.3×10^{2}	5.1×10^{-3}	1.5	2.4×10^{-4}
Hammer/anvil (1 m)	160	10^{4}	2.0×10^{3}	1.7×10^{-2}	4.7	7.5×10^{-4}
Large gun (1 m)	170	10^{5}	6.3×10^{3}	5.1×10^{-2}	15	2.4×10^{-3}
Rocket launch	180	10^{6}	2.0×10^{4}	1.7×10^{-1}	47	7.5×10^{-3}
Cannon	190	10^{7}	6.3×10^{4}	5.1×10^{-1}	150	2.4×10^{-2}

Table 3. Loudness, intensity, root-mean-squared perturbation pressure, root-mean-squared perturbation density, root-mean-squared perturbation velocity, and displacement for sound waves from various sources.

Frequencies

The human ear can detect sound waves with frequencies ranging from roughly 20 Hz to roughly 20 kHz (20,000 Hz) [*Neuroscience and Sensory-Motor Systems* ?.?]. Frequencies lower than this range are called infrasound or infrasonic and can be detected by some animals such as whales and elephants, while frequencies above the range of human hearing are called ultrasound or ultrasonic and can be detected by dogs, bats, and other animals. As humans age, sensitivity to the highest frequencies decreases, and the upper limit of detection in most adults is more like ~ 15 kHz or so.

On the musical scale, the note middle C (often designated C_4, using subscripts to denote octaves) has a frequency of 261.63 Hz. Each octave increases or decreases the frequency by a factor of 2; for example, the first C below middle C (C_3) has a frequency of 130.81 Hz, and the first C above middle C (C_5) has a frequency of 523.25 Hz. Since the same letter notes of different octaves are harmonics that are multiples of the same frequency, they sound "similar" despite their differences in pitch. There are 12 notes per octave: C, C♯/D♭, D, D♯/E♭, E, F, F♯/G♭, G, G♯/A♭, A, A♯/B♭, and B. If the notes are evenly spaced (the equal temperament system of tuning), each note is a factor of $2^{1/12} \approx 5.95\%$ higher in frequency than the preceding note. Usually the frequencies of the other notes are fixed by setting A_4, the A above middle C, to exactly 440 Hz, sometimes called a "Concert A." Standard 88-key pianos produce notes ranging from 27.5 Hz (A_0) to 4186 Hz (C_8).

Musical instruments produce sound waves in various ways. Stringed instruments such as pianos, guitars, and violins excite vibrations in strings of different lengths to produce different frequencies; the strings then vibrate the surrounding air to produce sound waves. Drums, cymbals, and xylophones excite vibrations in solid surfaces, which then vibrate the surrounding air. In woodwind reed instruments such as clarinets and saxophones, a vibrating reed produces numerous frequencies, and valves adjust the length of a resonant cavity of air to amplify one specific resonant frequency. Brass instruments such as trumpets, trombones, and tubas do the same thing using the vibrations of the player's lips instead of the vibrations of a reed. Reedless woodwind instruments like flutes also do the same thing, except blowing across an opening directly induces resonant vibrations inside a cavity of air, instead of requiring initial vibrations of a reed or the player's lips.

Vibrations in strings, solid surfaces, or air-filled tubes of given sizes have resonant frequencies that depend on the size of the vibrating structure. For simplicity, we will focus on air-filled tubes such as woodwind or brass instruments here, but similar principles apply to other vibrating structures. (For more information on vibrations in strings and surfaces, see *Classical Mechanics* ?.?.) Sound waves can travel through an air-filled tube, strike the end of the tube and reflect, travel the other way, reflect from the other end, and repeat the process. Constructive and destructive interference between waves traveling in each direction creates **standing waves** such as those illustrated in Fig. 15 for tubes of length L. As the name suggests, standing waves appear to stand in place instead of traveling back and forth. Standing waves are always wiggling back and forth to the maximum possible extent at **antinodes** and not wiggling at all at **nodes**. A closed end of a tube must be a node for displacement (physical motion of the air due to the wave), since no displacement is possible at the end wall of the tube. In contrast, an open end of a tube is an antinode for displacement; the air there is free to wiggle as much as it wants, so it wiggles to the maximum extent possible.

If the standing sound wave is viewed in terms of pressure instead of displacement, the antinodes and nodes are reversed–displacement nodes are pressure antinodes (all the wave energy locally is in the form of potential energy of pressure instead of kinetic energy of displacement wiggling), and displacement antinodes are pressure nodes (all the wave energy locally is in the form of kinetic energy of displacement wiggling instead of potential energy of pressure).

In order to satisfy the constraints at the tube ends, if both ends of a tube are closed as in Fig. 15(a) or if both ends are open as in Fig. 15(b), the relationship between the tube length L and the standing wave wavelength λ_n must be $L = n\lambda_n/2$, where n may be 1, 2, 3, 4, etc. Standing waves with different values of n are called different **modes**. The standing wave with the lowest value of n ($n = 1$) is called the **fundamental mode**. Using the velocity of sound v_s, the frequency $f_n = v_s/\lambda_n$ of each mode is:

$$f_n = \frac{nv_s}{2L} \qquad n = 1,\ 2,\ 3,\ 4,\ \text{etc.} \tag{193}$$

In Eq. (193), note that tubes with longer lengths L can support longer wavelengths and hence have lower frequencies. Of all the possible modes, the fundamental mode has the longest wavelength and lowest frequency.

Similarly, if a tube has one end closed and one end open as in Fig. 15(c), the relationship between the tube length and the standing wave wavelength must be $L = n\lambda_n/4$, where n is limited to only odd mode numbers of 1, 3, 5, 7, etc. The frequency of each mode $f_n = v_s/\lambda_n$ is then:

$$f_n = \frac{nv_s}{4L} \qquad n = 1,\ 3,\ 5,\ 7,\ \text{etc.} \tag{194}$$

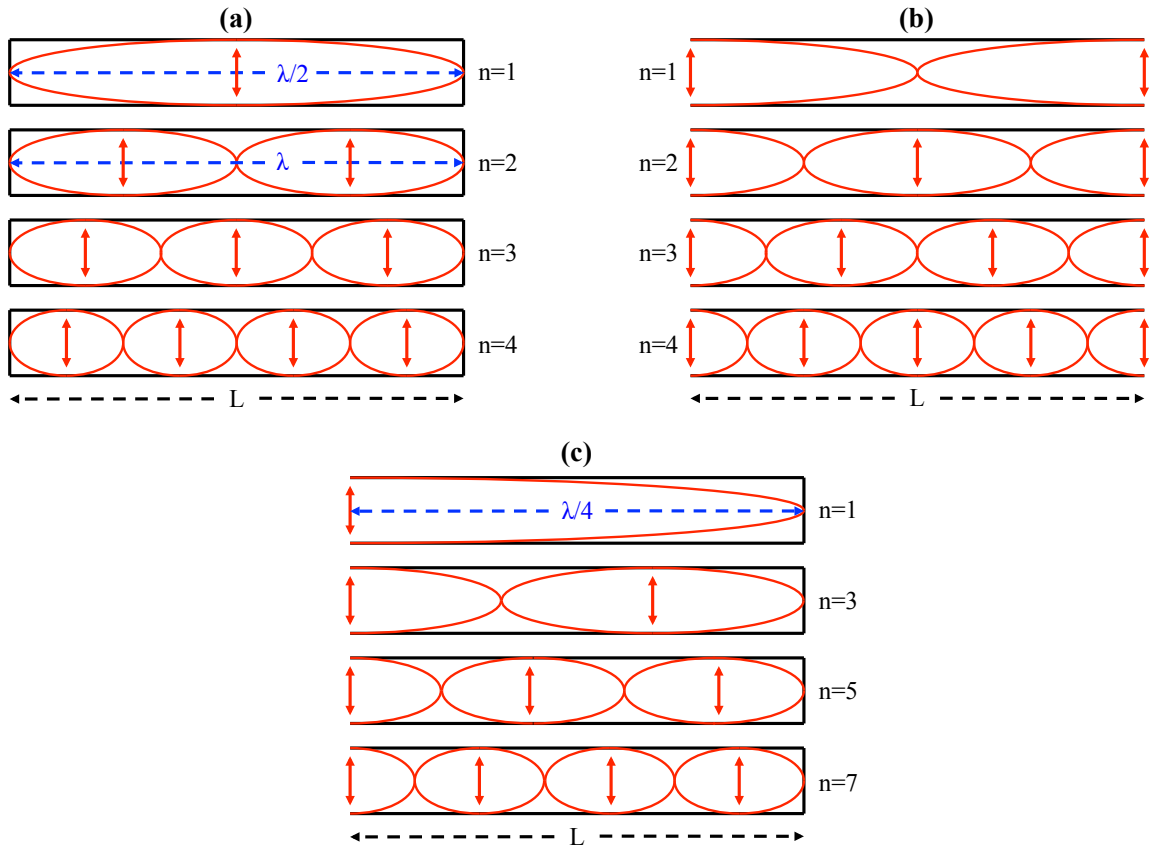

Figure 15. Standing waves with different mode numbers n in tubes of length L with (a) both ends closed, (b) both ends open, or (c) one end closed and one end open. The waves schematically illustrate antinodes (maximum wiggling) and nodes (zero wiggling) for displacement. For pressure instead of displacement, the antinodes and nodes would be reversed. The waves are shown as transverse only for purposes of easy visualization. In reality the waves are longitudinal along the length of the tubes.

As a concrete example, consider the human voice. The vocal cords or vocal folds are membranes in the larynx that can vibrate when air is expelled from the lungs. The vibrating membranes vibrate the air to create sound waves, which can be adjusted by the muscles and structures in the larynx and mouth to create a wide range of frequencies and sounds. For simple estimates, the human throat and mouth can be approximated as a tube that is open at the mouth and closed at the vocal cord end. Using Eq. (194), assuming this tube has a length $L \approx 0.16$ m, and using $v_s \approx 340$ m/sec for the speed of sound, the frequency of the fundamental mode in this system is:

$$f_1 \;=\; \frac{v_s}{4L} \;\approx\; 530 \text{ Hz} \tag{195}$$

This estimate is indeed in the right ballpark. Speaking and singing voices are generally in the range of $\sim 80 - 520$ Hz for adult men and $\sim 180 - 1100$ Hz for adult women.

Doppler Shift

The perceived frequency shift when an observer is moving toward or away from a sound source such as a siren or car horn is called the **Doppler shift**. Whereas there is no special frame of reference for special relativity or Doppler shifts of electromagnetic waves, for sound waves there is a special frame of reference, one in which the fluid through which the sound waves are propagating is at rest. The Doppler shift of sound waves is somewhat different depending on whether the sound source and/or observer are moving, as shown in Fig 16.

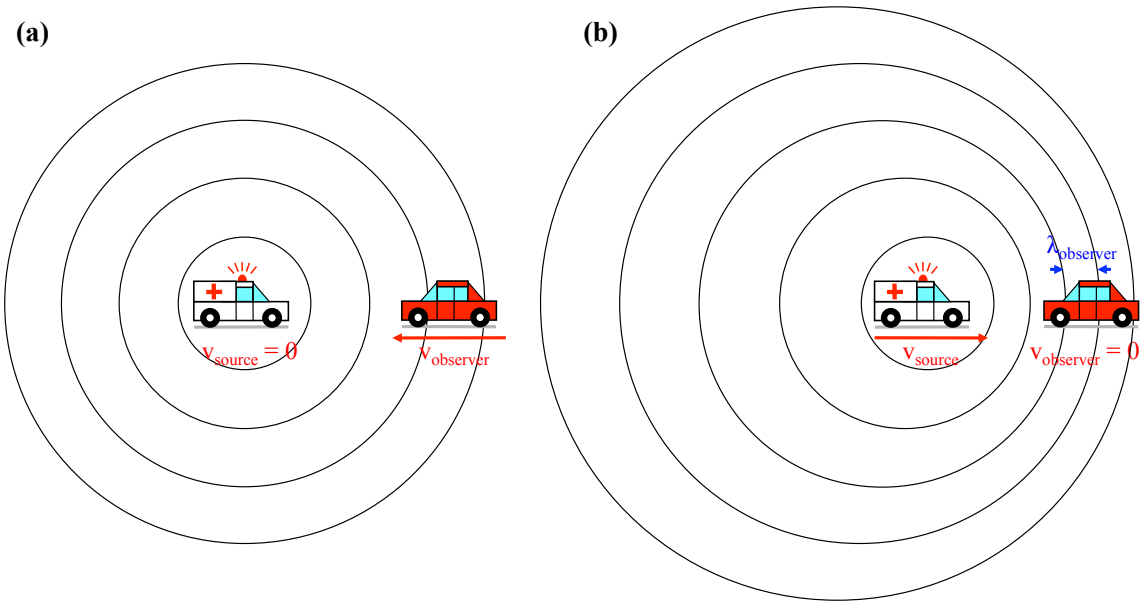

Figure 16. Doppler shift (a) when the sound source is motionless and the observer is moving, and (b) when the sound source is moving and the observer is motionless.

First consider the case in which the sound source is motionless and the observer is moving, as shown in Fig. 16(a). If the observer is moving toward the source at a velocity v_{observer} relative to the medium, the observer will encounter waves $1 + v_{\text{observer}}/v_s$ more often than if the observer were motionless and waited for the waves to arrive due solely to their own velocity v_s. Thus compared to the frequency f_{source} emitted by the source, the apparent acoustic frequency f_{observer} perceived by the observer is:

$$f_{\text{observer}} = f_{\text{source}}\left(1 + \frac{v_{\text{observer}}}{v_s}\right) = f_{\text{source}}\left(\frac{v_s + v_{\text{observer}}}{v_s}\right) \tag{196}$$

Now consider the case in which the observer is motionless and the sound source is moving, as illustrated in Fig. 16(b). If the source is moving toward the observer at a velocity v_{source} relative to the medium, the wavelength of sounds emitted toward the observer will be $\lambda_{\text{observer}} = (v_s - v_{\text{source}})/f_{\text{source}}$. Thus the frequency f_{observer} perceived by the observer is:

$$f_{\text{observer}} = \frac{v_s}{\lambda_{\text{observer}}} = f_{\text{source}}\left(\frac{v_s}{v_s - v_{\text{source}}}\right) \tag{197}$$

For the more general case in which the source and/or observer are moving, Eqs. (196) and (197) can be combined into one equation:

$$f_{\text{observer}} = f_{\text{source}} \left(\frac{v_s + v_{\text{observer}}}{v_s - v_{\text{source}}} \right) \tag{198}$$

The velocities v_{source} and v_{observer} are defined to be positive if they bring the source and observer closer together, and negative if they move the source and observer further apart. When the source and observer are getting closer, waves appear to be closer together, and the observed frequency f_{observer} is higher than the source frequency f_{source}. When the source and observer are moving further apart, the waves appear to be stretched out, and the observed frequency is lower than the source frequency. Equation (198) is not valid if the source and/or observer velocities are larger than the speed of sound (Section 3.9).

When the source and observer velocities are much smaller than the velocity of sound, $v_{\text{source}} \ll v_s$ and $v_{\text{observer}} \ll v_s$, Eq. (198) takes an approximate form which is more intuitive and more symmetrical between the source and the observer:

$$f_{\text{observer}} \approx f_{\text{source}} \left(1 + \frac{v_{\text{observer}}}{v_s} + \frac{v_{\text{source}}}{v_s} \right) \tag{199}$$

Because electromagnetic waves do not require a medium in which to propagate and thus do not have any special frame of reference, the equation for Doppler shifts of electromagnetic waves is somewhat different than that for sound waves in Eq. (198), although the physical reasoning and net effect are similar. See *Electromagnetism and Acoustics* ?.? for more information.

Acoustic Waves in Liquids, Solids, and Plasmas

For longitudinal compressional waves in a liquid or solid, the effective compressibility γp_0 of the gas in Eq. (178) is replaced with the compressibility $E = -dp\, V/dV$ of the material (pressure change dp due to change dV in the volume V), which is variously called the bulk, elastic, or Young's modulus:

$$v_s = \sqrt{\frac{E}{\rho}} \tag{200}$$

Propagation of sound waves in water is very important for sonar. For water with a bulk modulus of $E \approx 2.2 \times 10^9$ Pa and density $\rho \approx 1000$ kg/m^3, the speed of sound is $v_s \approx 1500$ m/sec, or approximately 4.5 times the speed of sound in air. Of course, the precise speed of sound in water will depend on the salt content, temperature and pressure. For more information, see *Oceanography* ?.? and the analogies between sonar and radar in *Electromagnetism and Acoustics* ?.?.

Likewise, propagation of sound waves in the earth is very important for seismology and geophysics. Although there is considerable variation from the earth's crust to the earth's core, representative values $E \approx 7 \times 10^{11}$ Pa and $\rho \approx 5500$ kg/m^3 yield an estimated speed of sound $v_s \approx 11,000$ m/sec. More detailed calculations find speeds of approximately 6000 m/sec in the earth's crust and 13,000 m/sec in the core. For more information, see *Geology* ?.?.

For steel with $E \approx 2 \times 10^{11}$ Pa and $\rho \approx 8000$ kg/m^3, the speed of sound is $v_s \approx 5000$ m/sec.

In solids (or even in fluids with enough viscosity), atoms can wiggle both parallel and perpendicular to the direction of motion of a wave, creating both conventional longitudinal and novel transverse (or shear) acoustic waves. Like the longitudinal waves just considered, transverse acoustic waves are also important in seismology and geophysics (*Geology* ?.?).

At a microscopic scale, acoustic waves, especially those in solid lattices such as metals and semiconductors, are often called phonons. An acoustic wave can be regarded as being composed of individual particles of wave energy or phonons, just as electromagnetic waves can be regarded as being composed of individual particles of wave energy or photons. For information on phonons, see *Solid State Physics* 3.

A plasma is a fluid that has so much energy that its atoms ionize, so the fluid has both positively charged ions and negatively charged free electrons. A wide variety of waves can occur in plasmas, and their behavior is complicated by the fact that the charged ions and electrons in the plasmas respond to electric and magnetic fields that they generate or that are applied externally. For information on plasma waves, see *Plasma Physics and Fusion* 4.

Mach Number and Compressibility

The Mach number of an object traveling at velocity v through a stationary fluid (or equivalently of a fluid flowing at velocity v past a stationary object) is defined as the ratio of the velocity to the speed of sound:

$$M \equiv \frac{v}{v_s} \tag{201}$$

One can use the Mach number to judge whether a fluid may be regarded as incompressible (as in Sections 1-2) or whether compressibility effects must be considered (as in this section).

By combining Eqs. (159) and (178), a change in pressure Δp induces a corresponding adiabatic change in fluid density $\Delta\rho$:

$$\Delta p = v_s^2 \, \Delta\rho \tag{202}$$

Assuming for the moment that compressibility effects are negligible, Eq. (10) gives the pressure change produced by fluid flow at a velocity v impacting on an object and decelerating:

$$\Delta p = \rho \frac{v^2}{2} \tag{203}$$

Combining Eqs. (202) and (203), the relative change in the fluid density upon deceleration, as a function of its initial velocity, is

$$\frac{\Delta\rho}{\rho} = \frac{1}{2}\left(\frac{v}{v_s}\right)^2 = \frac{1}{2} M^2 \tag{204}$$

At half the speed of sound, $M = 0.5$, Eq. (204) predicts a relatively small change in fluid density, $\Delta\rho/\rho = 12.5\%$. The change is this small because the effect varies as the square of the velocity or Mach number, as shown in Eq. (204). Thus for velocities not approaching or exceeding the speed of sound, fluid compressibility effects are small and the results of Sections 1-2 are fairly accurate.

However, as the velocity approaches the speed of sound, $M \to 1$, the relative change in the fluid density becomes quite large, $\Delta\rho \sim \rho/2$, as shown by Eq. (204). Of course, under these conditions the assumption of incompressibility underlying Eq. (203) in the derivation breaks down, so Eq. (204) is just a ballpark estimate. [A more accurate expression will be derived shortly in Eq. (209).] Nonetheless, it is clear that the fluid becomes highly compressed at velocities approaching the speed of sound.

3.4 Compressible Flow in Ducts

This section will analyze compressible, inviscid flow through a long duct in which the cross-sectional area A may change. For simplicity, only flow along the duct will be considered, making the problem essentially one-dimensional. We will derive relations for several cases: (a) stagnation flow in which an initially moving flow is decelerated to zero velocity downstream, (b) flow through a duct in which the cross-sectional area A increases or decreases along the length of the duct, (c) compressible flow in an isothermal pipe, and (d) compressible flow in an adiabatic pipe.

(a) Stagnation flow and properties

If fluid flow with initial enthalpy $h = c_pT$ and initial velocity v is adiabatically decelerated until its downstream velocity is zero, the flow is said to be stagnant, and its properties are then the **stagnation conditions** denoted with subscript "o." From Eq. (161), the stagnation enthalpy is

$$h_o = h + \frac{v^2}{2} \tag{205}$$

The stagnation enthalpy in Eq. (205) is simply $h_o = c_pT_o$, so the stagnation temperature T_o is:

$$c_pT_o = c_pT + \frac{v^2}{2} \tag{206}$$

$$\frac{T_o}{T} = 1 + \frac{v^2}{2c_pT} = 1 + \frac{\gamma-1}{2}M^2 \tag{207}$$

in which Eq. (207) used Eqs. (151), (178), and (201). In other words, when the flow is decelerated to zero velocity, all of its initial kinetic energy becomes extra thermal energy to heat the flow to the stagnation temperature T_o.

From Eqs. (157) and (207), the corresponding stagnation pressure is:

$$\frac{p_o}{p} = \left(\frac{T_o}{T}\right)^{\gamma/(\gamma-1)} = \left(1 + \frac{\gamma-1}{2}M^2\right)^{\gamma/(\gamma-1)} \tag{208}$$

Likewise, from Eqs. (156) and (207), the corresponding stagnation density is:

$$\frac{\rho_o}{\rho} = \left(\frac{T_o}{T}\right)^{1/(\gamma-1)} = \left(1 + \frac{\gamma-1}{2}M^2\right)^{1/(\gamma-1)} \tag{209}$$

Note that for $M \ll 1$, Eq. (209) reduces to $\rho_o/\rho \approx 1 + (\gamma-1)M^2/[2(\gamma-1)] = 1 + M^2/2$, in agreement with Eq. (204). Note also that for Mach 1 in air with $\gamma = 1.4$, the exact Eq. (209) predicts a density difference $\Delta\rho/\rho = (\rho_o - \rho)/\rho \approx 0.577$, so the estimate of 0.50 from Eq. (204) is not far off, even at $M = 1$.

Equations (207)-(209) are simplified when the initial flow is sonic, $M = 1$. When the flow is sonic, its temperature, pressure, and density are called the **critical** values and are denoted with asterisks. The ratios of the stagnation and critical values of temperature, pressure, and density are:

$$\frac{T_o}{T_*} = \frac{\gamma+1}{2} \tag{210}$$

$$\frac{p_o}{p_*} = \left(\frac{\gamma+1}{2}\right)^{\gamma/(\gamma-1)} \tag{211}$$

$$\frac{\rho_o}{\rho_*} = \left(\frac{\gamma+1}{2}\right)^{1/(\gamma-1)} \tag{212}$$

Equations (207)-(212) are building blocks of much scarier compressible flow equations to come.

(b) Flow through a duct of changing cross-sectional area

If the duct area changes by an amount dA as the flow moves from one region to another, the fluid density ρ will change by an amount $d\rho$, the fluid velocity v will change by an amount dv, and the fluid pressure p will change by an amount dp. We will combine three different equations to find how the change in cross-sectional area affects these other quantities.

The first equation is mass conservation, which requires the mass flow rate $\dot{m} = \rho\, v\, A$ to be constant. Differentiating the mass conservation equation yields a new form for that relation:

$$\dot{m} = \rho\, v\, A = \text{constant} \qquad \Longrightarrow \qquad d\rho\, v\, A + \rho\, dv\, A + \rho\, v\, A = 0$$

$$\Longrightarrow \qquad \frac{d\rho}{\rho} + \frac{dv}{v} + \frac{dA}{A} = 0 \tag{213}$$

The second equation is momentum conservation as expressed in the form of the Bernoulli equation from Eq. (10). Differentiating that yields:

$$p + \frac{1}{2}\rho\, v^2 = \text{constant} \qquad \Longrightarrow \qquad dp + \rho\, v\, dv = 0$$

$$\Longrightarrow \qquad \frac{dp}{\rho} + v\, dv = 0 \tag{214}$$

The third equation is the adiabatic relation from Eq. (159) using the speed of sound speed v_s:

$$dp = \gamma \frac{p}{\rho}\, d\rho \qquad\qquad v_s = \sqrt{\gamma \frac{p}{\rho}}$$

$$\Longrightarrow \qquad dp = v_s^2\, d\rho \tag{215}$$

Combining Eqs. (213)-(215) produces the **area-velocity relation**:

$$\frac{dv}{v} = -\frac{dp}{\rho v^2} = \frac{dA}{A}\,\frac{1}{M^2-1} \qquad \textbf{Area-velocity relation} \tag{216}$$

in which the Mach number is $M = v/v_s$ as usual.

Since $M^2 - 1$ appears in the denominator in Eq. (216), the area-velocity relation describes three different cases:

- **Subsonic flow**, $M < 1$. In a diverging duct ($dA > 0$), subsonic flow is decelerated ($dv < 0$) and pressurized ($dp > 0$), as in the case of the subsonic diffuser in Fig. 17(a). In a converging duct ($dA < 0$), subsonic flow is accelerated ($dv > 0$) and depressurized ($dp < 0$), as in the subsonic nozzle shown in Fig. 17(b).

- **Sonic flow**, $M = 1$. If the flow is exactly sonic ($M^2 - 1 = 0$), the area must remain constant, $dA = 0$, to keep Eq. (216) from blowing up. This must occur in a throat [Fig. 17(c)] that conveys flow from a converging section, which accelerates subsonic flow toward v_s or decelerates supersonic flow toward v_s, to a diverging section, which accelerates supersonic flow away from v_s or decelerates subsonic flow away from v_s. A constant-area bulge that conveys flow from a diverging section to a converging section could not have sonic flow; the diverging section would decelerate subsonic flow or accelerate supersonic flow away from v_s. Note that while sonic flow can only occur in a throat, flow through a throat need not be only sonic. If $dA = 0$ in Eq. (216), the Mach number can be less than or greater than 1 if $dv = 0$, or the throat has a constant-velocity subsonic or supersonic flow.

- **Supersonic flow**, $M > 1$. In a diverging duct ($dA > 0$), supersonic flow is accelerated ($dv > 0$) and depressurized ($dp < 0$), as in the supersonic nozzle in Fig. 17(d). In a converging duct ($dA < 0$), supersonic flow is decelerated ($dv < 0$) and pressurized ($dp > 0$), as in the supersonic diffuser in Fig. 17(e).

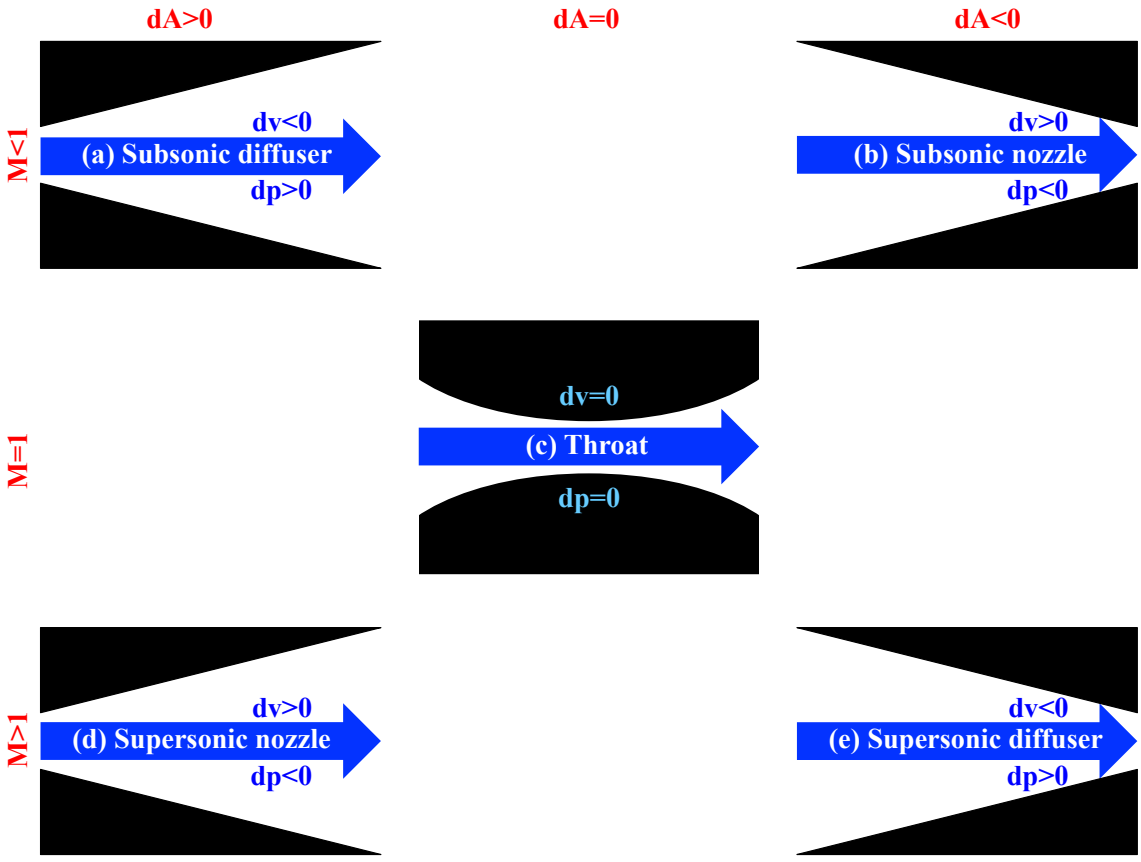

Fig. 17. Area-velocity relation for (a) a subsonic diffuser, (b) a subsonic nozzle, (c) a throat, (d) a supersonic nozzle, and (e) a supersonic diffuser.

Recall from Eq. (204) that density changes are generally small for subsonic flow. Since the mass flow rate $\rho v A$ is constant, if ρ is nearly constant for subsonic flow, increasing A decreases v, and decreasing A increases v, as found above. However, the density of supersonic flow can change over a wide range, provided that it obeys the adiabatic relation. If the area increases, supersonic flow expands and its density greatly decreases, so its velocity must increase to maintain the same flow rate. Thus subsonic and supersonic flow behave in opposite ways in converging and diverging ducts.

In a rocket engine, initially motionless propellant must be accelerated to as high an exit velocity as possible, so a convergent-divergent nozzle [Fig. 17(c)] is used. The convergent section of the nozzle accelerates the propellant from its initially motionless state to the speed of sound, and the divergent section of the nozzle further accelerates the propellant from the speed of sound to a higher exit velocity. For more information on rocket propulsion, see *Thermodynamics and Propulsion* ?.

The cross-sectional area A at any point in a duct can be related to the cross-sectional area A_* at the point in the duct where the flow is exactly sonic (local speed of sound v_{s*}). From conservation of the mass flow rate $\dot{m} = \rho\, v\, A = \rho_*\, v_{s*}\, A_*$, the ratio of the areas may be expressed as:

$$\begin{aligned}
\frac{A}{A_*} &= \frac{v_{s*}}{v}\,\frac{\rho_*}{\rho} = \frac{v_s}{v}\,\frac{v_{s*}}{v_s}\,\frac{\rho_*}{\rho_o}\,\frac{\rho_o}{\rho} \\
&= \frac{1}{M}\sqrt{\frac{T_*}{T}}\,\frac{\rho_*}{\rho_o}\,\frac{\rho_o}{\rho} = \frac{1}{M}\sqrt{\frac{T_*}{T_o}\,\frac{T_o}{T}}\,\frac{\rho_*}{\rho_o}\,\frac{\rho_o}{\rho} \\
&= \frac{1}{M}\left(\frac{2}{\gamma+1}\right)^{1/2}\left(1+\frac{\gamma-1}{2}M^2\right)^{1/2}\left(\frac{2}{\gamma+1}\right)^{1/(\gamma-1)}\left(1+\frac{\gamma-1}{2}M^2\right)^{1/(\gamma-1)} \qquad (217) \\
&= \frac{1}{M}\left[\frac{2}{\gamma+1}\left(1+\frac{\gamma-1}{2}M^2\right)\right]^{\frac{(\gamma+1)}{2(\gamma-1)}} \qquad (218)
\end{aligned}$$

in which Eq. (217) used Eqs. (207), (210), (209), and (212). In the final result of Eq. (218), note that the local Mach number changes as the local area changes relative to the sonic throat area A_*. For a given area ratio, both a subsonic ($M < 1$) and a supersonic ($M > 1$) solution are possible.

The **choked** or maximum mass flow rate is limited by how much flow can pass through the throat area A_* of the duct when the throat flow is at its maximum possible (sonic) speed:

$$\begin{aligned}
\dot{m}_{\max} &= \rho_*\, A_*\, v_{s*} = \rho_o\,\frac{\rho_*}{\rho}\; A_*\; v_{so}\sqrt{\frac{T_*}{T_o}} \\
&= \rho_o\left(\frac{2}{\gamma+1}\right)^{1/(\gamma-1)}\; A_*\,\sqrt{\gamma R T_o}\left(\frac{2}{\gamma+1}\right)^{1/2} \\
&= \sqrt{\gamma}\left(\frac{2}{\gamma+1}\right)^{\frac{(\gamma+1)}{2(\gamma-1)}}\; A_*\,\rho_o\sqrt{RT_o} \qquad (219)
\end{aligned}$$

(c) Compressible flow in an isothermal pipe

Compressible flow in an isothermal pipe is a good model for natural gas pipelines, in which the ground maintains the pipeline at an approximately constant temperature. For T = constant, the speed of sound $v_s = \sqrt{\gamma RT}$ is constant for the whole pipeline, and pressure and density changes are related by $dp = RT\,d\rho$. For a pipe of constant cross-sectional area A, mass conservation from Eq. (213) indicates that density and velocity changes are simply related by $d\rho/\rho = -dv/v$. Equation (5) for momentum conservation is valid with time variations ($\partial/\partial t$) and gravity (ρg) neglected and with $dp/dz = -f\,\rho\,v^2/(2D)$ from Eq. (100) used for viscous drag between the gas and pipe wall:

$$\rho\,v\,\frac{dv}{dz} \;=\; -\,\frac{dp}{dz} \;-\; \frac{f\,\rho\,v^2}{2D} \tag{220}$$

in which z is the position along the length of the pipeline, f is the Darcy friction factor, and D is the inner diameter of the pipe. The friction factor is constant down the length of the pipe since for laminar [Eq. (97)] or turbulent [Eq. (103)] flow f depends on the Reynolds number $\mathrm{Re}_D = \rho v D/\mu$, where ρv is constant from conservation of mass, D is constant, and the viscosity μ is constant for constant temperature. Multiplying both sides of Eq. (220) by $2\,dz/(\rho\,v^2)$, one finds:

$$-\,2\frac{dv}{v} \;-\; 2\frac{dp}{\rho\,v^2} \;=\; \frac{f\,dz}{D} \tag{221}$$

The second term in Eq. (221) may be rewritten as:

$$-\,2\frac{dp}{\rho\,v^2} \;=\; -\,2\,\frac{RT}{v^2}\,\frac{d\rho}{\rho} \;=\; 2\,\frac{RT}{v^2}\,\frac{dv}{v} \;=\; \frac{2}{\gamma M^2}\,\frac{dv}{v} \tag{222}$$

Using Eq. (222), Eq. (221) may be expressed as:

$$2\,\frac{dv}{v}\left(\frac{1}{\gamma M^2} - 1\right) \;=\; \frac{f\,dz}{D} \tag{223}$$

Using $dv/v = dM/M$ for isothermal flow, Eq. (223) may be expressed in terms of the Mach number:

$$\frac{2}{\gamma}\,\frac{dM}{M}\left(\frac{1}{M^2} - \gamma\right) \;=\; \frac{f\,dz}{D} \tag{224}$$

If the pipe is long enough, the flow reaches a limiting or choked velocity and ceases to accelerate as it moves further. The maximum Mach number can be found from Eq. (224) by setting $dM/dz = 0$:

$$M_{\text{choked}} \;=\; \frac{1}{\sqrt{\gamma}}, \qquad \text{or} \qquad v_{\text{choked}} \;=\; \sqrt{RT} \tag{225}$$

Integrating Eq. (224) over a pipeline of length L, the initial M_1 and final M_2 Mach numbers of the flow are related to the friction by:

$$\frac{1}{\gamma}\left(\frac{1}{M_1^2} \;-\; \frac{1}{M_2^2}\right) \;-\; \ln\left(\frac{M_2^2}{M_1^2}\right) \;=\; \frac{f\,L}{D} \tag{226}$$

where $M_1 < M_2 \le 1/\sqrt{\gamma}$. Setting $M_2 = M_{\text{choked}} = 1/\sqrt{\gamma}$ in Eq. (226), the pipe length the gas can traverse before reaching its choked state is:

$$L_{\text{choked}} \;=\; \frac{D}{f}\left[\frac{1}{\gamma M_1^2} \;-\; 1 \;+\; \ln\left(\gamma M_1^2\right)\right] \tag{227}$$

Other parameters in the choked state are:

$$\frac{p_{\text{choked}}}{p_1} \;=\; \frac{\rho_{\text{choked}}}{\rho_1} \;=\; \frac{M_1}{M_{\text{choked}}} \;=\; \sqrt{\gamma}\,M_1 \tag{228}$$

(d) Compressible flow in an adiabatic pipe

Equation (221) is also valid for adiabatic pipe flow with friction, sometimes called **Fanno flow**. Using the adiabatic relation $dp = \gamma RT\, d\rho$ (note the factor of γ, relative to the previous isothermal relation $dp = RT\, d\rho$), the second term in Eq. (221) may be rewritten as:

$$-\,2\frac{dp}{\rho\, v^2} \;=\; -\,2\,\frac{\gamma\, R\, T}{v^2}\,\frac{d\rho}{\rho} \;=\; 2\,\frac{\gamma\, R\, T}{v^2}\,\frac{dv}{v} \;=\; \frac{2}{M^2}\,\frac{dv}{v} \tag{229}$$

Using Eq. (229), Eq. (221) may be expressed as:

$$2\,\frac{dv}{v}\left(\frac{1}{M^2} - 1\right) \;=\; \frac{f\, dz}{D} \tag{230}$$

By differentiating the definition of Mach number ($v = M\sqrt{\gamma RT}$), variations in velocity, Mach number, and temperature are related by:

$$\frac{dv}{v} \;=\; \frac{dM}{M} \;+\; \frac{1}{2}\,\frac{dT}{T} \tag{231}$$

Differentiating the energy conservation equation for adiabatic flow, $h + v^2/2 = c_pT + v^2/2 =$ constant, and using $M^2 = v^2/(\gamma RT)$, another relation for velocity and temperature variations is:

$$\frac{dT}{T} \;=\; -\,\frac{v\, dv}{c_pT} \;=\; -\,\frac{\gamma RM^2}{c_p}\,\frac{dv}{v} \tag{232}$$

By combining Eqs. (231), (232), and (151), one can directly relate dv and dM without dT or T:

$$\frac{dv}{v} \;=\; \frac{dM}{M}\left(1 \;+\; \frac{\gamma - 1}{2}M^2\right)^{-1} \tag{233}$$

Using Eq. (233), Eq. (230) may be expressed in terms of the Mach number:

$$\frac{2}{\gamma}\,\frac{dM}{M}\left(\frac{1}{M^2} - 1\right)\left(1 \;+\; \frac{\gamma - 1}{2}M^2\right)^{-1} \;=\; \frac{f\, dz}{D} \tag{234}$$

If the pipe is long enough, the flow reaches a limiting or choked velocity and ceases to accelerate as it moves further. The maximum Mach number can be found from Eq. (234) by setting $dM/dz = 0$:

$$M_{\text{choked}} \;=\; 1, \qquad \text{or} \qquad v_{\text{choked}} \;=\; \sqrt{\gamma RT_{\text{choked}}} \tag{235}$$

Integrating Eq. (234) over a pipeline of length L, the initial M_1 and final M_2 Mach numbers of the flow are related to the average friction $\bar{f} = \int f\, dz/L$ by:

$$\frac{1}{\gamma}\left(\frac{1}{M_1^2} \;-\; \frac{1}{M_2^2}\right) \;+\; \frac{\gamma + 1}{2\gamma}\ln\left[\frac{(\gamma+1)M_1^2}{2 + (\gamma-1)M_1^2}\,\frac{2 + (\gamma-1)M_2^2}{(\gamma+1)M_2^2}\right] \;=\; \frac{\bar{f}\, L}{D} \tag{236}$$

Setting $M_2 = 1$ in Eq. (236), the distance the gas travels before reaching its choked state is:

$$L_{\text{choked}} \;=\; \frac{D}{\bar{f}}\left\{\frac{1}{\gamma M_1^2} \;-\; \frac{1}{\gamma} \;+\; \frac{\gamma + 1}{2\gamma}\ln\left[\frac{(\gamma+1)M_1^2}{2 + (\gamma-1)M_1^2}\right]\right\} \tag{237}$$

3.5 Shock Waves

Shock waves are basically very strong sound waves in a fluid, except fluid flow is supersonic behind the shock wave and subsonic ahead of it. Shock waves may be either stationary in oncoming flow [Fig. 18(a)] or moving through an initially motionless fluid [Fig. 18(b)], and shocks may be either normal [Fig. 18(c)] or oblique [Fig. 18(d)] to the fluid velocities. The shock is a layer only a few molecules thick separating the two regions, which have different values of density ρ, pressure p, velocity $v_\perp$ normal (or perpendicular) or $v_\parallel$ parallel to the shock, enthalpy h, and entropy s.

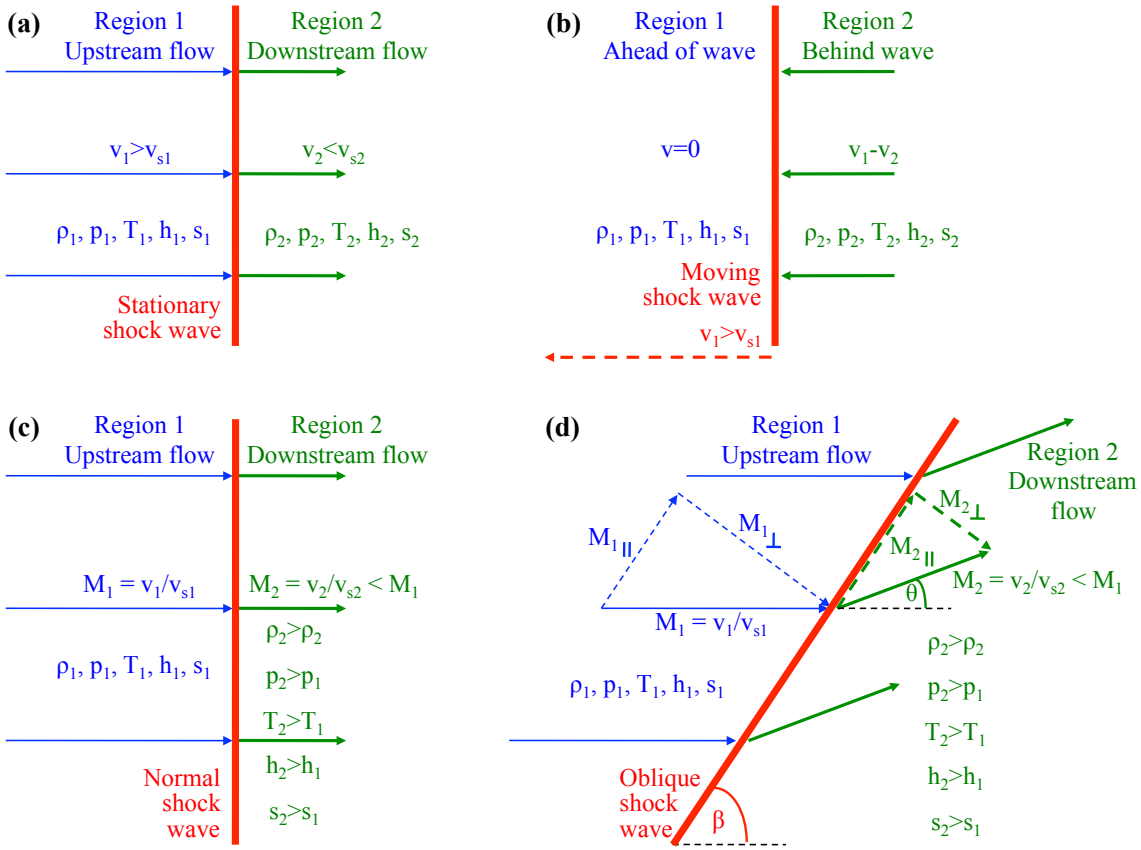

Figure 18. Some major properties of shock waves. (a) Stationary vs. (b) moving shock waves. (c) Normal vs. (d) oblique shock waves.

When evaluated across the shock in Fig. 18(c) or (d), Eqs. (3), (5), (9), and (159) become the **Rankine-Hugoniot shock equations** relating the properties in regions 1 and 2:

$$\rho_1 v_{1\perp} = \rho_2 v_{2\perp} \qquad \text{Conservation of mass} \tag{238}$$

$$p_1 + \rho_1 v_{1\perp}^2 = p_2 + \rho_2 v_{2\perp}^2 \qquad \text{Conservation of momentum perpendicular to shock} \tag{239}$$

$$v_{1\parallel} = v_{2\parallel} \qquad \text{Conservation of momentum parallel to shock} \tag{240}$$

$$h_1 + \frac{1}{2} v_{1\perp}^2 = h_2 + \frac{1}{2} v_{2\perp}^2 \qquad \text{Conservation of energy} \tag{241}$$

$$p_2 = \frac{\gamma - 1}{\gamma} \rho_2 h_2 \qquad \text{Equation of state} \tag{242}$$

Shock waves are easier to analyze when they are normal, or all fluid flow is perpendicular to the shock wave ($v_{1\parallel} = v_{2\parallel} = 0$), as shown in Fig. 17(c). By combining Eqs. (238)-(242) and slogging through several fun-filled pages of algebra [1, 3, 4, 5, 6, 9, 10], one can express the changes across the shock as functions of the upstream Mach number $M_1 = v_1/v_{s1} = v_{1\perp}/v_{s1}$ only [note that the speed of sound v_s may be different in the upstream and downstream regions, since the temperatures and other parameters in Eq. (178) are different]:

$$M_2 = \frac{v_2}{v_{s2}} = \sqrt{\frac{1 + [(\gamma-1)/2]M_1^2}{\gamma M_1^2 - (\gamma-1)/2}} \tag{243}$$

$$\frac{\rho_2}{\rho_1} = \frac{v_{1\perp}}{v_{2\perp}} = \frac{(\gamma+1)M_1^2}{2 + (\gamma-1)M_1^2} \tag{244}$$

$$\frac{p_2}{p_1} = 1 + \frac{2\gamma}{\gamma+1}\left(M_1^2 - 1\right) \tag{245}$$

$$\begin{aligned} \frac{T_2}{T_1} &= \frac{h_2}{h_1} = \frac{p_2}{p_1}\frac{\rho_1}{\rho_2} \\ &= \left[1 + \frac{2\gamma}{\gamma+1}\left(M_1^2 - 1\right)\right]\frac{2 + (\gamma-1)M_1^2}{(\gamma+1)M_1^2} \end{aligned} \tag{246}$$

$$\begin{aligned} s_2 - s_1 &= c_p \ln\left(\frac{p_2}{p_1}\frac{\rho_1}{\rho_2}\right) - R\ln\left(\frac{p_2}{p_1}\right) \\ &= c_p \ln\left\{\left[1 + \frac{2\gamma}{\gamma+1}\left(M_1^2 - 1\right)\right]\frac{2 + (\gamma-1)M_1^2}{(\gamma+1)M_1^2}\right\} \\ &\qquad -R\,\ln\left[1 + \frac{2\gamma}{\gamma+1}\left(M_1^2 - 1\right)\right] \end{aligned} \tag{247}$$

In crossing the shock wave, fluid is almost instantaneously decelerated from a supersonic velocity ($M_1 > 1$) to a subsonic velocity ($M_2 < 1$), causing its density, pressure, temperature, and entropy to suddenly rise ($\rho_2 > \rho_1$, $p_2 > p_1$, $T_2 > T_1$, and $s_2 > s_1$). Note that unlike small-amplitude sound waves, moving large-amplitude shock waves can travel faster than the speed of sound v_s.

An oblique or non-normal shock wave is shown in Fig. 18(d). The shock wave is inclined at an angle β relative to the upstream flow, so the component of the upstream Mach number that is normal to the shock wave is

$$M_{1\perp} = M_1 \sin\beta = \frac{v_1}{v_{s1}}\sin\beta \tag{248}$$

As shown in Fig. 18(d), passing through the shock wave deflects the downstream flow by an angle θ relative to the upstream flow. The shock wave is thus inclined at an angle $\beta - \theta$ relative to the downstream flow, so the component of the downstream Mach number that is normal to the shock wave is

$$M_{2\perp} = M_2 \sin(\beta - \theta) = \frac{v_2}{v_{s2}}\sin(\beta - \theta) \tag{249}$$

Since velocity components parallel to the shock wave are conserved across the shock wave as per Eq. (240), Eqs. (243)-(247) are valid for oblique shocks as long as we use the normal components of the Mach numbers:

$$M_{2\perp} = \sqrt{\frac{1+[(\gamma-1)/2]M_{1\perp}^2}{\gamma M_{1\perp}^2-(\gamma-1)/2}} \tag{250}$$

$$\frac{\rho_2}{\rho_1} = \frac{v_{1\perp}}{v_{2\perp}} = \frac{(\gamma+1)M_{1\perp}^2}{2+(\gamma-1)M_{1\perp}^2} \tag{251}$$

$$\frac{p_2}{p_1} = 1 + \frac{2\gamma}{\gamma+1}\left(M_{1\perp}^2-1\right) \tag{252}$$

$$\begin{aligned}\frac{T_2}{T_1} &= \frac{h_2}{h_1} = \frac{p_2}{p_1}\frac{\rho_1}{\rho_2} \\ &= \left[1+\frac{2\gamma}{\gamma+1}\left(M_{1\perp}^2-1\right)\right]\frac{2+(\gamma-1)M_{1\perp}^2}{(\gamma+1)M_{1\perp}^2}\end{aligned} \tag{253}$$

$$\begin{aligned}s_2-s_1 &= c_p \ln\left(\frac{p_2}{p_1}\frac{\rho_1}{\rho_2}\right) - R\ln\left(\frac{p_2}{p_1}\right) \\ &= c_p \ln\left\{\left[1+\frac{2\gamma}{\gamma+1}\left(M_{1\perp}^2-1\right)\right]\frac{2+(\gamma-1)M_{1\perp}^2}{(\gamma+1)M_{1\perp}^2}\right\} \\ &\qquad -R\,\ln\left[1+\frac{2\gamma}{\gamma+1}\left(M_{1\perp}^2-1\right)\right]\end{aligned} \tag{254}$$

Using $v_{1\parallel} = v_{2\parallel}$ from Eq. (240), and then utilizing the velocity triangles of Fig. 17(d) and Eq. (251), one finds:

$$\frac{\tan(\beta-\theta)}{\tan\beta} = \frac{v_{2\perp}}{v_{1\perp}} = \frac{\rho_1}{\rho_2} = \frac{2+(\gamma-1)M_1^2\sin^2\beta}{(\gamma+1)M_1^2\sin^2\beta} \tag{255}$$

Equation (255) can be rewritten to give the so-called $\theta-\beta-M$ relation connecting the shock wave angle β and flow deflection angle θ for any given value of the upstream Mach number M_1:

$$\theta = \tan^{-1}\left\{\frac{2}{\tan\beta}\left[\frac{M_1^2\sin^2\beta-1}{M_1^2(\gamma+\cos 2\beta)+2}\right]\right\} \tag{256}$$

Equation (256) is graphed in Fig. 19 as β vs. θ for various values of M_1, assuming $\gamma = 1.4$. Equation (256) yields a value for the deflection angle θ given an initial value for the shock wave angle β. In practice, however, one usually begins by knowing θ from the shape of the aircraft or other object encountering the supersonic flow, then uses θ and M_1 to graphically or numerically solve for the induced shock wave angle β from curves such as those in Fig. 19.

For very small deflections, $\theta \to 0$ (the far left side of Fig. 19), the numerator in Eq. (256) must go to zero, so in the limit of very weak shocks, the shock angle is

$$\beta = \sin^{-1}\left(\frac{1}{M_1}\right) \tag{257}$$

This minimum shock angle for a given Mach number is called the **Mach angle** and will be discussed in more detail in Section 3.9.

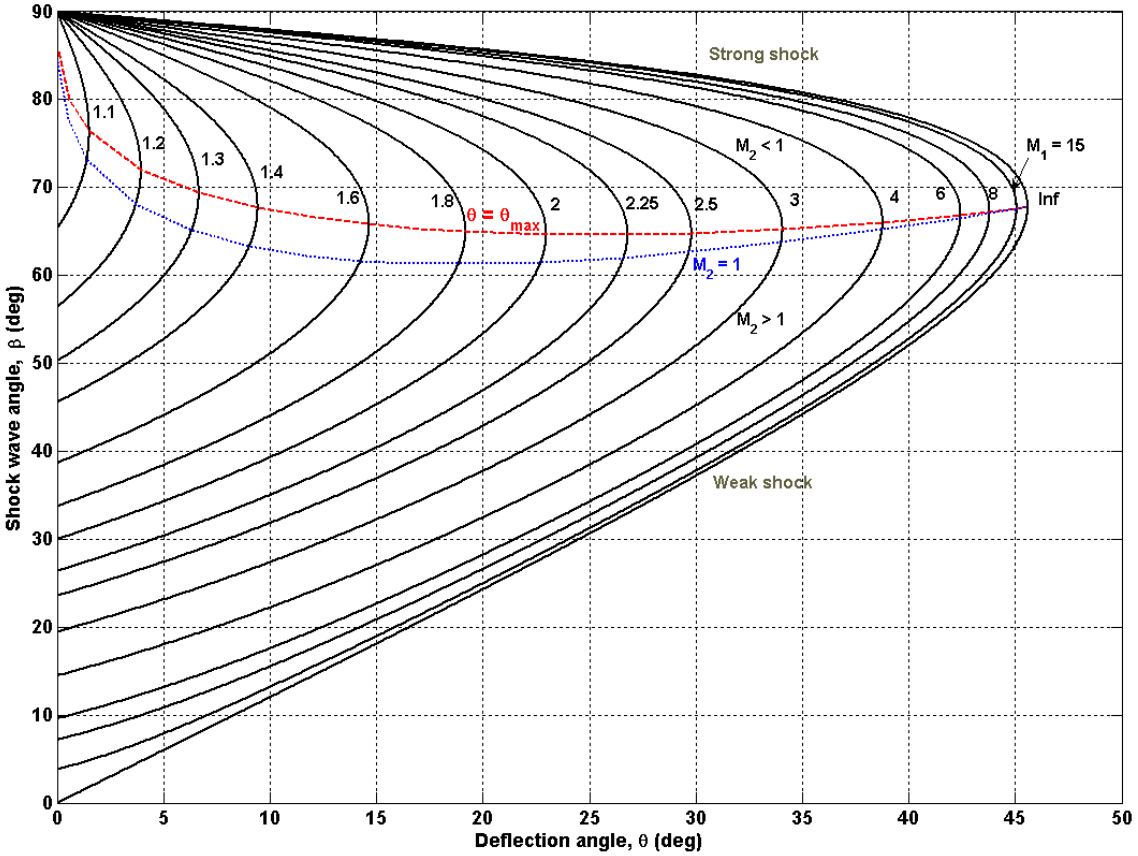

Figure 19. Shock wave angle β vs. flow deflection angle θ for various values of the upstream Mach number from $M_1 = 1.1$ to $M_1 = \infty$. (Public domain graph from http://en.wikipedia.org/wiki/File:ObliqueShockAngleRelation.png.)

Note that for a given value of M_1, there is some maximum allowed value for the deflection angle, $\theta_{\max}$, somewhere on the red curve in Fig. 19. As shown in Fig. 20(a)-(d), if a shape with deflection angle smaller than $\theta_{\max}$ encounters a supersonic flow, an **attached shock wave** will extend outward from the surface of the shape. Note that for a given value of the Mach number and $\theta < \theta_{\max}$, there are two possible shock wave angles β, a smaller shock angle called a weak shock because it compresses the flow less [Fig. 19 lower portion and Fig. 20(a)-(b)] and a larger shock angle called a strong shock because it compresses the flow more [Fig. 19 upper portion and Fig. 20(c)-(d)]. Flows almost always choose the weak shock solution with the smaller angle β, so one should generally assume that unless there is data to the contrary.

As shown in Fig. 20(e)-(f), if a shape with a deflection angle larger than $\theta_{\max}$ encounters a supersonic flow, no attached shock solutions are possible on the curves of Fig. 19, and a **detached shock wave** will form upstream from the shape. The detached shock wave may be regarded as a normal shock wave at the very front, connected to a large-β strong shock wave on the side, which in turn connects to a small-β weak shock wave. As we will see in Section 4.2, blunt shapes with large θ and detached shock waves create more aerodynamic drag than streamlined shapes with small θ and attached shock waves, but blunt shapes absorb much less of the heat generated by that drag, since there is an insulating layer of air between the shape and its shock wave.

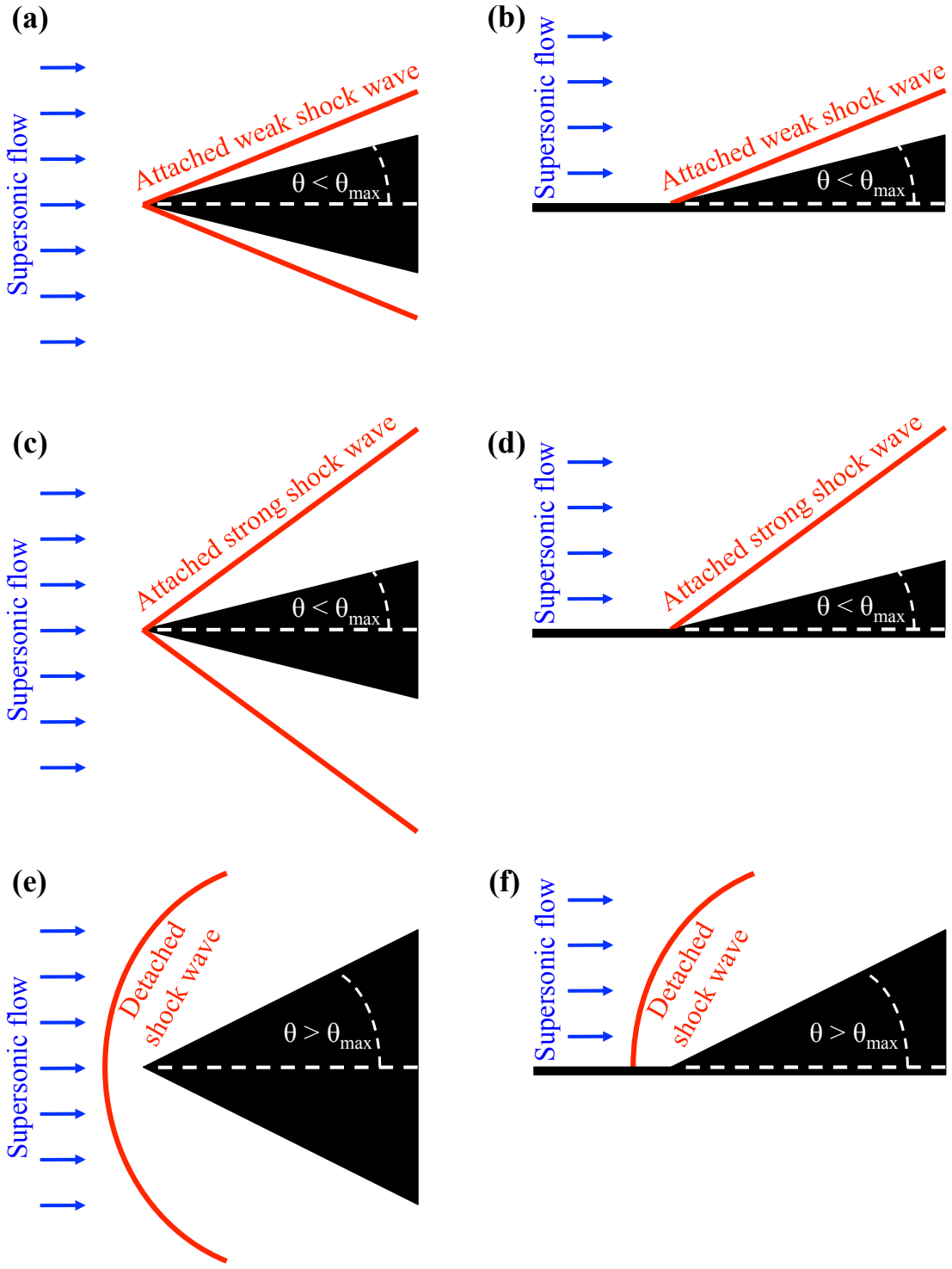

Figure 20. Attached weak shock waves for (a) a wedge and (b) a corner, attached strong shock waves for (c) a wedge and (d) a corner, and detached shock waves for (e) a wedge and (f) a corner in supersonic flow.

As has been discussed, if a surface bends into a supersonic flow, it creates an oblique shock wave that bends the flow away from the surface while decelerating the flow and increasing its density, pressure, and temperature [Fig. 21(a)]. However, if a surface bends away from a supersonic flow, it creates an expansion fan that bends the flow toward the surface while accelerating the flow and decreasing its density, pressure, and temperature [Fig. 21(b)]. Thus an expansion fan is the opposite of an oblique shock. Both cases will be considered in more detail in Section 3.9.

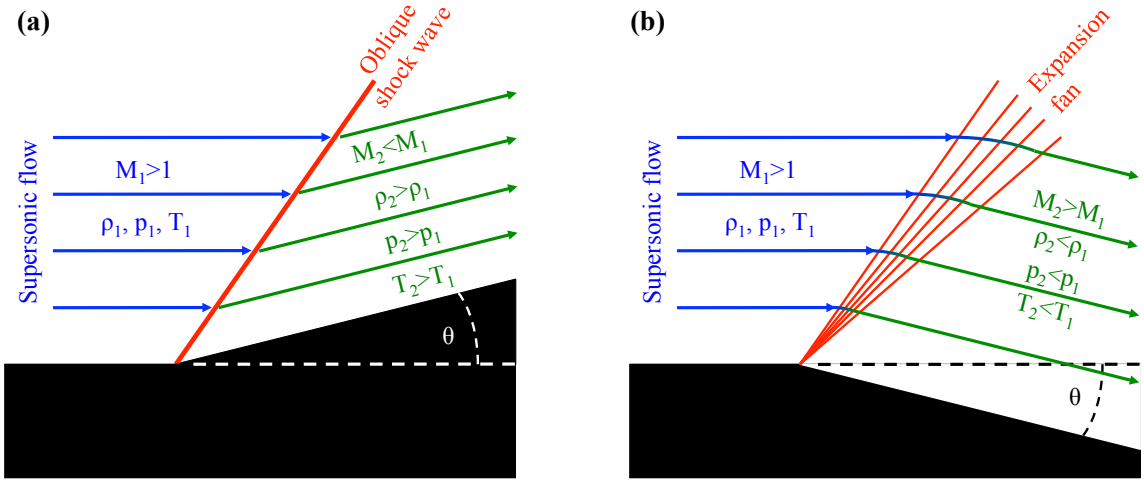

Figure 21. Oblique shock wave versus expansion fan. **(a)** If a surface bends into a supersonic flow, it creates an oblique shock wave. **(b)** If a surface bends away from a supersonic flow, it creates an expansion fan.

3.6 Explosive and Implosive Shock Waves

In addition to the plane shock waves considered in the previous section, other important cases include exploding shock waves expanding outward from a source and imploding shock waves converging inward to compress a material. We will consider four common examples (Fig. 22): the **Sedov solutions** for (a) a spherical mid-air explosion or (b) a hemispherical ground-level explosion of conventional or nuclear explosives (*Fission Power* 8.4), and the **Guderley solutions** for (c) a spherical or (d) a cylindrical implosion that may be used to increase the density of a material, particularly fission (*Fission Power* 8.3) or fusion (*Plasma Physics and Fusion* 6.2) fuel [6, 19, 20, 21, 22].

(a) Spherical explosive shock wave

For simplicity, we will assume that an energy E is released at a point source at position $r = 0$ and time $t = 0$ in a fluid with initial pressure p_1, initial density ρ_1, and initial temperature T_1, producing an explosive shock wave that propagates outward through the fluid. For reference, one ton of TNT high explosive produces an energy of 4.18×10^9 J. The characteristic radius and duration of the explosion may be easily estimated. The total energy E of the explosion creates an average energy density U_{avg} that decreases as the radius $R(t)$ of the shock wave expands with time:

$$U_{\text{avg}} = \frac{E}{(4/3)\pi R^3} \tag{258}$$

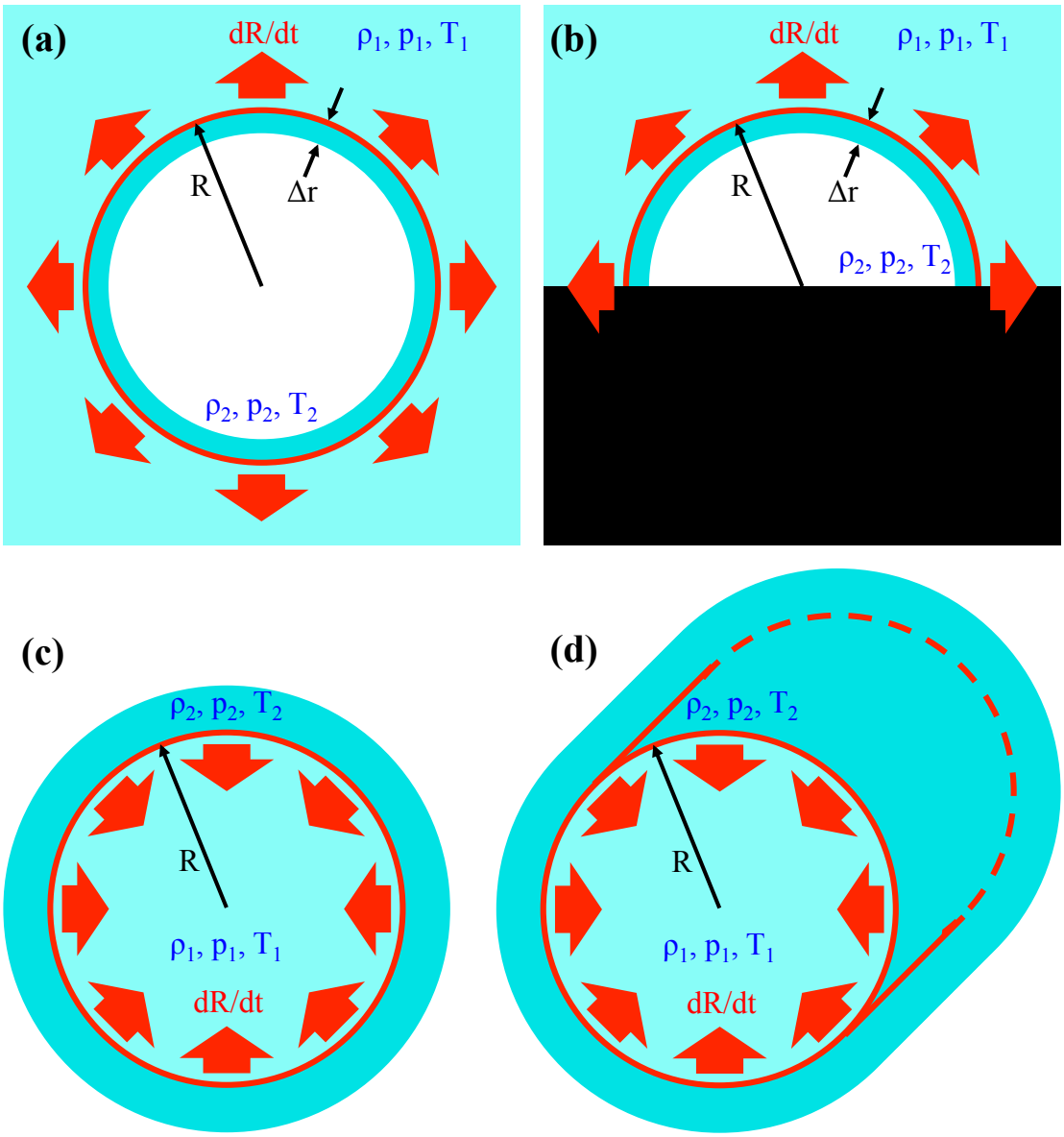

Figure 22. Explosive shock waves in (a) spherical and (b) hemispherical geometries and implosive shock waves in (c) spherical and (d) cylindrical geometries.

The average energy density falls to become equal to the initial pressure energy p_1 of the fluid when $U_{\text{avg}} = p_1$, or at a transition radius

$$R_{\text{trans}} = \left(\frac{3}{4\pi} \frac{E}{p_1} \right)^{1/3} \approx 21 \, E_{\text{tons}}^{1/3} \text{ m} \tag{259}$$

using sea-level atmospheric pressure $p_1 \approx 1.01 \times 10^5$ Pa and expressing E in equivalent tons of TNT. Before the shock wave reaches the radius R_{trans}, the shock has more energy than the surrounding medium, so it moves at a supersonic velocity as the previous section noted shock waves can do. After the shock wave passes the radius R_{trans}, the shock has less energy than the surrounding medium, so it smoothly transitions to become a relatively small perturbation on the background fluid, or in other words just a sound wave moving at the normal speed of sound v_{s1} in the undisturbed fluid.

However, a shock wave can still do severe damage to buildings, trees, or other structures until its average energy density falls to much less than the initial pressure energy p_1 of the fluid (remember Table 3), say $U_{\text{avg}} \approx p_1/100$, or at a characteristic blast radius

$$R_{\text{blast}} \;=\; \left(\frac{300}{4\pi}\,\frac{E}{p_1}\right)^{1/3} \;\approx\; 100\,E_{\text{tons}}^{1/3}\;\text{m} \tag{260}$$

Since $R_{\text{blast}} \gg R_{\text{trans}}$ and the shock wave propagates the vast majority of the distance R_{blast} at the speed of sound v_{s1}, the characteristic duration of the explosion is

$$t_{\text{blast}} \;\sim\; \frac{R_{\text{blast}}}{v_{s1}} \;=\; \left(\frac{1}{\gamma R T_1}\right)^{1/2}\left(\frac{300}{4\pi}\,\frac{E}{p_1}\right)^{1/3} \;\approx\; 0.3\,E_{\text{tons}}^{1/3}\;\text{sec} \tag{261}$$

in which the final numerical value assumes a sea-level atmospheric pressure $p_1 \approx 1.01 \times 10^5$ Pa and speed of sound $v_s \approx 346$ m/sec. Using Eqs. (259)-(261), some characteristic values for a wide range of explosives are given in Table 4.

Explosive	**Energy (TNT equivalent)**	R_{trans}	R_{blast}	t_{blast}
Small conventional explosive	1 kg (0.001 T)	2.1 m	10 m	0.03 sec
Large conventional explosive	1 T	21 m	100 m	0.3 sec
Early fission bombs	20 kT	580 m	2.7 km	8 sec
Largest thermonuclear bomb	100 MT	9.7 km	46 km	140 sec

Table 4. Characteristic energies, transition radii, blast radii, and durations of various types of explosions. The largest thermonuclear bomb known to have been built was the Soviet Union's Tsar Bomba, which was tested in 1961 in a 50 MT configuration but designed for a full yield of 100 MT.

From Eq. (244), a very strong ($M_1 \to \infty$) plane shock wave increases the density of the medium through which it passes by a factor of

$$\frac{\rho_2}{\rho_1} \;\approx\; \frac{\gamma+1}{\gamma-1} \tag{262}$$

Shock waves cannot compress a fluid more than this, since the shock waves also heat the fluid, and thermal expansion opposes further compression. In other words, as shock waves become arbitrarily strong, more and more of the shock energy goes into heating instead of compressing the fluid.

An explosive shock concentrates most of the fluid mass that was initially within the volume of the shock into a thin layer at the expanding surface of the shock, as shown in Fig. 22(a). If the initial fluid density is ρ_1, the fluid density within the shock layer is ρ_2, the radius of the shock wave is R, the thickness of the shock layer is $\Delta r \ll R$, and residual fluid not in the shock layer is ignored, conservation of mass equates the original fluid mass $M = (4/3)\pi R^3 \rho_1$ and its redistributed mass $4\pi R^2\,\Delta r\,\rho_2$:

$$\frac{4}{3}\pi R^3 \rho_1 \;=\; 4\pi R^2\,\Delta r\,\rho_2\;,\;\;\text{or} \tag{263}$$

$$\frac{\Delta r}{R} \;=\; \frac{1}{3}\,\frac{\rho_1}{\rho_2} \;=\; \frac{1}{3}\,\frac{\gamma-1}{\gamma+1} \tag{264}$$

in which the last step used Eq. (262). The value of γ depends on how much the explosion heats and ionizes the fluid. Ignoring such effects and using $\gamma = 1.4$ for air, Eq. (264) yields $\Delta r/R \approx 0.056$, confirming the assumption that the fluid is concentrated into a thin layer at the shock.

Pressure is a form of stored energy density, so the pressure p_2 in the expanding explosion is inversely proportional to the volume of the explosion, just like the energy density in Eq. (258):

$$p_2 \;\propto\; \frac{1}{R^3} \tag{265}$$

From the ideal gas law in Eq. (138), temperature is proportional to pressure, so the temperature T of the exploding shock wave varies just like Eq. (265):

$$T_2 \;\propto\; \frac{1}{R^3} \tag{266}$$

The velocity dR/dt of a shock wave is proportional to the speed of sound, which in turn is proportional to the square root of temperature from Eq. (178). Using this fact and Eq. (266) yields:

$$\frac{dR}{dt} \;\propto\; \frac{1}{R^{3/2}} \tag{267}$$

By integrating Eq. (267), one finds the time variation of the shock wave radius $R(t)$:

$$\int R^{3/2}\,dR \;\propto\; \int dt \qquad \Longrightarrow \qquad R^{5/2} \;\propto\; t\,, \qquad \text{or} \tag{268}$$

$$R \;=\; C_1\,t^{2/5} \tag{269}$$

in which C_1 is a constant. To determine this constant, consider the kinetic energy $K.E.$ of the mass $M = (4/3)\pi R^3\rho_1$ contained in the expanding shock wave:

$$K.E. \;=\; \frac{1}{2}M\left(\frac{dR}{dt}\right)^2 \;=\; \frac{1}{2}\left(\frac{4}{3}\pi R^3\rho_1\right)\left(\frac{dR}{dt}\right)^2 \tag{270}$$

$$=\; \frac{8\pi}{75}\,\rho_1\,C_1^5 \tag{271}$$

in which the last step in Eq. (271) used Eq. (269).

Assuming that the potential energy in the shock wave is comparable to the kinetic energy, the total energy is

$$E \;\approx\; 2\,K.E. \;=\; \frac{16\pi}{75}\,\rho_1\,C_1^5\,, \quad \text{or} \tag{272}$$

$$C_1 \;\approx\; \left(\frac{75}{16\pi}\right)^{1/5}\left(\frac{E}{\rho_1}\right)^{1/5} \;\approx\; \left(\frac{E}{\rho_1}\right)^{1/5} \tag{273}$$

Thus the complete expression for the shock wave radius is:

$$R \;\approx\; \left(\frac{E}{\rho_1}\right)^{1/5} t^{2/5} \;\approx\; 81\,E_{\text{tons}}^{1/5}\,t^{2/5} \tag{274}$$

in which the numerical result used $\rho_1 \approx 1.2$ kg/m^3 for sea-level air.

Differentiating Eq. (274), the complete expression for the shock wave velocity is

$$\frac{dR}{dt} \;\approx\; \frac{2}{5}\left(\frac{E}{\rho_1}\right)^{1/5} t^{-3/5} \;\approx\; 32\,E_{\text{tons}}^{1/5}\,t^{-3/5} \tag{275}$$

Using Eq. (274), Eqs. (265) and (266) become

$$p_2 \;\propto\; T_2 \;\propto\; \frac{1}{R^3} \;\propto\; \frac{1}{t^{6/5}} \tag{276}$$

Equations (274)-(276) are only valid before the shock wave radius R reaches the transition radius $R_{\rm trans}$ from Eq. (259). At around the transition radius, the shock wave gradually transitions to a sound wave and the radius starts to grow at the speed of sound v_{s1}. By rewriting Eq. (275) as

$$\frac{dR}{dt} \;\approx\; \frac{2}{5}\left(\frac{E}{\rho_1}\right)^{1/2} R^{-3/2} \;\approx\; 24,000\,\sqrt{E_{\rm tons}}\,R^{-3/2}\ \ {\rm m/sec} \tag{277}$$

one can verify dR/dt falls to v_{s1} at approximately $R_{\rm trans}$.

For more details on the internal structure and time evolution of explosions, see [21].

The above analysis assumes that the explosion occurs in an infinite, homogeneous, isotropic fluid. As shown in Table 4, for large nuclear explosions, the characteristic radii of the explosions become comparable to the scale height $H_o \sim 8$ km of the exponential atmosphere from Eq. (166). As a result, the high-pressure explosion will expand more toward lower-pressure high-altitude air and less in other directions. More detailed calculations of very large explosions take this effect into consideration [19, 20, 21].

(b) Hemispherical explosive shock wave

Whereas mid-air explosions may be modeled as spherical shock waves, an explosion at ground level may be idealized as a hemispherical explosion on a perfectly flat, non-absorbing surface [Fig. 22(b)]. If none of the energy goes into the ground, a hemispherical explosion of energy E may be regarded as half of the spherical explosion that would be created by twice that energy, $2E$. Thus Eqs. (258)-(276) may be applied to a hemispherical explosive shock wave with this one modification. For example, from Eq. (260) a hemispherical explosion of energy E will have a $2^{1/3} \approx 1.26$ times greater characteristic blast radius than a spherical explosion of the same energy E. Of course, this is only an idealization, since the surface may not be perfectly flat and some of the explosive energy may be coupled into the ground, creating seismic waves.

(c) Spherical implosive shock wave

Next we will consider a spherical implosion [Fig. 22(c)] and designate time $t = 0$ as the moment the shock wave converges on the center. For $t < 0$, the shock wave is approaching the center. At $t = 0$, the shock reflects from itself at the center, and for $t > 0$ the shock wave expands outward from the center, basically just the implosion played in reverse.

Shock waves are souped-up sound waves, and recall from Eq. (191) that the intensity of a spherical sound wave decreases as the inverse square of the radius from the source, $I \propto 1/R^2$, since as the radius increases, the intensity is spread over an area that increases like $4\pi R^2$. Also recall from Eq. (192) that the wave pressure is proportional to the square root of the intensity and thus decreases like $p \propto 1/R$ for a spherical sound wave. Likewise, the peak pressure of the imploding spherical shock wave varies like:

$$p_2 \;\propto\; \frac{1}{R} \tag{278}$$

Whereas $p \propto 1/R$ for sound waves, the nonlinearities of strong shock waves alter that power dependence slightly to more like $p \propto 1/R^{0.9}$ depending on the exact value of γ, but we will sweep such corrections under the rug.

Temperature is proportional to pressure, so the temperature T_2 of the imploding shock wave varies just like Eq. (278):

$$T_2 \propto \frac{1}{R} \tag{279}$$

As in the case of an explosive shock wave, the velocity dR/dt of an implosive shock wave is proportional to the speed of sound, which in turn is proportional to the square root of temperature. Using this fact and Eq. (279) yields:

$$\frac{dR}{dt} \propto \frac{1}{R^{1/2}} \tag{280}$$

By integrating Eq. (280), one finds the time variation of the shock wave radius $R(t)$ (for both the $t < 0$ implosion and $t > 0$ expansion phases):

$$\int R^{1/2}\, dR \propto \int dt \quad \Longrightarrow \quad R^{3/2} \propto t\,, \quad \text{or} \tag{281}$$

$$R = C_2\, |t|^{2/3} \tag{282}$$

in which C_2 is a constant. The exponent 2/3 in Eq. (282) is called the similarity exponent and its exact numerical value actually varies slightly depending on the value of γ, since nonlinearities that depend on γ slightly alter the power dependence on R in Eqs. (278)-(280) that led to the derivation of the similarity exponent. However, Eq. (282) is close enough for government work, so we'll stick with that.

Using Eq. (282), Eqs. (278)-(280) may be written as:

$$p_2 \propto T_2 \propto \frac{1}{R} \propto |t|^{-2/3} \tag{283}$$

$$\frac{dR}{dt} \propto \frac{1}{R^{1/2}} \propto |t|^{-1/3} \tag{284}$$

In reality, the shock wave radius does not go all the way to zero and the pressure, temperature, and velocity do not go all the way to infinity at $t = 0$ as in Eqs. (283)-(284). The minimum radius of compression is limited by the mean free path between collisions of particles within the fluid. For more information on individual particles, collisions, and mean free paths within a fluid, see *Plasma Physics and Fluids* 2.

From Eq. (262), a very strong ($M_1 \to \infty$) plane shock wave increases the density of the medium through which it passes by a factor of $(\gamma + 1)/(\gamma - 1)$. When a spherical shock wave converges at the center and starts to bounce back, the incoming shock wave increases the density by this factor $(\gamma+1)/(\gamma-1)$, and the reflected shock starting to propagate back outward further increases the density by the same factor again. Throwing in a factor of $1/\sqrt{2}$ obtained from more detailed calculations, the peak compression obtainable by an imploding spherical shock wave is:

$$\frac{\rho_{\text{peak}}}{\rho_1} \approx \frac{1}{\sqrt{2}} \left(\frac{\gamma+1}{\gamma-1}\right)^2 \tag{285}$$

For example, the peak compression is $16/\sqrt{2} \approx 11.3$ for a monatomic gas with $\gamma = 5/3$, or $36/\sqrt{2} \approx 25.5$ for a gas of diatomic molecules with $\gamma = 7/5$. As already noted, shock waves cannot compress a fluid more than this; as shock waves become arbitrarily strong, more and more of the shock energy goes into heating instead of compressing the fluid. In practice, the peak compression achievable by a spherical implosion will be somewhat less than the ideal value given by Eq. (285), due to viscosity, energy dissipation, nonlinearities, and other effects not considered here. For more information on spherical implosions, see *Plasma Physics and Fluids* 6.2.

(d) Cylindrical implosive shock wave

A cylindrical implosion [Fig. 22(d)] is very similar to a spherical implosion, with appropriate adjustments to the exponents. For sound waves in a cylindrical geometry, the intensity is inversely proportional to the radius from the source, $I \propto 1/R$, since as the radius increases, the intensity is spread over an area that increases like $2\pi R$. Using this fact and the relation to the peak wave pressure, $I \propto p^2$, the peak pressure of an imploding cylindrical shock wave varies like:

$$p_2 \quad \propto \quad \frac{1}{R^{1/2}} \tag{286}$$

Whereas $p \propto 1/R^{0.5}$ for sound waves, the nonlinearities of strong shock waves alter that power dependence slightly to more like $p \propto 1/R^{0.45}$, but we will continue to ignore such corrections.

Since temperature is proportional to pressure, the temperature T of the imploding shock wave varies just like Eq. (286):

$$T_2 \quad \propto \quad \frac{1}{R^{1/2}} \tag{287}$$

As in the spherical case, the velocity in the cylindrical shock wave is $dR/dt \propto \sqrt{T}$. Using Eq. (287), the velocity thus varies like:

$$\frac{dR}{dt} \quad \propto \quad \frac{1}{R^{1/4}} \tag{288}$$

By integrating Eq. (288), one finds the time variation of the shock wave radius $R(t)$ (for both the $t < 0$ implosion and $t > 0$ expansion phases):

$$\int R^{1/4}\, dR \quad \propto \quad \int dt \qquad \Longrightarrow \qquad R^{5/4} \;\propto\; t\,, \qquad \text{or} \tag{289}$$

$$R \quad = \quad C_3\; |t|^{4/5} \tag{290}$$

in which C_3 is a constant. As in the spherical case, the similarity exponent varies slightly depending on the value of γ, but 4/5 is a good representative value to use in Eq. (290).

Using Eq. (290), Eqs. (286)-(288) may be written as:

$$p_2 \quad \propto \quad T_2 \;\propto\; \frac{1}{R^{1/2}} \;\propto\; |t|^{-2/5} \tag{291}$$

$$\frac{dR}{dt} \quad \propto \quad \frac{1}{R^{1/4}} \;\propto\; |t|^{-1/5} \tag{292}$$

A spherical implosion compresses its central region in one more dimension than a cylindrical implosion does, so a cylindrical implosion cannot achieve as high a peak density as a spherical implosion can. Detailed calculations show that the cylindrical peak density is lower than the spherical peak density by a factor of $1/\sqrt{2}$. Modifying Eq. (285), the peak compression achievable in a cylindrical implosion is therefore:

$$\frac{\rho_{\text{peak}}}{\rho_1} \quad \approx \quad \frac{1}{2}\left(\frac{\gamma+1}{\gamma-1}\right)^2 \tag{293}$$

3.7 Subsonic Flow

Subsonic flow involves velocities that are less than Mach 1, the speed of sound, but may be high enough that compressibility effects must be considered. Using the definition of the velocity potential $\mathbf{v} = -\nabla\phi$, allowing for variation in the density ρ, and neglecting variation with time ($\partial/\partial t = 0$), the continuity equation from Eq. (3) may be written as

$$0 \;=\; \nabla\cdot(\rho\mathbf{v}) \;=\; \rho\nabla\cdot\mathbf{v} \;+\; \mathbf{v}\cdot\nabla\rho \;=\; -\rho\nabla^2\phi \;+\; \mathbf{v}\cdot\nabla\rho$$

$$\Rightarrow \quad \nabla^2\phi \;-\; \frac{\mathbf{v}\cdot\nabla\rho}{\rho} \;=\; 0 \tag{294}$$

For incompressible flow, the second term in Eq. (294) is zero, so this equation reduces to Laplace's equation with its usual solutions (Section 1.5). For compressible flow moving at high speed v_x in the x direction, one can approximate the second term of Eq. (294) and use the definition of the speed of sound $v_s^2 \equiv \partial p/\partial\rho$ from Eqs. (159) and (178):

$$\frac{\mathbf{v}\cdot\nabla\rho}{\rho} \;\approx\; v_x\,\frac{\partial\rho}{\partial x}\,\frac{1}{\rho} \;=\; v_x\,\frac{\partial\rho}{\partial p}\,\frac{\partial p}{\partial x}\,\frac{1}{\rho} \;=\; \frac{v_x}{v_s^2}\,\frac{\partial p}{\partial x}\,\frac{1}{\rho} \tag{295}$$

Using the momentum equation $v_x\partial v/\partial x = -(1/\rho)\partial p/\partial x$ from Eq. (5), the velocity potential ϕ, and the free-stream Mach number $M_\infty \equiv v_x/v_s$ (the subscript ∞ merely indicates that the free-stream Mach number is the speed of the flow far from objects passing through the flow and any flow perturbations that they induce), Eq. (295) may be rewritten as

$$\frac{\mathbf{v}\cdot\nabla\rho}{\rho} \;\approx\; -\,\frac{v_x^2}{v_s^2}\,\frac{\partial v}{\partial x} \;=\; M_\infty^2\,\frac{\partial^2\phi}{\partial x^2} \tag{296}$$

Inserting Eq. (296) into Eq. (294) yields:

$$\left[\left(1 - M_\infty^2\right)\frac{\partial^2}{\partial x^2} + \frac{\partial^2}{\partial y^2} + \frac{\partial^2}{\partial z^2}\right]\phi \;=\; 0 \tag{297}$$

Equation (297) leads back to Laplace's equation and its usual solutions if one simply rescales the effective dimension x in the direction of motion relative to the y and z coordinates:

$$x' \;=\; \frac{x}{\sqrt{1 - M_\infty^2}} \tag{298}$$

As a concrete example of the effect of Eq. (298), a given wing shape experiencing compressible flow is equivalent to a wing that is $1/\sqrt{1 - M_\infty^2}$ more elongated/swept back and experiencing incompressible flow; this **Prandtl-Glauert transformation** is shown in Fig. 23.

The effective scale change in the direction of the flow also alters the apparent density of the flow by the same factor of $1/\sqrt{1 - M_\infty^2}$ (effectively compressing the density in the direction of motion), in turn increasing the pressure exerted by the flow's density impacting the object by the same factor, leading to the **Prandtl-Glauert rule** for pressure, lift, and drag coefficients in compressible vs. incompressible flow:

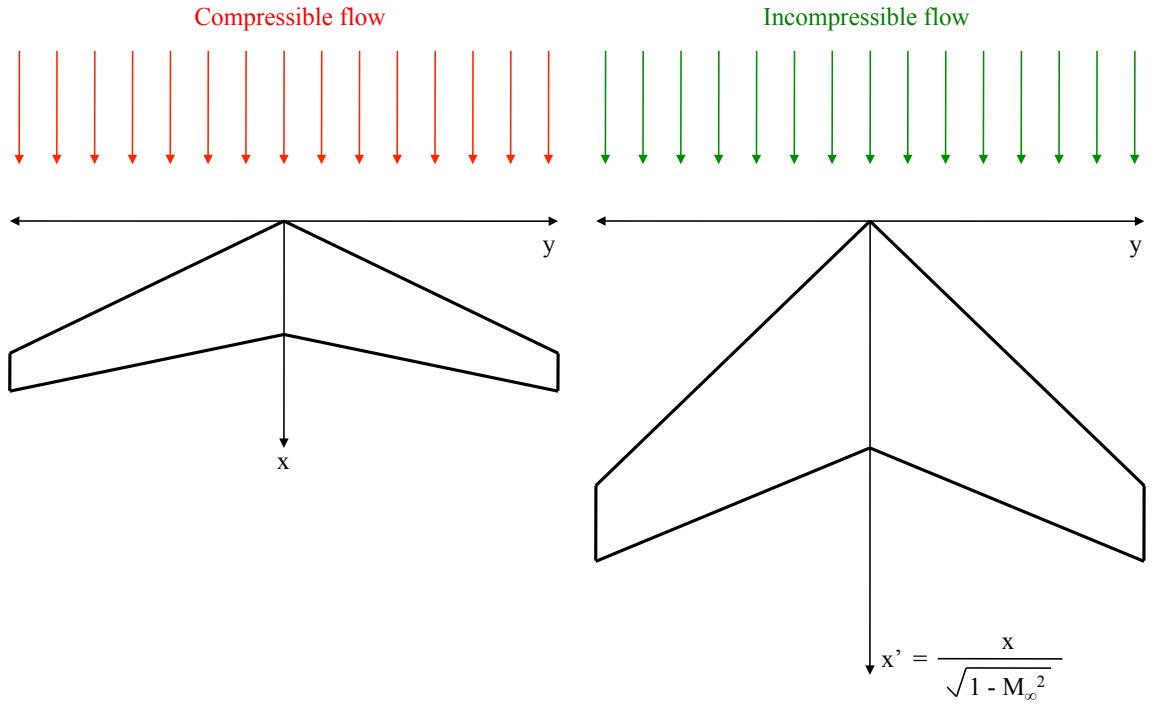

Figure 23. Prandtl-Glauert transformation. The aerodynamics of a shape traveling through compressible flow at Mach number M_∞ are equivalent to those of a shape that is traveling through incompressible flow and distorted by a factor of $1/\sqrt{1-M_\infty^2}$ in the direction of flow; dimensions perpendicular to the flow are unaffected.

$$C_{p,\,\text{comp}} = \frac{C_{p,\,\text{incomp}}}{\sqrt{1-M_\infty^2}} \tag{299}$$

$$C_{L,\,\text{comp}} = \frac{C_{L,\,\text{incomp}}}{\sqrt{1-M_\infty^2}} \tag{300}$$

$$C_{D,\,\text{comp}} = \frac{C_{D,\,\text{incomp}}}{\sqrt{1-M_\infty^2}} \tag{301}$$

The fundamental physics that led to Eqs. (298) and (299)-(301) is different than the physics underlying special relativity (*Classical Mechanics* ?). Nonetheless, it is somehow comforting that the results are basically the same, provided one uses the speed of sound waves v_s here instead of the speed of light waves c as in special relativity. As an object approaches the intrinsic wave speed, effective dimensions in the direction of motion are altered by $1/\sqrt{1-v^2/v_s^2}$ or $1/\sqrt{1-v^2/c^2}$, and resistance to further acceleration of the object increases by the same factor.

Simple linear approximations were used in Eqs. (295) and (296) in order to derive Eqs. (299)-(301). More accurate calculations yield a modified version called the **Karman-Tsien rule** [9, 10]:

$$C_{p,\,\text{comp}} = \frac{C_{p,\,\text{incomp}}}{\sqrt{1-M_\infty^2} + [M_\infty^2/(1+\sqrt{1-M_\infty^2})]C_{p,\,\text{incomp}}/2} \tag{302}$$

The first term in the denominator of Eq. (302) is simply the Prandtl-Glauert term. The other term in the denominator is a higher-order correction term obtained from nonlinear theory. Note that whereas the Prandtl-Glauert Eq. (299) blows up as the Mach number approaches 1, the more realistic Karman-Tsien Eq. (302) merely approaches a finite limiting value (in this case apparently 2, although nonlinearities make it tricky to correctly calculate the precise value).

3.8 Transonic Flow

Flow just below, at, or just above the speed of sound is called **transonic**. Equation (301) predicts that as a subsonic vehicle accelerates toward Mach 1, its drag coefficient C_D increases without limit. Similarly, Eq. (313) derived in the next section will show that as a supersonic vehicle decelerates toward Mach 1, C_D also blows up. Actually, the linear approximations underlying these derivations break down at Mach 1, where the flow equations become highly nonlinear. The peak transonic C_D is large but not infinite, as already observed from the Karman-Tsien Eq. (302). The nonlinearity makes the precise transonic C_D very difficult to calculate or even measure experimentally (since the nonlinearity can amplify very small changes in experimental conditions to yield very different results), but Fig. 24 plots a typical jet's C_D vs. Mach number.

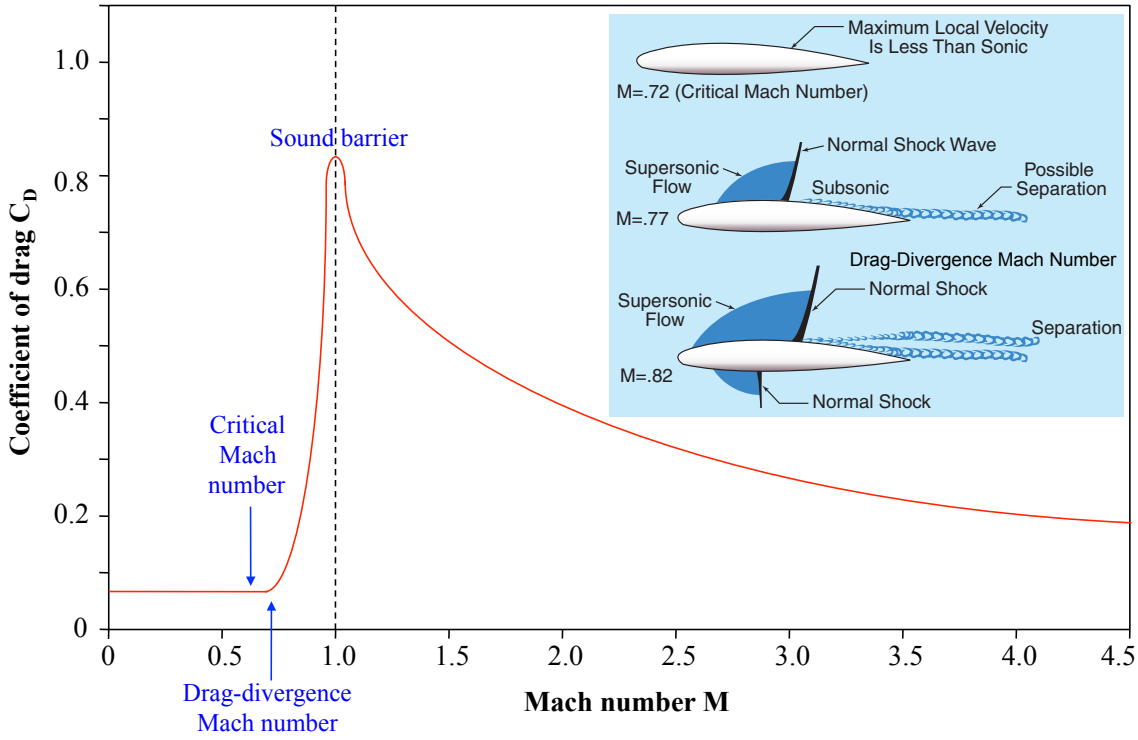

Figure 24. Sound barrier, or peak transonic drag coefficient. (Inset image by FAA and in public domain, from www.faa.gov/library/manuals/aircraft/airplane_handbook/media/faa-h-8083-3a-6of7.pdf, p. 15-7.)

From Section 1.8 and Fig. 24 inset, flow accelerates and decelerates as it moves around the contours of an airfoil, so the flow has different Mach numbers at different locations. As an airfoil begins to approach Mach 1, say at a free-stream Mach number of ~ 0.7, flow accelerated as it moves around the contours first reaches Mach 1 at some point on the surface; this speed is called the **critical Mach number** M_{cr}. A weak shock wave emanates from the surface at the point where the flow goes from supersonic back to subsonic. As the airfoil's speed increases closer to Mach 1, say Mach ~ 0.8, more of the surface is covered by supersonic flow and the shock wave moves toward the rear of the airfoil and becomes stronger. At the **drag-divergence Mach number** M_{ds}, the shock wave is strong enough that is causes the boundary layer to separate from the rear of the airfoil. This boundary layer separation is the main cause of the large transonic C_D that is sometimes called the sound barrier. Beyond Mach 1, a detached bow shock wave also forms ahead of the airfoil.

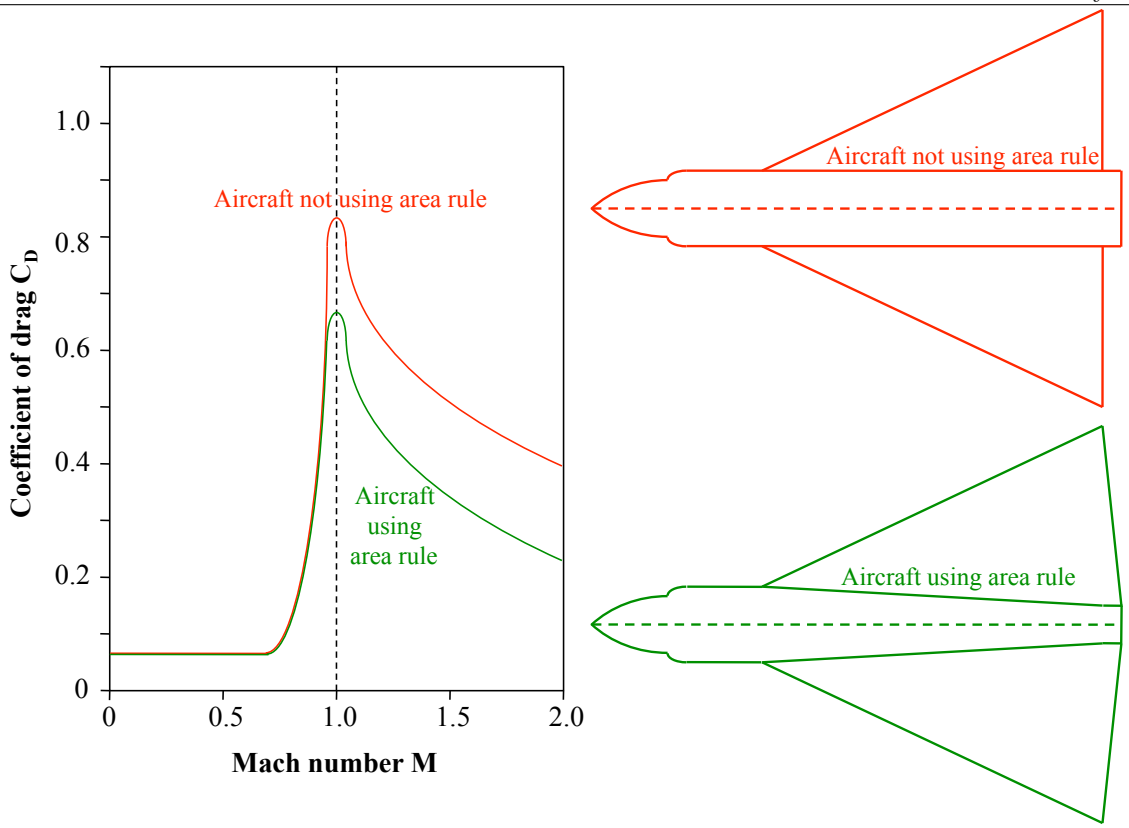

Figure 25. Area rule to reduce transonic drag. By keeping an aircraft's cross-sectional area that is presented to incoming flow relatively constant down the length of the craft, the flow can adjust to the contours of the vehicle with less compression and rarifaction, and hence less drag. For example, an aircraft's body should begin to narrow at the point where wings begin.

Four principles minimize drag in the transonic regime, and ideally all four should be employed:

1. **Area rule.** If transonic flow moving longitudinally down a vehicle encounters a sudden change in the vehicle's cross-sectional area, the flow cannot easily move out of the way; it is compressed or rarified and may separate from the vehicle's surface or launch a shock wave. By keeping the cross-sectional area relatively constant down the length of a vehicle, one can avoid such effects and thereby minimize the drag coefficient. For example, an aircraft's body should begin to narrow at the point where wings begin, as shown in Fig. 25.
2. **Supercritical airfoils.** As discussed in Section 1.7, the curvature of an airfoil makes airflow above the wing faster than flow below it. For aircraft at high subsonic speeds, this effect can accelerate air above the wings to Mach 1, creating a strong shockwave, separated boundary layer, and higher drag. By making the upper surface of the wings flatter or **supercritical**, aircraft can travel closer to Mach 1 before high-drag transonic flow occurs [Fig. 26(a)].
3. **Thinner airfoils.** Reducing the thickness of airfoils allows them to operate closer to Mach 1 before their drag coefficient rises [Fig. 26(b)]. In accordance with the Prandtl-Glauert transformation (Fig. 23), compressible flow at high supersonic speeds alters apparent lengths in the direction of travel relative to lengths perpendicular to the direction of travel, so a thin airfoil at high speeds appears to have the same proportions as a thick airfoil at low speeds.
4. **Swept wings.** Wings swept back at an angle in agreement with the Prandtl-Glauert transformation (Fig. 23) also reduce the drag coefficient in the transonic regime [Fig. 26(c)].

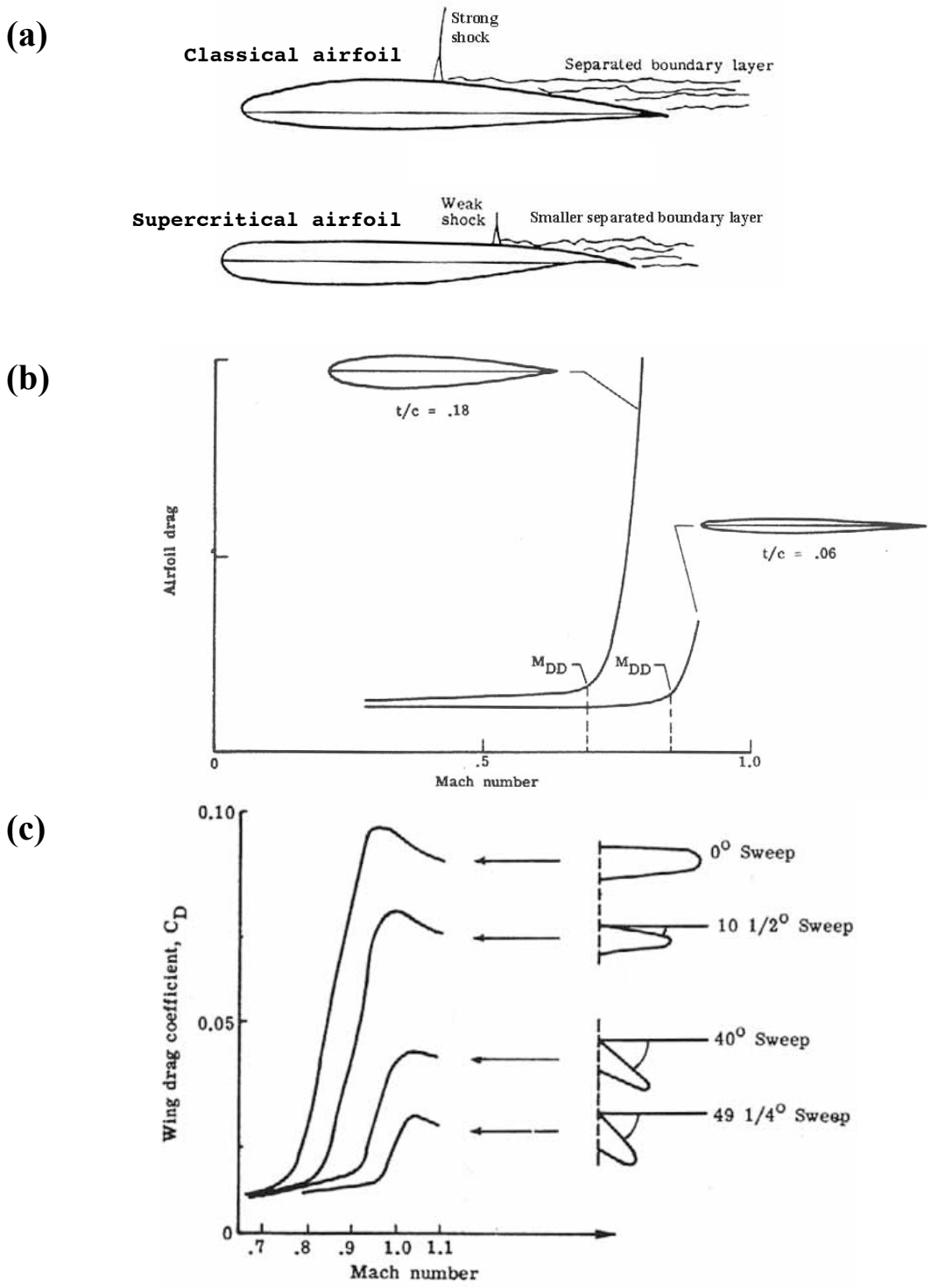

Figure 26. Other methods to reduce transonic drag. **(a)** The upper curve of a classical airfoil can increase subsonic flow to supersonic speeds, creating a strong shock wave, separated boundary layer, and higher drag. A supercritical airfoil is flatter on top to minimize these problems. **(b)** Reducing the thickness of airfoils allows them to operate closer to Mach 1 before their drag coefficient rises. **(c)** Swept-back wings also reduce the drag coefficient. (Images by NASA and in public domain, from www.centennialofflight.gov/timeline/ri_images.cfm.)

3.9 Supersonic Flow

Supersonic flow has a velocity greater than Mach 1. This section will only consider velocities between Mach 1 and approximately Mach 5; higher velocities are classified as hypersonic and will be analyzed in the next section.

If an object is traveling at or above Mach 1, sound waves emanating from the object behave very differently than those produced by an object moving at less than Mach 1 (Fig. 27). If an object travels at a subsonic velocity v, it produces waves that travel faster and further than the object in all directions–people can hear the object coming. Specifically, during a time Δt, the object moves a distance $v\Delta t$ from its original position, but a sound wave emitted from its initial position travels a greater distance $v_s\Delta t$ [Fig. 27(a)]. If an object travels at the speed of sound, $v = v_s$, people cannot hear it coming, since the object and its waves arrive at the same time. By the same token, the fluid ahead of the object is in a **zone of silence** where it is not forewarned about the object and cannot move out of the way until it is too late, increasing the drag on the object and producing the "sound barrier" [Fig. 27(b)]. Waves emitted by the object at various points in its trajectory pile up to form a flat shock wave or **Mach wave** moving with the object and extending perpendicular to its trajectory. If an object travels at a supersonic speed v, it arrives long before its sound waves, with the object covering a distance $v\Delta t$ in the time that a wave emitted from its initial location only travels a distance of $v_s\Delta t$ [Fig. 27(c)]. In this case, waves emitted by the object at various points in its trajectory pile up to form a **Mach cone**, a shock wave extending from the object and covering an angle μ, the **Mach angle**, on all sides of the object's trajectory. This is directly analogous to the physics and the direction of waves produced by a speedboat traveling faster than the normal speed of gravity waves in water (Section 3.11), or Cerenkov radiation emitted by a particle traveling faster than the speed of light in a medium (*Electromagnetism and Acoustics* ?.?) Using the right triangle in Fig. 27(c), one can find the Mach angle from

$$\sin\mu \;=\; \frac{v_s\Delta t}{v\Delta t} \;=\; \frac{v_s}{v} \tag{303}$$

Thus in terms of the free stream Mach number $M_\infty = v/v_s$, the Mach angle is

$$\mu \;=\; \sin^{-1}\frac{1}{M_\infty} \tag{304}$$

Measured in multiples of $v_s\Delta t$, the right triangle in Fig. 27(c) has a hypotenuse of length M_∞ and a side of length 1 opposite the angle μ. By the Pythagorean theorem, the side adjacent to the angle μ therefore has a length of $\sqrt{M_\infty^2 - 1}$ in these units, or the ratio of opposite to adjacent sides is:

$$\tan\mu \;=\; \frac{1}{\sqrt{M_\infty^2 - 1}} \tag{305}$$

The Mach angle is strictly valid only in the limit of very small waves or disturbances to the fluid, as was found earlier with Eq. (257). Stronger disturbances form a stronger shock wave with an angle β between μ and 90^o that must be found from Eq. (256) or Fig. 19. However, since the Mach angle is approximately valid and much easier to calculate, we will mostly just use it.

As shown in Fig. 28(a), if a flat surface in a supersonic flow has a sudden bend away from the flow at angle θ, the bend will produce a Mach wave at angle μ. Fluid flow near the surface will also bend by an angle θ, but the fluid does not find out about the bend until it passes through the Mach wave. The fluid flow changes from an initial velocity v_o to a final velocity $v = v_o + \Delta v$, where the height of the triangle highlighted in Fig. 28(b) is $v_o \sin\theta \approx v_o\theta$ for small angles θ. From the close-up of the highlighted triangle in Fig. 28(c), the height of the triangle may also be expressed as $\Delta v/\tan\mu$. Equating these two expressions for the height of the highlighted triangle yields:

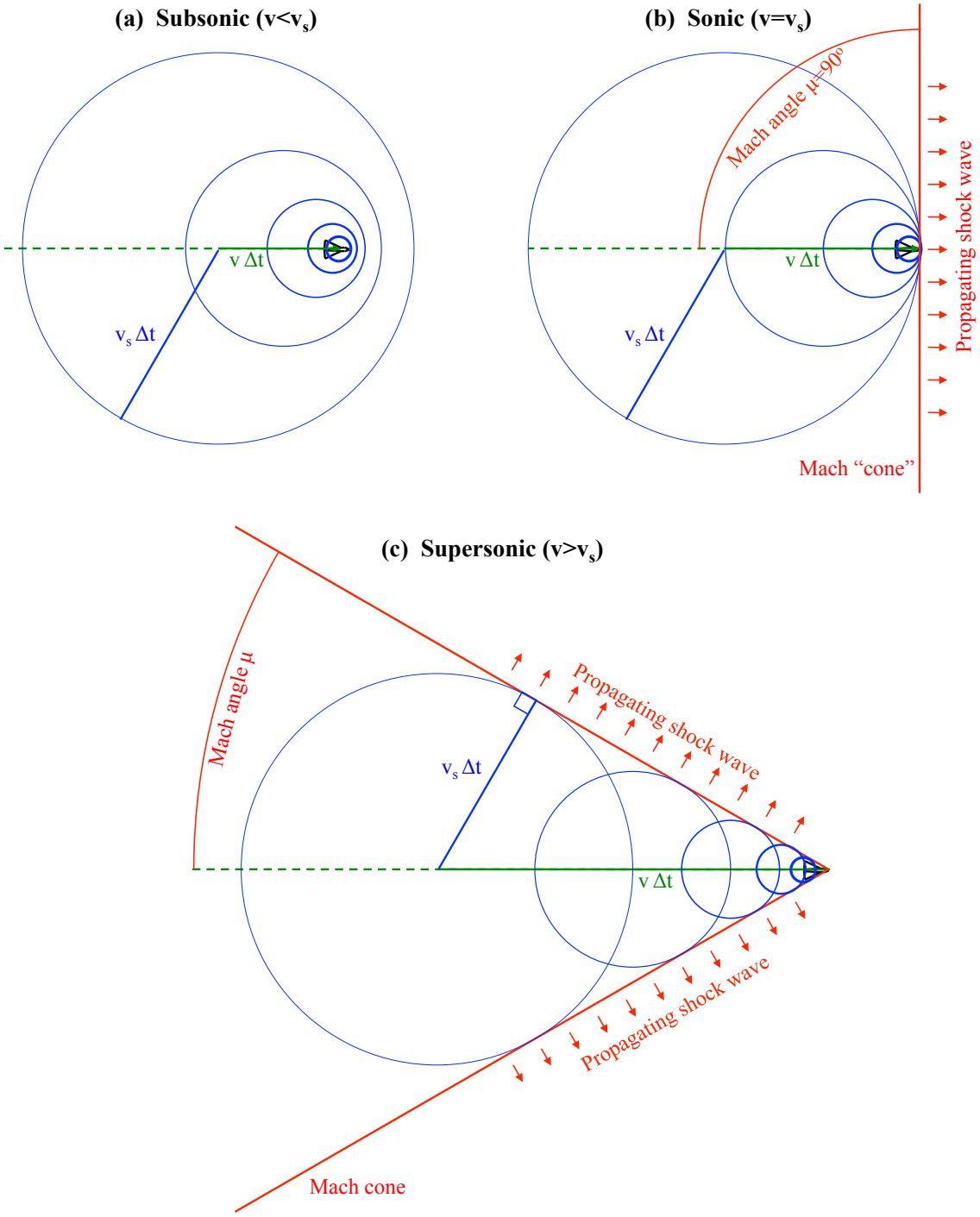

Figure 27. An object with velocity v travels a distance $v\Delta t$ in the time a sound wave emitted from the object's original position travels a distance $v_s\Delta t$. **(a)** In the subsonic case ($v < v_s$), the waves travel faster and further than the object in all directions. **(b)** In the sonic case ($v = v_s$), the waves emitted by the object at different times pile up to create a flat Mach wave moving with the object and extending perpendicular to its trajectory. **(c)** In the supersonic case ($v > v_s$), the object outruns its own waves, and the waves pile up to create a Mach cone trailing the object with an angle μ relative to the object's trajectory.

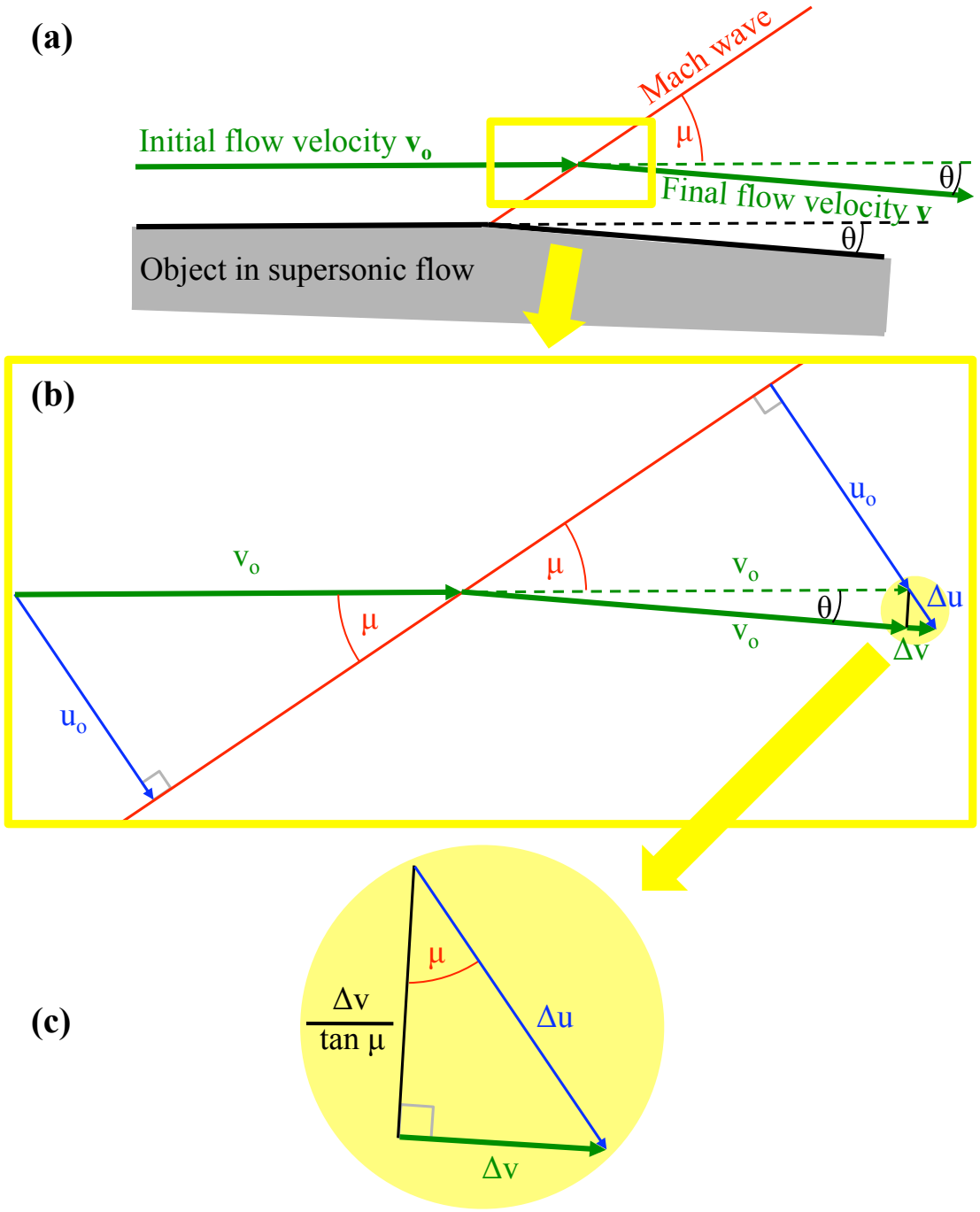

Figure 28. Finding the supersonic pressure coefficient. **(a)** If a flat surface in a supersonic flow has a sudden bend away from the flow at angle θ, the bend will produce a Mach wave at angle μ. Fluid flow near the surface will also bend by an angle θ, but the fluid does not find out about the bend until it passes through the Mach wave. **(b)** The fluid flow changes from an initial velocity v_o to a final velocity $v = v_o + \Delta v$, where the height of the highlighted triangle is $v_o \sin\theta$. If the surface bends away from the flow as shown, Δv is positive and the flow accelerates. However, if the surface bends into the flow, Δv is negative and the flow decelerates. **(c)** From this close-up of the highlighted triangle, the height of the triangle may also be expressed as $\Delta v / \tan\mu$.

$$\frac{\Delta v}{v_o} \;=\; -\theta \tan\mu \;=\; \frac{-\theta}{\sqrt{M_\infty^2 - 1}} \tag{306}$$

The surface deflection angle θ is defined to be positive for a leading edge or a bend into the flow [Fig. 21(a)] and negative for a trailing edge or a bend away from the flow [Figs. 21(b) and 28(a)]. Thus a leading edge creates a shock wave that decelerates the flow [($\Delta v < 0$ in Eq. (306)], whereas a trailing edge creates an expansion fan that accelerates the flow [($\Delta v > 0$ in Eq. (306)].

The coefficient of pressure at an object's surface is the local pressure relative to the free-stream pressure ($p - p_o$), divided by the pressure equivalent to the free stream's kinetic energy ($\rho_o v_o^2/2$):

$$C_p \;\equiv\; \frac{p - p_o}{\rho_o v_o^2/2} \tag{307}$$

Since the flow velocity increases ($\Delta v > 0$) for a trailing edge, by the conservation of energy, the pressure of the flow must decrease ($p < p_o$). Thus the pressure difference is:

$$\begin{aligned} p - p_o &= \frac{1}{2}\rho_o v_o^2 - \frac{1}{2}\rho_o (v_o + \Delta v)^2 \\ &\approx -\rho_o v_o \Delta v \end{aligned} \tag{308}$$

We have neglected compressibility effects by assuming $\rho_o \approx$ constant, and also neglected the term involving $(\Delta v)^2$, since those effects are smaller for small perturbations to the flow.

Combining Eqs. (306)-(308), the **Ackeret (linearized) supersonic pressure coefficient** is

$$C_p \;=\; 2\,\frac{\Delta v}{v_o} \;=\; \frac{2\theta}{\sqrt{M_\infty^2 - 1}} \tag{309}$$

On a leading surface, C_p is positive and the pressure is higher than the ambient pressure p_o, but on a trailing surface, C_p is negative–a supersonic vehicle pulls a partial vacuum in its wake.

It is reassuring that the denominator of the supersonic C_p in Eq. (309) is the same as that of the subsonic C_p in Eq. (299) but with $M_\infty^2 - 1$ instead of $1 - M_\infty^2$. Special relativity predicts a similar sign reversal for objects traveling faster vs. slower than light (*Classical Mechanics* ?.?). Like the subsonic C_p, the supersonic C_p in Eq. (309) becomes infinite at Mach 1, but this should not be taken seriously, since the assumptions underlying the derivation break down as explained in Section 3.8. As an aside, when one goes from subsonic to supersonic speeds, the factor $1 - M_\infty^2$ shifts from positive to negative, so Eq. (297) changes from Laplace's equation into a hyperbolic equation:

$$\left[\left(M_\infty^2 - 1\right)\frac{\partial^2}{\partial x^2} - \frac{\partial^2}{\partial y^2} - \frac{\partial^2}{\partial z^2}\right]\Phi \;=\; 0 \tag{310}$$

More detailed calculations show that the right side of Eq. (309) is just the first term of a Taylor series in powers of θ. The higher terms bring in the nonlinearities of supersonic flow (such as the more accurate oblique shock wave angle $\beta > \mu$ from Section 3.5) that are not described by the first-order linear term. The **Busemann supersonic pressure coefficient** [13] retains the first two terms of the Taylor series for greater accuracy:

$$C_p \;=\; \frac{2\theta}{\sqrt{M_\infty^2 - 1}} \;+\; \left[\frac{(\gamma+1)M_\infty^4 - 4M_\infty^2 + 4}{2(M_\infty^2 - 1)^2}\right]\theta^2 \tag{311}$$

Equation (308) can be used to calculate the lift and drag of vehicles. Figure 29 shows a simple example, a flat plate inclined at angle α to a supersonic flow. The pressure on the bottom of the plate is positive relative to p_o and given by Eq. (308) with $\theta = \alpha$. Likewise, the pressure on the top of the plate is negative and given by Eq. (308) with $\theta = -\alpha$. The net pressure force normal to the surface is the difference of these two quantities, and by the geometry of Fig. 5(c) a fraction $\cos\alpha$ of that force is directed upward (perpendicular to the incoming flow) as lift. For small angles of attack α, one may use $\cos\alpha \approx 1$. Thus the supersonic lift coefficient of a flat plate is

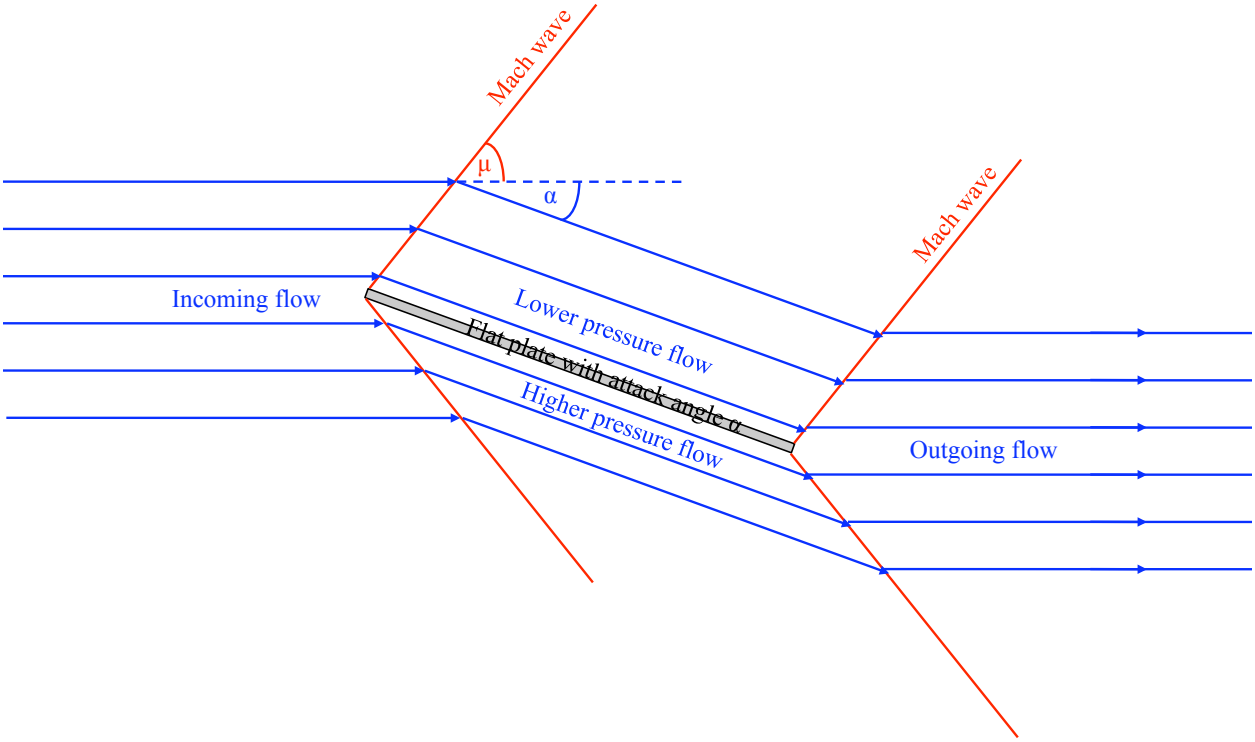

Figure 29. A flat plate in supersonic flow. The flat plate is inclined at an angle of attack α relative to the incoming flow. The leading and trailing edges of the plate generate Mach waves at angle μ relative to the incoming flow. The supersonic flow adjusts its path when it passes through each Mach wave. Note that the pressure of the supersonic flow decreases above the plate (the lines of flow become further apart), whereas the pressure increases below the plate (the lines of flow become closer together). This pressure difference produces both lift and drag forces on the plate.

$$C_L = \left[\frac{2\alpha}{\sqrt{M_\infty^2 - 1}} - \left(- \frac{2\alpha}{\sqrt{M_\infty^2 - 1}} \right) \right] \cos\alpha \approx \frac{4\alpha}{\sqrt{M_\infty^2 - 1}} \tag{312}$$

Using the small-angle approximation $\sin\alpha \approx \alpha$ for the component of the pressure force parallel to the incoming flow (Fig. 29), the supersonic drag coefficient on a flat plate is likewise:

$$C_D = \left[\frac{2\alpha}{\sqrt{M_\infty^2 - 1}} - \left(- \frac{2\alpha}{\sqrt{M_\infty^2 - 1}} \right) \right] \sin\alpha \approx \frac{4\alpha^2}{\sqrt{M_\infty^2 - 1}} \tag{313}$$

Thus for small angles of attack α, the lift-to-drag ratio of the supersonic plate is:

$$\frac{L}{D} = \frac{C_L}{C_D} = \cot\alpha \approx \frac{1}{\alpha} \tag{314}$$

Note that Eq. (314) for the supersonic case is the same result and for the same reason as Eq. (57) for the incompressible subsonic case. The same methods used above may be used to approximate the supersonic lift and drag of more complex objects if the angles of their surfaces relative to the incoming flow are fairly small.

3.10 Hypersonic Flow

By convention, **hypersonic flow** generally means Mach 5 or higher, and it is relevant for spacecraft leaving or re-entering the earth's atmosphere, some missiles, and a few proposed advanced aircraft. As will be shown, hypersonic airflow behaves differently than merely supersonic flow, leading to unique pressure, lift, and drag coefficients that are independent of Mach number. Aerodynamic heating is also important at hypersonic speeds, as will be discussed in Section 4.

Due to its extreme forward speed, hypersonic flow travels in a straight line until it hits an object, then it follows the contours of the object very closely, as shown in Fig. 30. Shock waves also follow along the body very closely instead of diverging off to each side. Isaac Newton considered this sort of fluid behavior first, so this is called the Newtonian theory.

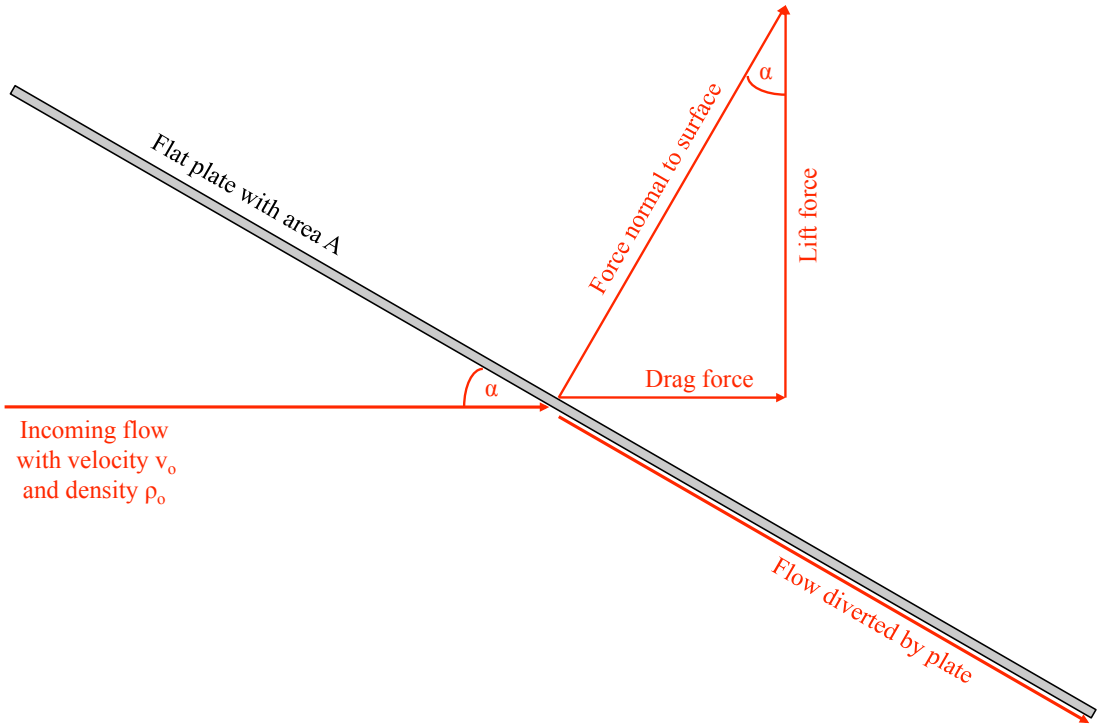

Figure 30. Hypersonic flow hitting a surface is diverted to closely follow along the surface, producing a force normal to the surface, which has lift and drag components.

The force of a hypersonic flow around an object can be found by considering a flat surface of area A with angle of attack α relative to the flow (Fig. 30). The mass flow rate hitting the surface is $\dot{m} = \rho_o v_o A \sin\alpha$. The flow velocity component perpendicular to the surface stops when it hits the surface, causing a change in flow velocity $\Delta v = v_o \sin\alpha$ and a force F perpendicular to the surface:

$$F \;=\; \dot{m}\,\Delta v \;=\; \rho_o v_o^2 A \sin^2\alpha \tag{315}$$

This force exerts on the surface a pressure F/A in addition to the ambient background pressure p_o, and this pressure may be written in terms of a coefficient of pressure C_p:

$$p - p_o \;=\; \frac{F}{A} \;=\; \rho_o v_o^2 \sin^2\alpha \;=\; C_p\,\frac{1}{2}\rho_o v_o^2 \tag{316}$$

$$\text{where}\quad C_p \;\equiv\; 2\sin^2\alpha \tag{317}$$

Even for objects other than flat plates, Eq. (317) can be used to find the local pressure at a point with inclination α on the object. Note that for a blunt body ($\alpha = \pi/2$), the pressure coefficient for hypersonic flow is twice what it would be for a flow much slower than the speed of sound.

A more accurate version of Eq. (317) can be found from the oblique shock wave equations of Section 3.5. Using Eq. (256) with the angle of attack as the deflection angle ($\theta = \alpha$) and assuming that the Mach number is very large and the angles are very small, the relation between the shock wave angle β and the angle of attack or deflection angle α is linear:

$$\beta \approx \frac{\gamma+1}{2}\,\alpha \tag{318}$$

For air with $\gamma = 1.4$, the shock wave angle from Eq. (318) is just 20% larger than the surface angle, so at hypersonic speeds, shock waves do closely follow along a vehicle's body as noted earlier.

Analogous to the Newtonian derivation of Eqs. (316)-(317), the excess pressure exerted on a surface by hypersonic flow may be found from Eq. (252) by setting $p_2 = p$ and $p_1 = p_o$, and assuming that $p \gg p_o$ and that the Mach number is very large:

$$\frac{p-p_o}{p_o} \approx \frac{p}{p_o} \approx \frac{2\gamma}{\gamma+1}\sin^2\beta\ M^2 = \frac{2}{\gamma+1}\sin^2\beta\ \frac{1}{RT_o}\,v_o^2\,, \quad \text{or} \tag{319}$$

$$p-p_o \approx \frac{2}{\gamma+1}\sin^2\beta\ \frac{p_o}{RT_o}\,v_o^2 = \frac{4}{\gamma+1}\sin^2\beta\ \frac{1}{2}\rho_o v_o^2 = C_p\,\frac{1}{2}\rho_o v_o^2 \tag{320}$$

$$\text{where } C_p \approx \frac{4}{\gamma+1}\sin^2\beta \tag{321}$$

For air with $\gamma = 1.4$, the pressure coefficient from Eqs. (320) and (318) is $C_p \approx 1.67\sin^2(1.2\alpha)$.

Shock wave compression often heats hypersonic flow around an object to such high temperatures that γ for the air changes from its usual value 1.4. For example, diatomic oxygen dissociates in the temperature range 2000-4000 ^{o}K ($O_2 \rightarrow 2O$), diatomic nitrogen dissociates at 4000-9000 ^{o}K ($N_2 \rightarrow 2N$), and atoms ionize at $T > 9000^o$K ($N \rightarrow N^+ + e^-$ and $O \rightarrow O^+ + e^-$). It is difficult to calculate the effective γ under such conditions, but it is generally lower than 1.4 and closer to 1. Note that if γ is 1, Eqs. (320) and (318) become exactly the Newtonian result of Eq. (317).

Since C_p is the coefficient for pressure normal to a surface, the lift coefficient may be found by taking the fraction $\cos\alpha$ that is perpendicular to the flow (Fig. 29):

$$C_L = C_p\cos\alpha = C_{\text{p max}}\sin^2\alpha\cos\alpha \tag{322}$$

This lift coefficient is reaches a maximum of $C_L \approx 0.77$ at an angle of attack $\alpha \approx 54.7^o$.

Likewise, the drag coefficient is found from the pressure component parallel to the flow (which is proportional to $\sin\alpha$, as shown in Fig. 29):

$$C_D = C_p\sin\alpha = C_{\text{p max}}\sin^3\alpha \tag{323}$$

For small angles, the drag coefficient is $C_D \approx C_{\text{p max}}\alpha^3$, proving that hypersonic aerodynamics can be very nonlinear, even for small perturbations. From Eqs. (322)-(323), the ratio of lift to drag is

$$\frac{L}{D} = \frac{C_L}{C_D} = \cot\alpha \tag{324}$$

Equation (324) is the same result as Eq. (57) for the subsonic case and Eq. (314) for the supersonic case, and it is generally accurate except for $\alpha < 10^o$. Due to skin friction effects not included in this analysis, L/D actually drops to zero at $\alpha = 0$ instead of exploding as Eq. (324) suggests.

Note that coefficients C_p, C_L, and C_D are independent of Mach number at hypersonic velocities, just as they are at low subsonic velocities. The only velocity dependence is the v^2 by which they are multiplied to find the actual pressure, lift, and drag.

3.11 Analogy Between Acoustic Waves and Gravity Waves at a Fluid's Surface

Acoustic or shock waves in a compressible fluid are analogous to gravity waves at the surface of an incompressible fluid. Just as acoustic or shock waves could be either stationary or moving [Fig. 18(a)-(b)], gravity waves at the surface of a fluid may be either stationary or moving, as illustrated in Fig. 31(a) and (b). As with shock waves, a moving gravity wave may be treated as a stationary gravity wave (or vice versa) by means of the velocity transformations shown in Fig. 31.

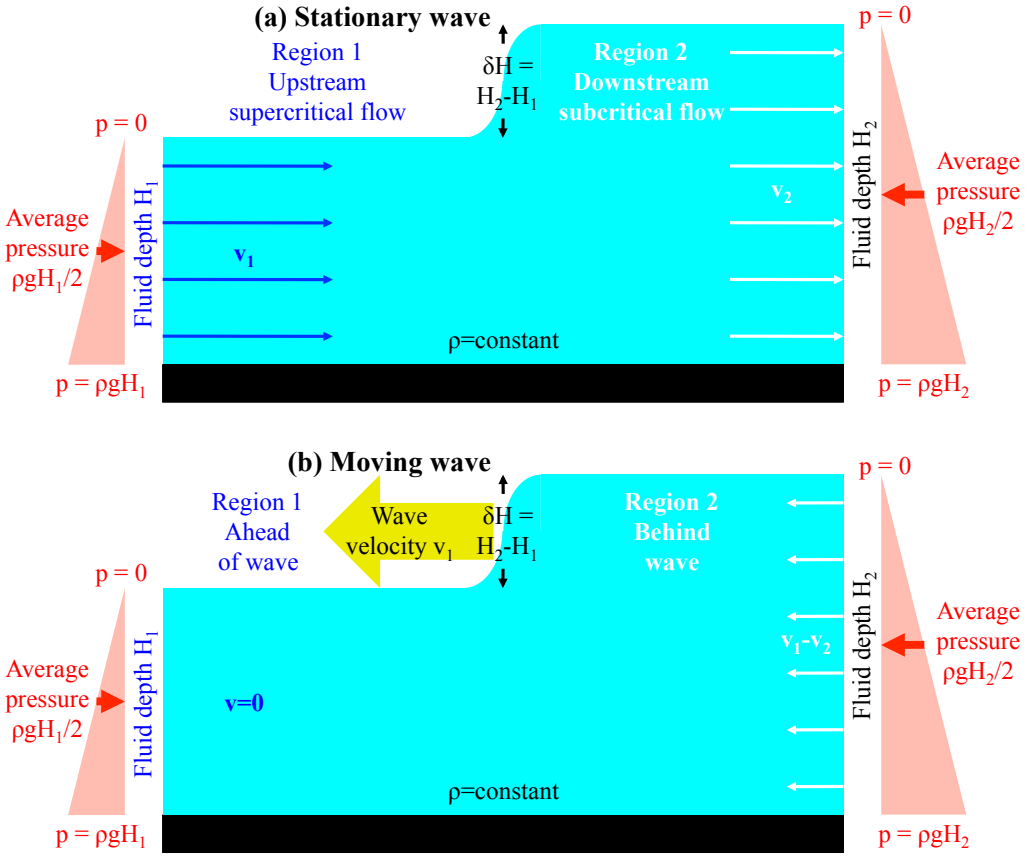

Figure 31. Gravity wave at the surface of a fluid for cases in which (a) the fluid is flowing at upstream velocity v_1 and the wave is stationary, and (b) the fluid is initially motionless and the wave is moving at velocity v_1.

Assuming constant density ρ and some constant fluid channel width into the page, conservation of mass from Eq. (4) for the wave in Fig. 31(a) (evaluated for fluid velocity v_1 and depth H_1 in region 1 ahead of the wave and fluid velocity v_2 and depth H_2 in region 2 behind the wave) is simply:

$$v_1 H_1 \quad = \quad v_2 H_2 \tag{325}$$

Momentum conservation from Eq. (5) may be simplified for the stationary wave in Fig. 31(a) by neglecting time variation ($\partial/\partial t = 0$) and viscosity ($\mathbf{F}_{\text{viscous}} = 0$) and only considering effects parallel to the fluid flow (thus the vertical $\rho\mathbf{g}$ term may be ignored):

$$\rho\mathbf{v}\cdot\nabla\mathbf{v} = -\nabla p \qquad \text{(from the momentum conservation equation)} \tag{326}$$

$$\rho v_1 \Delta v = -\Delta p \qquad \text{(evaluated across the jump from region 1 to region 2)} \tag{327}$$

$$\int \rho v_1 \Delta v \, dh = -\Delta \int p \, dh \qquad \text{(integrating over depth)} \tag{328}$$

$$v_1 H_1(\rho v_1 - \rho v_2) = -(H_1 p_{1,\,\text{avg}} - H_2 p_{2,\,\text{avg}}) = -\frac{1}{2}\rho g(H_1^2 - H_2^2) \tag{329}$$

The physical meaning of Eq. (329) is simply that the decrease in the momentum of fluid flowing from region 1 to region 2 in Fig. 31(a) is due to the imbalance in pressure forces on the fluid. There is a higher average pressure on the right side of the deeper region 2, and a lower average pressure on the left side of the shallower region 1, or a net pressure force toward the left to decrease the fluid's forward momentum. The factor $v_1 H_1$ on the left side of Eq. (329) gives the flux (per unit channel width into the page) flowing across the boundary from region 1 to region 2.

By combining Eqs. (325) and (329) and using some algebra, one can solve for the fluid velocities in regions 1 and 2 if the respective depths are known:

$$v_1 = \sqrt{\frac{gH_2}{2H_1}\,(H_1 + H_2)} \tag{330}$$

$$v_2 = \frac{H_1}{H_2} v_1 = \sqrt{\frac{gH_1}{2H_2}\,(H_1 + H_2)} \tag{331}$$

In the limit of a very small wave ($H_2 \to H_1 \equiv H$), the velocities in Eqs. (330)-(331) become:

$$v_1 \;\to\; v_2 \;\to\; v_{\text{wave}} \;\equiv\; \sqrt{gH} \tag{332}$$

The small-wave limit corresponds to the same fluid velocity $v_1 = v_2$ upstream and downstream of a stationary wave [Fig. 31(a)], or zero fluid velocity ahead of and behind a moving wave [Fig. 31(b)].

Equation (332) is the velocity v_{wave} of small waves on a fluid of depth H subject to gravitational acceleration g. For example, the surface wave velocity from Eq. (332) would be ~ 10 m/sec for a lake with a depth of 10 m, or ~ 100 m/sec for a sea with a depth of 1000 m. (For sufficiently deep water, the surface wave speed can become independent of the depth [4].) The speed v_{wave} of small gravity waves is analogous to the speed v_s of sound waves of small amplitude from Section 3.3. Just as large-amplitude shock waves can travel faster than v_s (Section 3.5), large gravity waves can travel faster than v_{wave} as shown by Eq. (330) with $H_2 > H_1$.

The **Froude number** F compares any velocity v to the small-gravity-wave velocity v_{wave} for the local depth H, just as the Mach number compares any velocity to the local speed of sound:

$$F \equiv \frac{v}{v_{\text{wave}}} = \frac{v}{\sqrt{gH}} \tag{333}$$

Instead of solving for the velocities, one can solve Eqs. (325) and (329) for the depth ratio:

$$\frac{H_2}{H_1} = \frac{1}{2}\left[\sqrt{1+8\left(\frac{v_1^2}{gH_1}\right)}-1\right] = \frac{1}{2}\left(\sqrt{1+8F_1^2}-1\right) \tag{334}$$

Note that $H_2/H_1 \to 1$ in Eq. (334) as $F_1 \to 1$ as expected.

Just like a shock wave, a gravity wave dissipates energy and creates entropy. The energy density loss E_{loss} or head loss h_{loss} of the fluid passing through the wave between region 1 and region 2 is:

$$E_{\text{loss}} = \rho g h_{\text{loss}} = \left(\rho g H_1 + \frac{1}{2}\rho v_1^2\right) - \left(\rho g H_2 + \frac{1}{2}\rho v_2^2\right) \tag{335}$$

$$\Rightarrow \quad h_{\text{loss}} = \frac{(H_2 - H_1)^3}{4H_1H_2} \tag{336}$$

A stationary wave such as that shown in Fig. 31(a) is often encountered in situations in which water in a channel is flowing so quickly that the flow velocity is greater than the local wave velocity $\sqrt{gH_1}$ for that depth. Such flow is called **supercritical flow** and is analogous to supersonic flow. The flow would much rather be traveling at less than the local wave velocity (**subcritical flow**), just as compressible flow would rather be subsonic. Since the density ρ must remain constant, the only way that supercritical flow can become subcritical is to increase its depth to H_2 and slow its velocity to v_2, as illustrated in Fig. 31(a). Such a stationary wave in open-channel flow is called a **hydraulic jump** due to the sudden increase in fluid height.

The moving wave of Fig. 31(b) may be a tidal wave, a tsunami generated by an earthquake, or a wave produced by a passing ship. A particularly interesting case is that of waves produced by a speedboat that is traveling faster than the local wave velocity $v_{\text{wave}} = \sqrt{gH}$, or with a Froude number $F > 1$. Just as sound waves emitted by a supersonic object (with a Mach number $M_\infty > 1$, or traveling faster than the local sound speed v_s) add up to produce a V-shaped shock wave trailing behind the object [Fig. 27(c)], waves produced by a speedboat moving at $F > 1$ add up to produce a V-shaped gravity wave trailing behind the speedboat. The angle of the waves made by the speedboat can be found from Eqs. (303)-(305) by simply replacing $v_s \to v_{\text{wave}}$ and $M_\infty \to F$.

The analogy between sound waves in a compressible fluid and gravity waves at the surface of an incompressible fluid may be especially elucidated by comparing the respective wave velocities from Eqs. (200) and (332):

- In sound waves, more fluid can accumulate at a given location by increasing the local density ρ. In gravity waves, more fluid can accumulate at a given location by increasing the local depth H.
- In sound waves, any local increase in density is resisted by the compressibility $E = \gamma p$. In gravity waves, any local increase in depth is resisted by the gravitational acceleration g.
- Sound waves result when the total energy sloshes back and forth between potential energy (stored in regions with higher density) and kinetic energy (fluid moving from higher-density to lower-density regions). Gravity waves result when the total energy sloshes back and forth between potential energy (stored in regions with greater depth) and kinetic energy (fluid moving from deeper to shallower regions).

4 Compressible, Viscous Fluid Mechanics

In general, detailed fluid flow calculations get really scary when both compressibility and viscosity must be considered at the same time. This situation applies when one must consider boundary layers and skin friction (hence involving viscosity) for objects traveling at high speeds (hence involving compressibility). Detailed predictions of these effects require computational fluid dynamic models and/or experimental measurements, neither of which we will cover here. Rather, we will begin by showing how the inclusion of compressibility alters some of the incompressible viscous flow results from Section 2 by a correction factor. Then we will spend the rest of this section considering several different examples of one of the most important applications of compressible viscous fluid mechanics, atmospheric reentry of spacecraft. These reentry examples can be simplified by treating compressibility and viscosity effects separately to obtain approximate results.

4.1 Fundamental Effects of Compressibility on Viscous Fluid Flow

Flow that is both compressible and viscous can be simplified by treating it as essentially inviscid compressible flow with an approximate correction factor for viscous effects, or as essentially incompressible viscous flow with an approximate correction factor for compressibility effects. In Section 3.4 (c) and (d), compressible, viscous internal flows were treated primarily as compressible inviscid flows; viscous effects were greatly simplified by assuming that the fluid all moved at the same velocity v across the cross-sectional area of the flow and that any viscous effects could be lumped into an average Fanno friction factor f for viscous drag between the fluid and the wall.

In contrast, for external compressible viscous flows such as will be considered in Section 4, it is easier to treat the flow as an incompressible viscous fluid but introduce a correction factor for compressibility effects. In most cases this correction factor is a factor of two or less, even at hypersonic speeds. Here we will find approximate expressions for this correction factor for a flat plate, but the same principles apply to other shapes and flow geometries.

When an object is subjected to a compressible viscous flow at ambient temperature T, some of the kinetic energy of the flow is converted to thermal energy in the boundary layer formed around the object. This makes the average effective temperature in the boundary layer, commonly dubbed the **reference temperature** T^*, higher than the ambient temperature T. If the fluid's ambient (or incompressible) properties are denoted by ρ for density and μ for viscosity, the fluid properties in the boundary layer must be evaluated at the reference temperature T^*, giving the values ρ^* for density and μ^* for viscosity. In turn, these modified density and viscosity values will affect the boundary layer thickness and frictional drag coefficient in ways we will now estimate.

In Eq. (207), we found that when a flow at Mach number M_∞ stops in an adiabatic manner, its kinetic energy is converted to thermal energy, raising its temperature by an amount $(\gamma-1)M_\infty^2 T/2 = M_\infty^2 T/5$ for air with $\gamma = 1.4$. To average between the flow that is heated in this manner by directly interacting with an adiabatic (perfectly insulating) wall, and the ambient flow further away from the wall, we can divide this temperature increase by a factor of two, $\approx M_\infty^2 T/10$. Thus the reference temperature for viscous compressible flow on an adiabatic wall is

$$\frac{T^*}{T} \approx 1 + \frac{1}{10}M_\infty^2 \tag{337}$$

Instead of an adiabatic wall, a different boundary condition is to stipulate that the wall temperature is fixed at a value T_w, for example due to cooling to prevent overheating of the vehicle. This reduces the effect of flow-deceleration-produced heating, say by a factor of ~ 3 to $\sim M_\infty^2 T/30$. In the boundary layer, one must take the average of the wall temperature T_w and the ambient flow temperature T, or $T^* \approx (T + T_w)/2$, then add the $\sim M_\infty^2 T/30$ temperature increase produced by slowing the flow. Therefore the reference temperature for viscous compressible flow on a fixed-temperature wall is

$$\frac{T^*}{T} \approx \frac{1}{2} + \frac{1}{2}\frac{T_w}{T} + \frac{1}{30}M_\infty^2 \tag{338}$$

A much scarier and more detailed calculation in [14] arrived at exactly the same answer as Eq. (338). Some references such as [2] and [11] give Eqs. (337) and (338) with numerical coefficients determined from empirical measurements, which have minor differences from the values given here. Note that Eqs. (337) and (338) reduce to $T^*/T = 1$ for low speeds and no wall temperature difference.

Using the ideal gas law in Eq. (138) and assuming constant pressure, the reference temperature modifies the density by a factor of:

$$\frac{\rho^*}{\rho} \approx \frac{T}{T^*} \tag{339}$$

The variation of viscosity with temperature is given by Sutherland's law:

$$\frac{\mu}{\mu_0} \approx \left(\frac{T}{T_0}\right)^{3/2} \frac{T_0 + S}{T + S} \tag{340}$$

For air, $\mu_0 \approx 1.72 \times 10^{-5}$ Pa·sec, $T_0 \approx 273^o$K, and $S \approx 111^o$K. At the high temperatures characteristic of hypersonic flight, Sutherland's law may be simplified to

$$\frac{\mu^*}{\mu} \approx \left(\frac{T^*}{T}\right)^{1/2} \tag{341}$$

From Eq. (133), the incompressible viscous drag force F_D on one side of a flat plate of width W and length L may be expressed in terms of a frictional drag coefficient C_f:

$$F_D = \frac{1}{2} C_f \rho v_\infty^2 W L \tag{342}$$

Likewise, the compressible viscous drag force F_D^* on one side of a flat plate can be expressed in terms of a drag coefficient C_f^*:

$$F_D^* = \frac{1}{2} C_f^* \rho v_\infty^2 W L = \frac{C_f^*}{C_f} F_D \tag{343}$$

In Eqs. (134) for incompressible viscous laminar flow and (136) for incompressible turbulent flow over a flat plate, the frictional drag coefficient was found to depend on the Reynolds number, which in turn depends on the density and viscosity in the boundary layer. Note that in Eq. (343), the compressible drag force is evaluated using ρ, not ρ^*. Thus the ratio C_f^*/C_f must be defined to include both compressible changes to the Reynolds number and changes ρ^*/ρ that would technically lie outside the definitions of the drag coefficients from Eqs. (134) and (136).

Using Eqs. (130), (339), and (341), compressibility increases the thickness of a laminar boundary layer on a flat plate by a factor of:

$$\frac{\delta(x)^*}{\delta(x)} = \left(\frac{\rho}{\rho^*}\frac{\mu^*}{\mu}\right)^{1/2} \approx \left(\frac{T^*}{T}\right)^{3/4} \tag{344}$$

For an adiabatic wall, Eq. (337) should be used in Eq. (344), and for a fixed-temperature wall, Eq. (338) should be used in Eq. (344). Relative to the incompressible result, the boundary layer thickness increases due to expansion of the heated boundary layer, since the density is now allowed to vary. Note that the thickness increases almost linearly with increasing reference temperature. At the same Mach number, a wall that is cooled to maintain a fixed temperature will have a thinner boundary layer than an adiabatic wall, because the cooled wall partially cools the boundary layer and keeps it from expanding as much.

Similarly, using Eqs. (134), (339), and (341), and incorporating a factor of ρ^*/ρ as discussed above, compressibility alters the laminar drag coefficient on a flat plate by a factor of:

$$\frac{C_f^*}{C_f} = \frac{\rho^*}{\rho}\left(\frac{\rho}{\rho^*}\frac{\mu^*}{\mu}\right)^{1/2} \approx \left(\frac{T}{T^*}\right)^{1/4} \tag{345}$$

The drag coefficient decreases with increasing reference temperature (and hence increasing velocity) since high-speed aerodynamic heating increases the boundary layer thickness, thereby decreasing the velocity gradient across the boundary layer and hence decreasing the shear and drag. The laminar drag coefficient declines slowly with increasing Mach number because of the weak power dependence on T^*/T in Eq. (345). The ratio declines to $C_f^*/C_f \sim 1/2$ around a Mach number of roughly $M_\infty \sim 17$, depending on the specific assumptions made about wall temperature or whether the wall is adiabatic. At the same Mach number, a wall that is cooled to maintain a fixed temperature will have a thinner, denser boundary layer and larger drag coefficient than an adiabatic wall. Note that the actual drag force still goes up drastically with increasing velocity even though the drag coefficient decreases somewhat with velocity, since the drag force is proportional to $C_f^* v^2$.

Using Eqs. (135), (339), and (341), compressibility increases the thickness of a turbulent boundary layer on a flat plate by a factor of:

$$\frac{\delta(x)^*}{\delta(x)} = \left(\frac{\rho}{\rho^*}\frac{\mu^*}{\mu}\right)^{1/7} \approx \left(\frac{T^*}{T}\right)^{3/14} \tag{346}$$

Like the laminar result in Eq. (344), the compressibility increases the turbulent boundary layer thickness, but now it increases more slowly, varying roughly like the fourth root of the reference temperature.

Likewise, using Eqs. (136), (339), and (341), and absorbing the factor of ρ^*/ρ as discussed, compressibility alters the turbulent drag coefficient on a flat plate by a factor of:

$$\frac{C_f^*}{C_f} = \frac{\rho^*}{\rho}\left(\frac{\rho}{\rho^*}\frac{\mu^*}{\mu}\right)^{1/7} \approx \left(\frac{T}{T^*}\right)^{11/14} \tag{347}$$

This result for turbulent flow has a much stronger temperature dependence than the laminar case in Eq. (345). Thus it declines more rapidly with Mach number, falling to $C_f^*/C_f \sim 1/2$ around a Mach number of roughly $M_\infty \sim 5$, depending on the specific assumptions made about wall temperature or whether the wall is adiabatic.

4.2 General Principles of Atmospheric Reentry

An important application of compressible viscous fluid mechanics is the reentry of spacecraft or ballistic missile warheads into the earth's atmosphere [23, 24]. The typical velocity of vehicles reentering the atmosphere may be found by considering a vehicle of mass m in a circular orbit just above the earth's atmosphere, say at a height $H = 150$ km above the earth's surface. Because H is much smaller than the radius of the earth $R_\oplus \approx 6380$ km, one may simply use $R_\oplus$ for the orbital radius and the surface value $g \approx 9.807$ m/sec^2 for the gravitational acceleration. In a circular orbit at velocity v_o, viewed in a rotating reference frame, the outward centrifugal force $mv_o^2/R_\oplus$ balances the inward gravitational force mg:

$$\frac{mv_o^2}{R_\oplus} = mg \ , \ \text{or} \tag{348}$$

$$v_o = \sqrt{gR_\oplus} \approx 7.91 \ \text{km/sec} \approx \text{Mach } 23 \tag{349}$$

At this speed, each kg of the vehicle has a kinetic energy 1 kg $\cdot \ v_o^2/2 \approx 3.13 \times 10^7$ J that is equivalent to the explosive energy of roughly 7 kg of TNT–the vehicle's energy is equivalent to seven times its mass in high explosives. This enormous kinetic energy must be safely dissipated before the vehicle reaches the earth's surface. A rocket could slow an orbiting vehicle to a stop, but such a decelerating rocket would need to be as large as the one that initially accelerated the vehicle to orbital speed, and then sending the decelerating rocket into orbit would require an unimaginably large initial launch vehicle.

The simplest solution is to use aerodynamic drag in the atmosphere to steadily dissipate a vehicle's kinetic energy before it lands. However, the reentry trajectory must be chosen so that both:

1. Deceleration of the vehicle is not too severe for the instrumentation or the passengers (if there are any). The deceleration must be prolonged over at least a few minutes to limit it to levels that can be tolerated by humans. At the upper limit of human endurance, a $\sim 10g \sim 100$ m/sec^2 deceleration would require 80 seconds to brake an initial velocity of 8000 m/sec, and a more readily tolerated $\sim 3g \sim 30$ m/sec^2 deceleration would require ~ 4.5 minutes.

2. Heating of the vehicle from aerodynamic drag is not too great. The kinetic energy ~ 30 MJ/kg that must be dissipated is 2-4 times larger than the energy required to vaporize most materials. Methods for safely dissipating this much energy without vaporizing the vehicle will now be discussed.

When air flow impacts a reentering vehicle, the kinetic energy density $\rho v^2/2$ of the flow relative to the vehicle is converted to thermal energy density $\rho c_p T$, heating the air to a temperature T far higher than the ambient air temperature. As the temperature rises, air molecules first are excited into higher energy states, then dissociate into individual atoms, and then finally are progressively stripped of their electrons and ionized. While the specific heat capacity at constant pressure c_p is a constant for air at lower temperatures, at higher temperatures c_p is a function of temperature, to account for these various effects. From Section 3.1, air is mostly nitrogen, and monatomic nitrogen would have $c_p \approx 717.5$ J/(kg ^{o}K). As the nitrogen atoms are excited and partially ionized, they gain more degrees of freedom (the electrons can be in various energy levels), so c_p increases. The extent of excitation and ionization and hence the value of c_p vary over the temperature range characteristic of reentry, but in general a good value to use for earth reentry is:

$$c_p \approx 5000 \ \frac{\text{J}}{\text{kg } ^o\text{K}} \tag{350}$$

Thus a vehicle reentering at velocity v heats the flow directly impacting it to a **stagnation temperature** of

$$T \approx \frac{v^2}{2c_p} \approx 10^{-4}\, v^2_{\mathrm{m/sec}} \ {}^{\circ}\mathrm{K} \tag{351}$$

For a vehicle with orbital velocity $v \sim 8000$ m/sec, the stagnation temperature is $T \sim 6400^o$K. This is high enough to melt or vaporize virtually all materials, and is even hotter than the surface of the sun, which is approximately 5800^oK.

Since the drag force per cross-sectional area of a vehicle is $C_D \rho v^2/2$ and power is the product of force and velocity, the rate at which a reentering vehicle's kinetic energy is converted to heat is $C_D \rho v^3/2$. Using $C_D \approx 2$ for a blunt hypersonic vehicle from Eq. (317), the heat production rate is

$$q_{\mathrm{total}} \approx \rho\, v^3 \ \frac{\mathrm{W}}{\mathrm{m}^2} \tag{352}$$

For a typical high-altitude atmospheric density $\rho \sim 10^{-4}$ kg/m^3 and vehicle velocity $v \sim 8000$ m/sec, the total heat production rate is an incredible $q_{\mathrm{total}} \sim 50$ MW/m^2.

Fortunately, for a well-designed vehicle, only a small fraction of this heat is transferred to the vehicle, and the rest is imparted to the surrounding air. As shown in Fig. 32, a reentry vehicle should have blunt instead of sharp leading surfaces, in order to minimize heating of the vehicle. At hypersonic speeds, a streamlined vehicle creates a weaker shock wave and heats the air less, but the vehicle absorbs much more of the heat that is generated, since the shock and boundary layers are so close to the vehicle, especially where the shock wave is attached at the vehicle's nose. (For such a streamlined design, reentry would first melt the nose, and then proceed to destroy the rest of the vehicle.) In contrast, a very blunt vehicle creates a stronger shock wave and heats the air more, but the vehicle absorbs much less of the heat that is generated, since the shock wave is detached from the vehicle, and the intervening boundary layer serves to insulate the vehicle from most of the heat. (In a realistic reentry, the capsule would actually be tilted at some angle of attack to generate lift, as will be described in Section 4.4 for lifting reentry trajectories.) Thus reentry capsules have broad, flattened heat shields facing the oncoming flow, and space-shuttle-type reentry vehicles have blunt noses and rounded leading wing edges and also reenter at a high angle of attack with the flat underside facing the oncoming flow.

At the velocities that will be considered in this section, convection is the dominant mode of heat transfer, although at higher velocities, radiative heat transfer would also need to be considered [24]. From *Heat Transfer* 2.1, the heat transferred from a medium at temperature T_∞ through a boundary layer of thickness δ and thermal conductivity κ to a vehicle of surface temperature T_s and radius R is

$$q_{\mathrm{vehicle}} \approx \frac{\kappa(T_\infty - T_s)}{\delta(R)} \tag{353}$$

From Eq. (130), the laminar boundary layer thickness for a vehicle of size R is $\delta \sim R/\sqrt{\mathrm{Re}_R}$, so the heat transfer is

$$q_{\mathrm{vehicle}} \sim \sqrt{\mathrm{Re}_R}\ \frac{\kappa(T_\infty - T_s)}{R} \tag{354}$$

Empirical measurements yield the best numerical factor for heat transfer to a sphere:

$$q_{\mathrm{vehicle}} \approx 2\sqrt{\mathrm{Re}_R}\ \frac{\kappa(T_\infty - T_s)}{R} \tag{355}$$

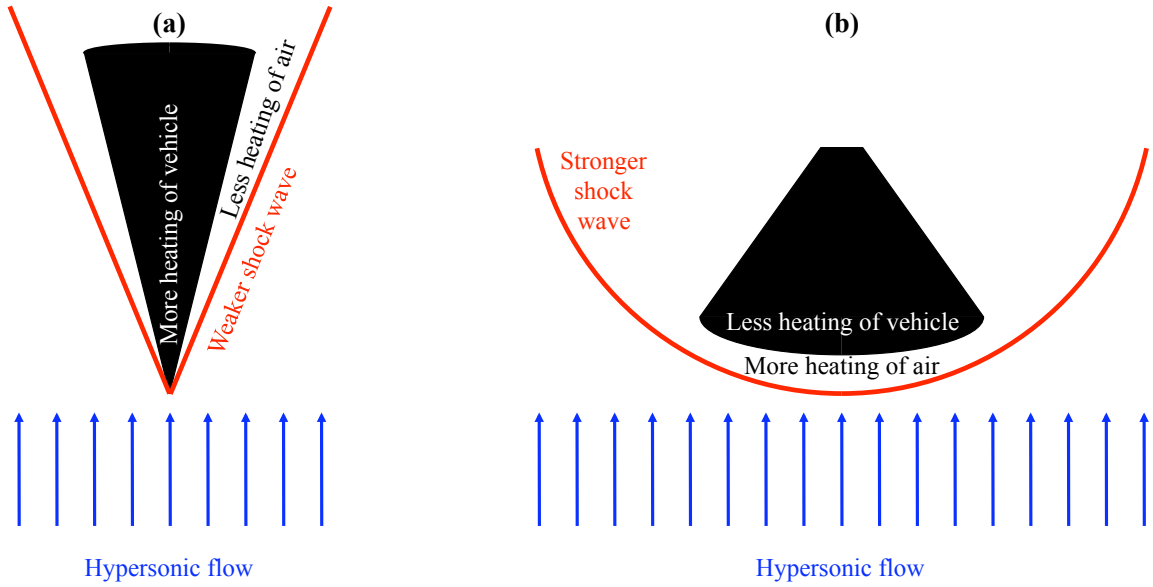

Figure 32. A reentry vehicle should have blunt instead of sharp leading surfaces to minimize heating of the vehicle. **(a)** At hypersonic speeds, a streamlined vehicle creates a weaker shock wave and heats the air less, but the vehicle absorbs much more of the heat that is generated, since the shock and boundary layers are so close to the vehicle, especially at the vehicle's nose. **(b)** A very blunt vehicle creates a stronger shock wave and heats the air more, but the vehicle absorbs much less of the generated heat, since the shock wave is detached from the vehicle, and the intervening boundary layer helps to insulate the vehicle from the heat.

Assuming that the air temperature just beyond the boundary layer is the stagnation temperature $T_\infty = v^2/(2c_p)$, that the stagnation temperature is much higher than the vehicle temperature ($T_\infty \gg T_s$), and that the Reynolds number is $\text{Re}_R = \rho v R/\mu$, Eq. (355) becomes

$$q_{\text{vehicle}} \approx \frac{\kappa/c_p}{\sqrt{\mu}} \sqrt{\frac{\rho}{R}}\, v^{2.5} \approx \sqrt{\mu} \sqrt{\frac{\rho}{R}}\, v^{2.5} \tag{356}$$

in which Eq. (356) used the relation $\mu \approx \kappa/c_p$ from the Prandtl number for air, $\text{Pr} = c_p\mu/\kappa \approx 1$.

The viscosity of air varies with temperature according to Sutherland's law from Eq. (340). Assuming $\mu_0 \approx 1.72 \times 10^{-5}$ Pa·sec and $T_0 \approx 273^o$K, neglecting S in comparison to the temperatures, and using Eq. (207), the viscosity may be expressed as:

$$\mu \approx 1.0 \times 10^{-6} \sqrt{T_{^oK}}\ \frac{\text{kg}}{\text{m sec}} \approx 1.0 \times 10^{-8}\, v_{\text{m/sec}}\ \frac{\text{kg}}{\text{m sec}} \tag{357}$$

Combining Eqs. (356) and (357), the heat transfer becomes

$$q_{\text{vehicle}} \approx 1 \times 10^{-4} \sqrt{\frac{\rho}{R}}\, v^3\ \frac{\text{W}}{\text{m}^2} \tag{358}$$

Of course, a reentering vehicle is generally not spherical, and the precise local and total heat transfer rates will depend on the specific shape of the vehicle. However, Eq. (358) is extremely useful for obtaining initial estimates of reentry heat transfer before doing more detailed calculations.

Taking the ratios of Eqs. (358) and (352), the fraction of the heat transferred to the vehicle is

$$\frac{q_{\text{vehicle}}}{q_{\text{total}}} \approx 10^{-4} \frac{1}{\sqrt{\rho R}} \tag{359}$$

For ballpark values of high-altitude atmospheric density $\rho \sim 10^{-4}$ kg/m^3 and reentry capsule size $R \sim 1$ m, the ratio is $q_{\text{vehicle}}/q_{\text{total}} \sim 10^{-2}$. Thus only $\sim 1\%$ of the produced heat is imparted to the vehicle, but that is still a very considerable ~ 0.5 MW/m^2. Likewise, the boundary layer insulates the vehicle from the $\sim 6000^o$K stagnation temperature of the airflow, although heat transfer across the boundary layer can still heat the leading surfaces of the vehicle to $1000 - 2000^o$K.

To protect the vehicle, these leading surfaces are covered by a heat shield. The underside of the space shuttle was covered with low-density tiles made of silica fibers (the tiles had a net density only $\sim 6\%$ that of solid silica, the remainder of the volume being empty space to minimize thermal conductivity) covered with black borosilicate paint, and the shuttle's nose and leading wing edges had tiles of carbon-carbon composite (graphite fibers for strength embedded in amorphous carbon for lower thermal conductivity than carbon lattices) better able to withstand the higher temperatures in those locations. Because these tiles were very good thermal radiators and insulators, they reradiated most of the heat they acquired back to the airflow, and conducted very little of the heat to the rest of the shuttle. Most other reentry vehicles are single-use and employ ablative heat shields that are gradually vaporized during reentry in order to remove the thermal energy they have absorbed before it can be conducted to the rest of the vehicle. For example, each Apollo command module used a fiberglass heat shield that was initially $\sim 25\%$ silica fibers and $\sim 75\%$ epoxy resin; after reentry most of the silica fibers remained, but the epoxy resin had been charred until only carbon remained from its initial composition.

An added complication of reentry is that the layer of partially ionized air below and around a reentering vehicle blocks electromagnetic communications between the vehicle and the ground. There is little ionization directly in the wake of the vehicle, however, so the vehicle can still communicate with satellites in that direction, and thereby indirectly communicate with the ground through those satellites. The space shuttle commonly employed this technique.

Since the power dissipated by atmospheric deceleration is $\sim \rho v^3$, to limit deceleration and heating to tolerable levels, it is important to choose reentry trajectories that remain as high as possible (to minimize ρ) while the velocity v is still very large. Reentry trajectories suitable for different types of vehicles will be considered [Fig. 33]: (a) ballistic reentry, (b) lifting reentry, (c) skip reentry, and (d) double-dip reentry. These four reentry approaches will be considered in Sections 4.3-4.6.

The stratosphere is the most important layer of the atmosphere for reentry, so one can use the exponential atmosphere approximation, Eq. (165). A vehicle of cross-sectional area A has aerodynamic drag D and lift L forces given by Eqs. (45) and (48), where the drag and lift coefficients C_D and C_L are assumed to be constant for simplicity. Although centrifugal force is considered (in a rotating frame of reference that effectively follows the vehicle around the earth), curvature of the earth with respect to the flight path is generally neglected. To convert the equations of motion into an easily solvable form, reentry calculations commonly change the independent variable in differential equations by taking the ratio of derivatives, as will be shown.

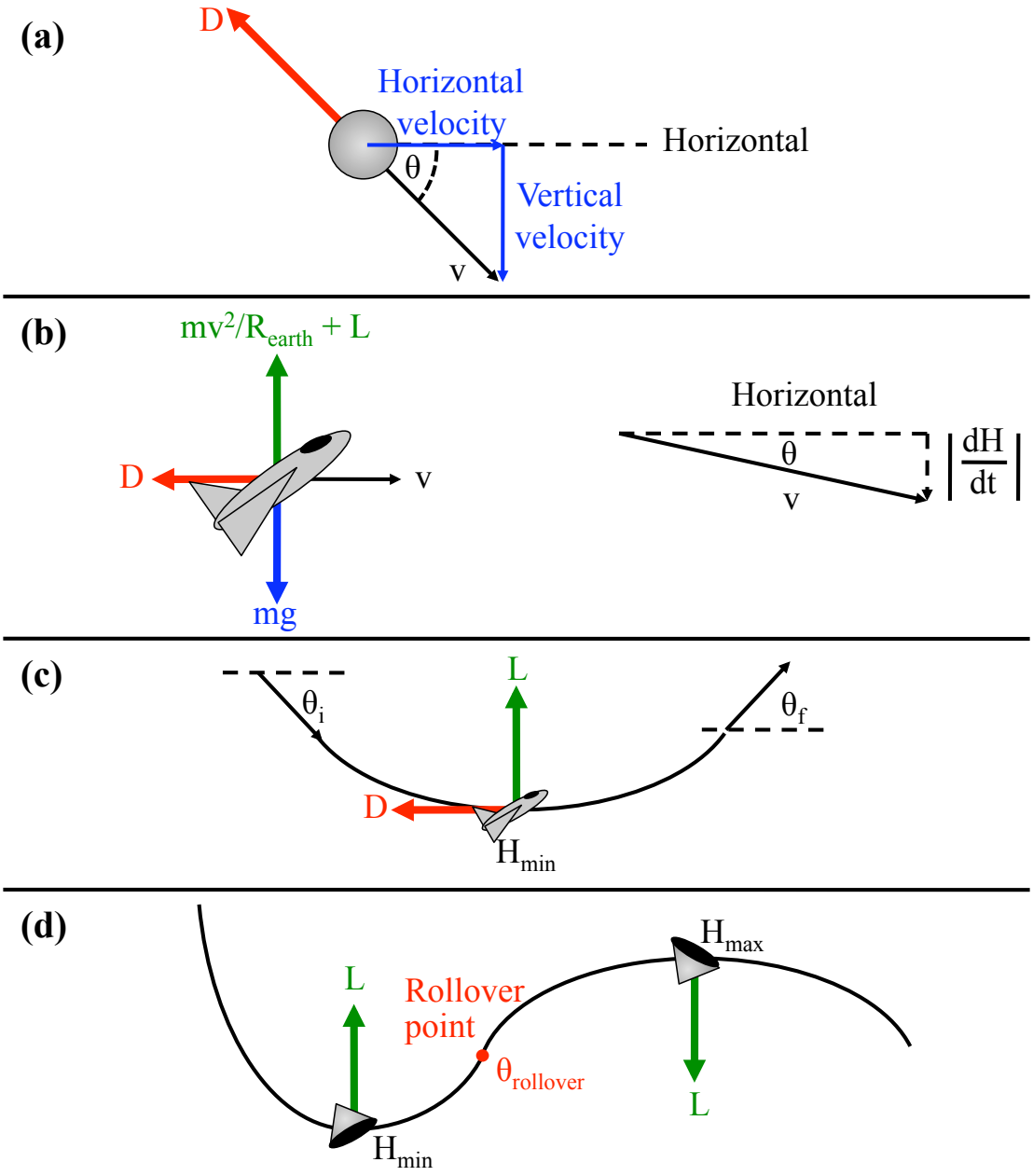

Figure 33. Atmospheric reentry approaches. **(a)** Ballistic reentry. **(b)** Lifting-body reentry. **(c)** Skip reentry. **(d)** Double-dip reentry.

4.3 Ballistic Reentry

In a ballistic reentry [Fig. 33(a)], the vehicle cannot generate aerodynamic lift; this applies to many warheads and the first manned spacecraft. The effective gravitational acceleration, the difference between the downward gravitational acceleration and the upward centrifugal acceleration, is between 0 and 1 g. (0 g would be a circular orbit with the gravitational and centrifugal forces balanced, and 1 g would be falling with no forward velocity.) As will be shown, the vehicle deceleration due to aerodynamic drag is far larger than this, so gravity and centrifugal force may be neglected. The vehicle's initial velocity v_i is typically of the order of v_o from Eq. (349). The pitch angle θ between the trajectory and the local horizontal is defined to be negative when downward; for simplicity it is assumed to be constant. Using Eq. (45), Newton's second law for the acceleration a along the trajectory is

$$a \;=\; \frac{dv}{dt} \;=\; -\,\frac{1}{2m}\,C_D A \rho v^2 \tag{360}$$

Taking the ratio of $d\rho/dH = -\rho/H_o$ [using Eq. (165)] and $dH/dt = -v\,|\sin\theta|$, one finds:

$$\frac{d\rho}{dt} \;=\; \frac{d\rho}{dH}\,\frac{dH}{dt} \;=\; \frac{\rho v}{H_o}\,|\sin\theta| \tag{361}$$

Equation (361) may be used to rewrite Eq. (360), changing the independent variable from t to ρ:

$$\frac{dv}{d\rho} \;=\; \frac{dv/dt}{d\rho/dt} \;=\; -\,\frac{C_D A H_o}{2m\,|\sin\theta|}\,v \tag{362}$$

Equation (362) is simply an equation for exponential decay, so its solution is

$$v \;=\; v_i\,\exp\left(-\,\frac{C_D A H_o}{2m\,|\sin\theta|}\,\rho\right) \tag{363}$$

$$\;=\; v_i\,\exp\left(-\,\frac{C_D A H_o \rho_o}{2m\,|\sin\theta|}\,e^{-H/H_o}\right) \tag{364}$$

Inserting Eq. (363) into Eq. (360) yields the acceleration as a function of the local density:

$$a \;=\; -\,\frac{C_D A \rho v_i^2}{2m}\,\exp\left(-\,\frac{C_D A H_o \rho}{m\,|\sin\theta|}\right) \tag{365}$$

Setting $d/d\rho$ of Eq. (365) equal to zero, one finds the density at which maximum deceleration occurs:

$$\frac{da}{d\rho} \;=\; -\,\frac{C_D A v_i^2}{2m}\,\exp\left(-\,\frac{C_D A H_o \rho}{m\,|\sin\theta|}\right)\left(1 \,-\, \frac{C_D A H_o \rho}{m\,|\sin\theta|}\right) \;=\; 0$$

$$\Longrightarrow\quad \rho_{\text{max decel}} \;=\; \frac{m\,|\sin\theta|}{C_D A H_o} \tag{366}$$

Inserting Eq. (366) into (363) and (164) gives the velocity and altitude for the maximum deceleration:

$$v_{\text{max decel}} \;=\; e^{-1/2}\,v_i \;\approx\; 0.607\,v_i \tag{367}$$

$$H_{\text{max decel}} \;=\; H_o \ln\left(\frac{\rho_o}{\rho_{\text{max decel}}}\right) \;=\; H_o \ln\left(\frac{C_D A H_o \rho_o}{m\,|\sin\theta|}\right) \tag{368}$$

Note that for an object with a sufficiently large mass and small cross section for drag ($m/A \to \infty$), atmospheric drag does not slow an object much, and Eq. (368) predicts that maximum deceleration would not occur until a theoretical negative altitude, whereas of course the solid ground (not included in the equation) intervenes to cause maximum deceleration at $H = 0$. The reentry and impact of a large, dense meteorite would be a good example.

Plugging Eq. (366) into Eq. (365) gives the maximum deceleration:

$$\begin{aligned} |a|_{\text{max decel}} &= \frac{v_i^2 \, |\sin\theta|}{2H_o e} = \frac{R_\oplus}{2H_o e} \, |\sin\theta| \left(\frac{v_i}{v_o}\right)^2 \text{ g} \\ &\approx 180 \, |\sin\theta| \left(\frac{v_i}{v_o}\right)^2 \text{ g} \end{aligned} \tag{369}$$

From Eq. (369), the maximum deceleration is independent of the vehicle drag coefficient. For a given reentry angle, vehicles with different values of C_D experience the same maximum deceleration, though higher-drag vehicles experience it at a higher altitude, according to Eq. (368).

The deceleration can be over 100 g for $v_i \sim v_o$ and large reentry angles θ. This justifies the original assumption that the effective gravitational acceleration could be neglected. If the reentry angle could be made arbitrarily small, Eq. (369) shows that the deceleration would approach zero. Unfortunately, even in a ballistic reentry into the atmosphere from a circular orbit with $v_i = v_o$, the decelerating vehicle will begin to lose altitude as its decreasing upward centrifugal acceleration fails to balance the downward gravitational acceleration, so there is a minimum achievable value of θ and hence a minimum achievable value for the peak deceleration. At the point of maximum deceleration, this difference between the gravitational and centrifugal forces produces a net downward effective gravitational acceleration of

$$|g_{\text{effective}}|_{\text{max decel}} = g - \frac{(v_o/\sqrt{e})^2}{R_\oplus} = \frac{e-1}{e} \, g \tag{370}$$

Assuming that θ is small, the vehicle's horizontal velocity at the point of maximum deceleration is approximately

$$\frac{v_o}{\sqrt{e}} = v_o - |a|_{\text{avg}} \, \Delta t \tag{371}$$

$$\implies \Delta t = \frac{v_o}{|a|_{\text{avg}}} \, \frac{\sqrt{e}-1}{\sqrt{e}} \, , \tag{372}$$

in which Δt is the time between the beginning of reentry and the point of maximum deceleration, and $|a|_{\text{avg}}$ is the average deceleration during that time.

Similarly, for small θ the downward vertical velocity at the point of maximum deceleration is approximately

$$\frac{v_o}{\sqrt{e}} \, \theta = |g_{\text{effective}}|_{\text{avg}} \, \Delta t \tag{373}$$

$$\implies \theta = (\sqrt{e}-1) \, \frac{|g_{\text{effective}}|_{\text{avg}}}{|a|_{\text{avg}}} \tag{374}$$

$$\approx (\sqrt{e}-1) \, \frac{|g_{\text{effective}}|_{\text{max decel}}}{|a|_{\text{max decel}}} \, , \tag{375}$$

which may be used to find the minimum achievable ballistic reentry angle.

Inserting Eqs. (377) and (369) into Eq. (375) and solving for θ yields

$$\theta = \left[\frac{(\sqrt{e}-1)(e-1)}{180e}\right]^{1/2} \approx 0.0477 \text{ radians} \quad (\text{or } 2.73^o) \tag{376}$$

$$|a|_{\text{max decel}} = 180\theta \text{ g} \approx 8.6 \text{ g} \tag{377}$$

This result is very close to that found by much more detailed numerical calculations [23]. The Soviet Vostok and U.S. Mercury capsules executed a shallow-angle ballistic reentry and hence experienced $\sim 8-9$ g of deceleration, at the upper limit of what their pilots could tolerate. Reducing $|a|_{\text{max}}$ below this value requires aerodynamic lift, so that the spacecraft can remain longer at very high altitudes, where the air is less dense and the aerodynamic drag less severe.

For a Vostok or Mercury reentry with typical values $H_o \approx 6500$ m, $C_D \approx 2$, $A \sim 3$ m^2, $\rho_o \approx 1.225$ kg/m^3, $m \sim 2000$ kg, and $\theta \approx 0.0477$, Eqs. (366) and (368) indicate that maximum deceleration for a capsule reentering from circular orbit occurs at an atmospheric density $\rho_{\text{max decel}} \approx 2 \times 10^{-3}$ kg/m^3 and an altitude $H_{\text{max decel}} \approx 40$ km.

Inserting Eq. (363) into Eq. (358), the heat transfer rate to the vehicle during ballistic reentry is

$$q_{\text{vehicle}} \approx 1 \times 10^{-4}\, v_i^3 \sqrt{\frac{\rho}{R}}\, \exp\left(-\frac{3C_D A H_o}{2m\,|\sin\theta|}\,\rho\right) \frac{\text{W}}{\text{m}^2} \tag{378}$$

Using Eq. (378) and setting $dq_{\text{vehicle}}/d\rho = 0$, one finds that the maximum heat transfer occurs when the atmospheric pressure is

$$\rho_{\text{max heat}} = \frac{m\,|\sin\theta|}{3C_D A H_o} = \frac{1}{3}\,\rho_{\text{max decel}}\,, \tag{379}$$

or $\rho_{\text{max heat}} \sim 7 \times 10^{-4}$ kg/m^3 for the Vostok/Mercury case.

Inserting Eq. (379) into Eq. (378) gives the maximum heat transfer:

$$q_{\text{vehicle, max}} \approx 1 \times 10^{-4}\, v_i^3 \sqrt{\frac{m\,|\sin\theta|}{3eC_D A H_o R}}\ \frac{\text{W}}{\text{m}^2} \tag{380}$$

For a Vostok or Mercury capsule with $v_i = v_o \approx 8000$ m/sec, $m \sim 2000$ kg, $\theta \sim 0.0477$, $C_D \approx 2$, $A \sim 3$ m^2, $H_o \approx 6500$ m, and $R \sim 1$ m, the maximum heat transfer is $q_{\text{vehicle, max}} \sim 1$ MW/m^2. As predicted by Eqs. (352) and (359), this is indeed only a small fraction of the total generated heat, although it is still a large number and required a very good ablative heat shield.

Inserting Eq. (379) into Eq. (363) and (164) gives the velocity and altitude for the maximum heating:

$$v_{\text{max heat}} = e^{-1/6}\, v_i \approx 0.846\, v_i \tag{381}$$

$$H_{\text{max heat}} = H_o \ln\left(\frac{\rho_o}{\rho_{\text{max heat}}}\right) = H_o \ln\left(\frac{3C_D A H_o \rho_o}{m\,|\sin\theta|}\right) \tag{382}$$

$$= H_o \ln\left(\frac{3C_D A H_o \rho_o}{m\,|\sin\theta|}\right) + H_o \ln 3 \approx H_{\text{max decel}} + 1.10 H_o \tag{383}$$

Thus the point of maximum heating occurs earlier during reentry than the point of maximum deceleration, or when the vehicle is approximately 1.1 $H_o \approx 7$ km higher.

4.4 Lifting-Body Reentry

Lifting reentry [Fig. 33(b)] covers the case in which the vehicle generates aerodynamic lift as well as drag. For simplicity, the ratio of the lift and drag forces from Eqs. (48) and (45), $L/D = C_L/C_D$, is assumed to remain constant during the reentry, and the initial velocity is assumed to be the orbital velocity v_o from Eq. (349). Because very small angles minimize the deceleration (as shown for ballistic reentry) and the vehicle now has lift to help support it, one can assume that the trajectory is essentially horizontal.

Neglecting vertical acceleration, the downward gravitational and upward centrifugal and lift forces must balance:

$$mg \;=\; \frac{mv^2}{R_\oplus} \;+\; L \tag{384}$$

Using Eq. (48) for L in Eq. (384) and solving for the velocity v yields:

$$mg \;=\; \frac{mv^2}{R_\oplus} \;+\; \frac{1}{2}C_L A\rho v^2 \tag{385}$$

$$\Longrightarrow\; v \;=\; \frac{v_o}{\sqrt{1+\frac{R_\oplus C_L A\rho}{2m}}} \;=\; \frac{v_o}{\sqrt{1+\frac{R_\oplus C_L A\rho_o}{2m}\,e^{-H/H_o}}} \tag{386}$$

$$\approx\; \sqrt{\frac{2mg}{C_L A\rho_o}}\,e^{H/2H_o} \tag{387}$$

The approximation in the last step is valid once the velocity is low enough that the centrifugal force is much smaller than the lift.

Equation (384) may be turned around into a form that will be useful in a moment:

$$\frac{1}{m} \;=\; \frac{g}{L}\left[1-\left(\frac{v}{v_o}\right)^2\right] \tag{388}$$

Newton's second law along the trajectory is:

$$\frac{dv}{dt} \;=\; -\frac{D}{m} \tag{389}$$

Substituting Eq. (388) into Eq. (389), one finds the acceleration:

$$\frac{dv}{dt} \;=\; -g\,\frac{D}{L}\,\left[1-\left(\frac{v}{v_o}\right)^2\right] \tag{390}$$

Thus the magnitude of the deceleration increases as the velocity v decreases, asymptotically approaching gD/L. The Gemini, Apollo, and Soyuz capsules had a lift-to-drag ratio $L/D \approx 0.5$, giving a maximum deceleration ~ 2 g, much better than the earlier Mercury and Vostok. Due to the space shuttle's larger ratio, $L/D \approx 2.5$, its peak deceleration was even more gentle, ~ 0.4 g.

The reentry trajectory of a lifting body actually deviates from the horizontal by a small negative (downward) angle θ, which may be found from the relation:

$$\sin\theta \;=\; \frac{1}{v}\,\frac{dH}{dt} \;=\; \frac{1}{v}\,\frac{dv/dt}{dv/dH} \tag{391}$$

Taking the derivative d/dH of both sides of Eq. (387) produces

$$\frac{dv}{dH} \;=\; \frac{Lv}{2mgH_o} \tag{392}$$

Inserting Eqs. (389) and (392) into Eq. (391), one finds:

$$\sin\theta \;=\; 2\,\frac{D}{L}\,\frac{H_o g}{v^2} \tag{393}$$

Equation (393) shows that the magnitude of θ increases (the vehicle drops more rapidly) as the velocity v decreases, since there is less centrifugal force and lift to keep the vehicle aloft.

θ is small enough that the approximation $\sin\theta \approx \theta$ is valid. Using a mid-reentry value of the velocity, $v \sim v_o/2$, yields an estimate of θ during reentry:

$$\theta \;\sim\; 8\,\frac{D}{L}\,\frac{H_o}{R_\oplus} \;\approx\; \frac{D}{L}\,0.5^{\,o}\,, \tag{394}$$

validating the initial assumption of nearly horizontal flight.

The ground range Δx travelled during reentry may be estimated from θ and the altitude drop during that time, say $\Delta H \sim 2H_o$:

$$\Delta x \;\sim\; \frac{\Delta H}{\sin\theta} \;\sim\; \frac{2H_o}{\theta} \;\sim\; \frac{1}{4}\,\frac{L}{D}\,R_\oplus \tag{395}$$

Since the space shuttle had $L/D \approx 2.5$, Eq. (395) shows that it could travel ~ 4000 km during reentry. Thus the reentry began very far from the actual landing site. Because the shuttle had no fuel to maneuver during landing, it arrived at the landing site with excess altitude to ensure that it would not fall short of the runway. If the extra altitude was not needed for contingencies, the shuttle banked back and forth to burn off the extra altitude before approaching the runway.

Inserting Eqs. (165) and (386) into Eq. (358), the heat transfer to a lifting reentry vehicle is

$$q_{\text{vehicle}} \;\approx\; 1\times10^{-4}\,\sqrt{\frac{\rho_o}{R}}\,v_o^3\,e^{-H/2H_o}\,\left(1+\frac{R_\oplus C_L A\rho_o}{2m}\,e^{-H/H_o}\right)^{-3/2}\;\frac{\text{W}}{\text{m}^2} \tag{396}$$

Setting $dq_{\text{vehicle}}/dH = 0$ and solving for H yields the altitude where peak heat transfer occurs:

$$H_{\text{max heat}} \;=\; H_o \ln\left(\frac{R_\oplus C_L A\rho_o}{m}\right) \tag{397}$$

Inserting Eq. (397) into Eq. (396), the maximum heat transfer to a lifting reentry vehicle is

$$q_{\text{vehicle, max}} \;\approx\; 5\times10^{-5}\,v_o^3\,\sqrt{\frac{\rho_o m}{RR_\oplus C_L A\rho_o}}\;\frac{\text{W}}{\text{m}^2} \tag{398}$$

For a space shuttle reentry with typical values $H_0 \approx 6500$ m, $R_\oplus \approx 6.38\times10^6$ m, $C_L \approx 2$, $A \sim 400$ m^2, $\rho_o \approx 1.225$ kg/m^3, and $m = 1\times10^5$ kg, Eq. (397) indicates that maximum heat transfer occurs at an altitude $H_{\text{max heat}} \sim 70$ km, or an atmospheric pressure $\rho_{\text{max heat}} = m/(R_\oplus C_L A) \sim 2\times10^{-5}$ kg/m^3. Also using the representative values $R \sim 20$ m and $v_o \approx 8000$ m/sec, the maximum heat transfer is $q_{\text{vehicle, max}} \sim 25$ kW/m^2, or $\sim$40x lower than the ballistic case. Note that the large lift means the decelerating vehicle can stay much higher in the atmosphere much longer than a ballistic vehicle with no lift, changing the point of maximum heating to a much higher altitude, much lower atmospheric density, and much lower peak heat transfer. In fact, the heat transfer is sufficiently low that silica tiles were sufficient to insulate the vehicle and re-radiate the heat to the surrounding atmosphere, whereas higher heat transfer values would require single-use ablative heat shields.

4.5 Skip Reentry

If desired, a vehicle can skip off the upper atmosphere like a fast-moving flat rock skipping off the surface of a pond, and this is called a skip reentry [Fig. 33(c)]. The prototypical example was the Sänger-Bredt intercontinental bomber proposed during WWII, which would have used rocket power to achieve a suborbital flight and then would have repeatedly skipped off the atmosphere to travel most of the way around the earth before reentering for a final time and landing [23]. One skip with initial velocity v_i will be considered here to illustrate the basic principle.

Gravity and centrifugal force are negligible relative to the strong aerodynamic forces involved in skipping off the atmosphere. Newton's second law parallel and perpendicular to the trajectory is

$$m \frac{dv}{dt} = -D \tag{399}$$

$$mv \frac{d\theta}{dt} = L \tag{400}$$

Taking the ratio of Eqs. (399) and (400) gives the variation of velocity with vehicle pitch angle,

$$\frac{dv}{d\theta} = \frac{dv/dt}{d\theta/dt} = -\frac{D}{L} v \tag{401}$$

Equation (401) describes exponential decay due to drag during the skip, so its solution is

$$v = v_i \exp\left[-\frac{D}{L}(\theta - \theta_i)\right], \tag{402}$$

in which θ_i is the initial pitch angle for atmospheric entry. If the vehicle does not lose much of its velocity during the skip, its pitch angle θ_f leaving the atmosphere is approximately the mirror image of the angle entering the atmosphere, $\theta_f = -\theta_i$, like a light ray reflecting off a surface. Using these angles in Eq. (402) yields

$$v_f = v_i \exp\left(-2\theta_i \frac{D}{L}\right) \tag{403}$$

Newton's second law perpendicular to the trajectory in Eqs. (399) and (400) indicates that

$$\frac{d\theta}{dt} = \frac{C_L A \rho v}{2m} \tag{404}$$

An equation for the altitude may be found by taking the ratio of $dH/dt = v \sin\theta$ and Eq. (404):

$$\frac{dH}{d\theta} = \frac{dH/dt}{d\theta/dt} = \frac{2m \sin\theta}{C_L A \rho}$$

$$= \frac{2m \sin\theta}{C_L A \rho_o e^{-H/H_o}} \tag{405}$$

Separating variables in Eq. (405) and integrating gives the minimum altitude during the skip:

$$\frac{C_L A \rho_o}{2m} \int_\infty^{H_{\min}} dH \, e^{-H/H_o} = \int_{\theta_i}^0 d\theta \, \sin\theta$$

$$\implies H_{\min} = H_o \ln\left[\frac{C_L A \rho_o H_o}{2m(1 - \cos\theta_i)}\right] \tag{406}$$

Pilots are generally happier if $H_{\min}$ is greater than 0, which means that the argument of the logarithm in Eq. (406) must be greater than 1. For small values of θ_i, the approximation $\cos\theta_i \approx 1 - \theta_i^2/2$ may be used, and the positive altitude requirement reduces to:

$$\theta_i^2 \;<\; \frac{C_L A \rho_o H_o}{m} \tag{407}$$

Thus skipping requires a small entry angle θ_i and/or large coefficient of lift C_L.

Using Eq. (406), the atmospheric density at the minimum altitude is

$$\rho_{\text{at min}} \;=\; \rho_o\, e^{-H_{\min}/H_o} \;=\; \frac{2m(1-\cos\theta_i)}{C_L A H_o} \tag{408}$$

The maximum acceleration is lateral due to the lift and occurs at the minimum altitude:

$$\begin{aligned} |a|_{\max} \;&=\; \frac{L_{\text{atmin}}}{m} \;=\; \frac{C_L A \rho_{\text{at min}} v_{\text{at min}}^2}{2m} \\ &=\; \frac{v_i^2}{H_o}\,(1-\cos\theta_i)\exp\left(-2\theta_i\,\frac{D}{L}\right) \\ &\approx\; 490\left(\frac{v_i}{v_o}\right)^2 \theta_i^2\,\exp\left(-2\theta_i\,\frac{D}{L}\right)\;\text{g} \end{aligned} \tag{409}$$

Using $v_i \sim v_o$ and $\theta_i = 5^o \approx 0.087$ rad and neglecting the exponential factor yields $|a|_{\max} \approx 3.7$ g.

The ground range Δx traversed while the angle changes by $\Delta\theta$ may be estimated from Eq. (404):

$$\Delta\theta \;\sim\; \frac{C_L A \rho}{2m}\, v\,\Delta t \;\sim\; \frac{C_L A \rho}{2m}\,\Delta x \tag{410}$$

Using Eq. (410) with $\Delta\theta = 2\theta_i$, the ground range covered during the entire skip maneuver is

$$(\Delta x)_{\text{skip}} \;\sim\; \frac{2m}{C_L A \rho_{\text{atmin}}}\,2\theta_i \;=\; \frac{2\theta_i}{1-\cos\theta_i}\,H_o \;\approx\; \frac{26\ \text{km}}{\theta_i}\,, \tag{411}$$

which is ~ 300 km for $\theta_i = 5^o \approx 0.087$ rad.

Even though skip reentries were never used for suborbital bombers, they are extremely useful for **aerobraking**, or slowing an interplanetary spacecraft into orbit when it arrives at its target planet. By plotting the spacecraft's trajectory so that its perigee slightly dips into the planet's upper atmosphere, one can cause the spacecraft to lose enough velocity to lower its apogee from infinity (escape velocity) to some finite value for an orbit around the planet. If the velocity loss on one skip is not too great, just the trajectory of the spacecraft tangentially grazing the curved atmosphere of the planet is enough to cause the spacecraft to "pull up" from the skip, even if the vehicle is not capable of lift. In practice, though, it is better to employ lift as in the skip example calculated above, since it affords much more control over the aerobraking process to deal with fluctuations in atmospheric density. If necessary to minimize the forces and heating the spacecraft experiences during each skip, several successive passes through a planet's atmosphere with a small skip each time can be used to aerobrake from very large initial velocities. For more information on orbital and interplanetary trajectories, see *Classical Mechanics* ?.?.

Skip reentries are also useful as part of a more complicated maneuver called a double-dip reentry, which is used by spacecraft returning to the earth from deep space, as will be considered next.

4.6 Double-Dip Reentry

A spacecraft with negligible initial kinetic energy that "falls" from deep space to the earth's surface acquires a kinetic energy equal to the earth's gravitational well depth:

$$\frac{1}{2}mv^2 \;=\; \frac{GM_\oplus m}{R_\oplus} \;=\; mgR_\oplus \;\;,\;\; \text{or} \tag{412}$$

$$v \;=\; \sqrt{2gR_\oplus} \;=\; \sqrt{2}\,v_o \;\approx\; 11.2 \;\text{km/sec} \tag{413}$$

Thus the spacecraft has a velocity of Mach 33 or twice the kinetic energy of a vehicle that is simply in low earth orbit. The vehicle deceleration and aerodynamic heating would be too great if such a large amount of kinetic energy were expended during just one pass into the earth's atmosphere. For this reason, the U.S. Apollo and Soviet Zond capsules that returned from the moon executed a double-dip reentry, making two passes into the atmosphere before landing.

As shown in Fig. 33(d), a double-dip reentry begins like a skip. If the skip were completed, the vehicle would simply travel far out into space again due to its high remaining velocity. To avoid this, at pitch angle $\theta_{\text{rollover}} < |\theta_i|$ the vehicle rolls over before completing the skip, then (with its aerodynamic lift directed downward) executes an inverted skip to remain in the upper atmosphere. From Eq. (411), the ground range during a skip is inversely proportional to the atmospheric density where the skip is carried out. Thus the ground range traveled during the inverted skip is far longer than that of the initial upright skip, by the ratio of the low- and high-altitude atmospheric densities:

$$\frac{(\Delta x)_{\text{inverted}}}{(\Delta x)_{\text{skip}}} \;\sim\; \frac{\rho_{\text{at min}}}{\rho_{\text{at max}}} \;=\; \exp\left(\frac{H_{\max} - H_{\min}}{H_o}\right) \tag{414}$$

Therefore the ground range can easily be thousands of km.

From Eq. (407), a vehicle traveling from space to the ground encounters an effective amount of atmosphere $\sim \rho_o H_o$, and the aerodynamic lift it can generate during that transit can produce a net squared deflection θ_i^2 in the trajectory. To maximize the upward part of the double-dip maneuver without leaving the atmosphere, a vehicle can use half of the effective atmosphere to raise its pitch angle from $\theta = 0$ to θ_{rollover} and the other half to lower the pitch angle back to $\theta = 0$ so the vehicle stays within the atmosphere. This limits the rollover angle:

$$\theta_{\text{rollover}}^2 \;<\; \frac{1}{2}\,\theta_i^2 \tag{415}$$

Toward the end of the inverted phase of a double-dip reentry, the velocity is low enough that downward lift is no longer needed to hold the vehicle within the atmosphere. The lift may then be used to glide or steer toward a preferred landing site. For capsules such as Apollo that cannot eliminate their aerodynamic lift, the lift vector is slowly rolled about the velocity vector to cancel out the effects of lift once the vehicle is on its final course to the landing site.

References

[1] Frank M. White, *Fluid Mechanics* (7th ed., McGraw-Hill, New York, 2010). In terms of clear explanations and comprehensive coverage, this is by far the best single textbook on fluid mechanics. Make it your first and if necessary your only book on the subject.

[2] Frank M. White, *Viscous Fluid Flow* (3rd ed., McGraw-Hill, New York, 2005). Supplements White's introductory textbook and offers thorough coverage of incompressible and compressible viscous fluid mechanics, mostly emphasizing analytical calculations and approximations instead of scary computer stuff.

[3] Bruce R. Munson, Alric P. Rothmayer, Theodore H. Okiishi, and Wade W. Huebsch, *Fundamentals of Fluid Mechanics* (7th ed., Wiley, New York, 2012). Based on the topics and order of coverage, this book appears to consciously imitate White's *Fluid Mechanics* (or perhaps vice versa). It omits a considerable amount of information that is included in White's book, but every once in a long while it includes something that White does not.

[4] Pijush K. Kundu, Ira M. Cohen, and David R. Dowling, *Fluid Mechanics* (5th ed., Elsevier, New York, 2011). This textbook is a good complement to the general books by White or Munson. It covers the same basic topics as those books, but then skips some of their advanced topics in favor of a completely different set of advanced topics, such as instabilities, geophysical fluid dynamics, and biofluid mechanics.

[5] James A. Fay, *Introduction to Fluid Mechanics* (MIT Press, Cambridge, MA, 1994). Fay's book is more introductory than those by White, Munson, and Kundu. It omits many of the more advanced topics covered in those books, although the topics that Fay does include are covered very clearly and in detail.

[6] L.D. Landau and E.M. Lifshitz, *Fluid Mechanics* (2nd ed., Pergamon Press, New York, 1987). Far more math than physical intuition, but amazingly rigorous and comprehensive. Once the authors blow through ordinary fluid mechanics, they start on *really* advanced topics.

[7] Eugene A. Avallone, Theodore Baumeister III, and Ali M. Sadegh, *Marks' Standard Handbook for Mechanical Engineers* (11th ed., McGraw-Hill, New York, 2006), Section 3. Very terse but very useful treatment of fluid mechanics and related topics, including tables of properties.

Aerodynamics

John D. Anderson Jr.'s textbooks on aerodynamics and related topics are wonderfully clear and organized and also discuss the pioneers of aerodynamics. They are significantly better than competing textbooks on aerodynamics, and they go into compressible fluid flow in far greater detail than the above general books on fluid mechanics do. There is considerable overlap among Anderson's books, though, so you don't necessarily need to buy them all. If you can only buy one, get *Fundamentals of Aerodynamics*.

[8] *Introduction to Flight* (7th ed., McGraw-Hill, New York, 2011).

[9] *Fundamentals of Aerodynamics* (5th ed., McGraw-Hill, New York, 2010).

[10] *Modern Compressible Flow* (3rd ed., McGraw-Hill, New York, 2002).

[11] *Hypersonic and High Temperature Gas Dynamics* (2nd ed., AIAA, Washington, DC, 2006).

[12] *Aircraft Performance and Design* (McGraw-Hill, New York, 1999).

[13] John J. Bertin and Russell M. Cummings, *Aerodynamics for Engineers* (6th ed., Prentice Hall, Englewood Cliffs, NJ, 2013). In general, this textbook does not explain things as well as Anderson's books and is less organized. However, every few hundred pages it mentions something useful that Anderson does not.

[14] William H. Dorrance, *Viscous Hypersonic Flow* (McGraw-Hill, New York, 1962). A forerunner of Anderson's more recent hypersonic textbook, and especially noteworthy for its theoretical derivation of the reference temperature for compressible viscous flow on pp. 134-140.

[15] J. Gordon Leishman, *Principles of Helicopter Aerodynamics* (2nd ed., Cambridge University Press, New York, 2006). By far the clearest and best out of the handful of helicopter textbooks.

Acoustics

[16] Lawrence E. Kinsler, Austin R. Frey, Alan B. Coppens, James V. Sanders, *Fundamentals of Acoustics* (4th ed., Wiley, New York, 1999).

[17] Allan D. Pierce, *Acoustics* (Acoustical Society of America, Woodbury, NY, 1989).

[18] David T. Blackstock, *Fundamentals of Physical Acoustics* (Wiley, New York, 2000).

Shock waves

[19] Ya. B. Zel'dovich and Yu. R. Raizer, *Physics of Shock Waves and High-Temperature Hydrodynamic Phenomena* (Dover, New York, 2002). A classic.

[20] P. L. Sachdev, *Shock Waves and Explosions* (Chapman and Hall/CRC, Boca Raton, FL, 2004). Very mathematical, but one of the few books on the subject.

[21] Samuel Glasstone and Philip J. Dolan, *The Effects of Nuclear Weapons* (U.S. Government Printing Office, Washington, D.C., 1977). Detailed phenomenology of explosive shock waves.

[22] Carey Sublette, *The Nuclear Weapon Archive/Nuclear Weapons Frequently Asked Questions* (http://nuclearweaponarchive.org, 2007). Detailed unclassified discussion of implosive shock waves for compressing fission and fusion fuel.

Atmospheric reentry

[23] William E. Wiesel, *Spaceflight Dynamics* (3rd ed., Aphelion Press, Beavercreek, Ohio, 2010). The clearest and most concise presentation of reentry approaches, and a wonderfully written book in general. Unfortunately it only covers reentry trajectories, not reentry heat transfer.

[24] Wilbur Hankey, *Re-Entry Aerodynamics* (AIAA, Washington, DC, 1988). The best and most recent book on reentry heat transfer, which isn't saying much. You also need to translate the calculations from units such as BTUs per slug per fortnight into real units.